TABLE OF CONTENTS

LIST OF FIGURES

LIST OF TABLES

Intentionally Blank

8. ANALYSIS OF DESIGN EVENTS

In previous chapters of this SAR, the features of the TMI-2 ISFSI NUHOMS®-12T system that are important to safety have been identified and discussed. The purpose of this chapter is to present the engineering analyses for normal and off-normal operating conditions, and to establish and qualify the system for a range of credible and hypothetical accidents. The term "NUHOMS®-12T" refers to the TMI-2 ISFSI NUHOMS®-12T system.

In accordance with NRC Regulatory Guide 3.48 [8.1], the design events identified by ANSI/ANS 57.9-1984 [8.2] form the basis for the accident analyses performed for the NUHOMS®-12T system. Three categories of design events are defined. Normal operating and off-normal events and are addressed in Section 8.1. Accident conditions as postulated in ANSI/ANS 57.9-1984 due to natural phenomena and manmade events are addressed in Section 8.2. These events provide a means of establishing that the NUHOMS®-12T system design satisfies the applicable operational and safety acceptance criteria as delineated herein.

This chapter presents the engineering analysis for normal, off-normal, and accident conditions if the NUHOMS®-12T system using the NRC 10 CFR 71 certified MP-187 for transportation from TAN to INTEC. Appendix E of this SAR presents the normal, off-normal and accident conditions of the NUHOMS®-12T system using the NRC 10 CFR 72 approved OS-197 Transfer Cask for transportation from TAN to INTEC.

8.1 Normal and Off-Normal Operations

Normal operating design conditions consist of a set of events that occur regularly, or frequently, in the course of normal operation of the NUHOMS®-12T system. These normal operating conditions are addressed in Section 8.1.1. Off-normal operating design conditions are events that could occur with moderate frequency, possibly once during any calendar year of operation. These off-normal operating conditions are addressed in Section 8.1.2. The thermal-hydraulic, structural, and radiological analyses associated with these events are presented in the sections that follow.

8.1.1 Normal Load Structural Analysis

Table 8.1-1 shows the normal operating loads for which the NUHOMS®-12T safety-related components are designed. The table also lists the individual NUHOMS®-12T components that are affected by each loading. The magnitude and characteristics of each load are described in Section 8.1.1.1.

The method of analysis and the analytical results for each load are described in Sections 8.1.1.2 through 8.1.1.8. The load combinations for the affected components are given in Table 8.1-1and Table 8.1-2. The mechanical properties of materials employed in the structural analysis of the NUHOMS®-12T system components are presented in Table 8.1-3.

8.1.1.1 Normal Operating Loads

The normal operating loads for the NUHOMS®-12T system components are:

1. Dead Weight Loads
2. Design Basis Internal Pressure Loads
3. Design Basis Thermal Loads
4. Operational Handling Loads
5. Design Basis Live Loads

These loads are described in detail in the following paragraphs.

A. Dead Weight Loads

Table 8.1-4 shows the weights of various components of the NUHOMS®-12T system. The dead weight of the component materials is determined based on nominal component dimensions.

A density value of 0.283 pound per cubic inch for carbon steel and 0.285 pound per cubic inch for stainless steel are used in the dead weight calculations. A nominal concrete density of 140 pounds per cubic foot is conservatively selected as a design basis for the shielding and thermal evaluations. A nominal density of 150 pounds per cubic foot is assumed for the structural evaluation of the HSM.

B. Design Basis Internal Pressure

The range of NUHOMS®-12T DSC internal pressures for operating conditions and postulated accident conditions and the associated air temperatures are shown in Table 8.1-5. For normal and off-normal operating conditions, the NUHOMS®-12T DSC is vented to the atmosphere and therefore the normal operating pressure is 0 psig.

The maximum fuel debris temperature under normal, off-normal, or accident conditions from Table 8.1-10 is 219°F. To be conservative, the maximum fuel debris temperature is used for the air temperature in the DSC. To add additional conservatism, a temperature of 250°F is used as the temperature of the air in the DSC for pressure calculation.

The free volume of the DSC is calculated to be 3.4×10^6 cc. From Appendix C, the maximum hydrogen production rate with 12 TMI-2 canisters is 7 x 12 = 84 cc/hr. Using the stoichiometric production rate of hydrogen and oxygen, the total gas production rate in the DSC from 12 TMI-2

canisters is 84 + 84/2 = 126 cc/hr. Assuming that the vents on the DSC are plugged and the DSC is left in the HSM for a one year period, the total gas production in the DSC will be 1.1×10^6 cc/year.

Using the above temperatures, the DSC free volume and the total gas produced for a period of one year, the maximum pressure in the DSC is calculated to be 11.4 psig for the DSC in the HSM case.

Therefore, a design pressure of 15 psig is used for the DSC which bounds the pressure in the DSC during normal, off-normal, or accident conditions.

C. Design Basis Thermal Loads

The range of ambient temperature cases analyzed are defined in Section 8.1.3. The resulting temperature distributions in the HSM and DSC are determined by performing thermal analyses for these ambient conditions. Thermal properties for the materials are given in Table 8.1-6 and Table 8.1-7. The thermal analyses described in Section 8.1.3 provide temperature distributions for the HSM and DSC. They are shown in Table 8.1-8 through Table 8.1-10, and in Figure 8.1-1 through Figure 8.1-5. These temperature distributions are developed for the range of normal ambient temperatures shown in Table 8.1-10.

Table 8.1-9 summarizes the maximum calculated temperatures for normal operating conditions for the DSC shell. A more detailed tabulation of the thermal results used for the HSM structural design is shown in Table 8.1-8. The HSM reinforced concrete design is controlled by these thermal gradients.

The effect of DSCs being emplaced at varying locations throughout the HSM array are represented by the single module analysis presented herein since the prefabricated HSMs which make up HSM arrays are free-standing units. The appropriate inside and outside surface temperatures corresponding to peak temperatures and thermal gradients from Table 8.1-8 are applied to the HSM analytical model shown in Figure 8.1-15 and the resulting forces and moments calculated.

The temperature distributions derived from the three normal operating cases (-20°F, 45°F, 87°F) are considered in the structural analysis of the DSC and HSM as discussed in Sections 8.1.1.2. through 8.1.1.9. The temperature distributions for each component are used to determine the effects of thermal stresses and thermal cycling on the NUHOMS®-12T components. These results are also used to evaluate the effects of creep on the HSM reinforced concrete.

D. Operational Handling Loads

The most significant operational loading condition for the NUHOMS®-12T system components is sliding of the DSC from the transfer cask into the HSM. Sliding is achieved by the push/pull forces induced by the hydraulic ram system. These forces are applied to the grapple ring assembly, which is an integral part

of the DSC bottom end assembly. The forces induced by the ram system are reacted by friction forces which develop between the sliding surfaces of the DSC, the transfer cask, and HSM support rails.

Based on the surface finish and contact angle of the DSC support rails inside the HSM (as described in Chapter 4), a bounding coefficient of friction is conservatively assumed to be 0.25. Therefore, the nominal ram load required to slide the DSC under normal operating conditions is:

$$P = \frac{0.25\ W}{\text{Cos}\ \theta} = 0.29\ W$$

Where:

P = Push/Pull Load

W = Loaded DSC Weight

θ = 30 degrees, Angle of the Canister Support Rail

The DSC bottom cover plate and grapple ring assembly are designed to withstand a normal operating push/pull force equal to 100% of the loaded DSC weight (conservatively set at 70,000 pounds). To ensure retrievability for a postulated jammed DSC condition, the ram is sized with a capacity for an enveloping load of 70,000 pounds, as described in Section 8.1.2. These ram forces bound those friction forces postulated to develop between the sliding surfaces of the DSC and transfer cask during worst case off-normal conditions.

E. Design Basis Live Loads

As discussed in Section 3.2.4, a live load of 130 pounds per square foot is conservatively selected to envelope all postulated live loads acting on the HSM, including the effects of snow and ice.

8.1.1.2 Dry Shielded Canister Confinement Boundary Analysis

Stresses are evaluated in the NUHOMS® DSC shell and closure plates due to:

1. Dead Weight

2. Design Basis Normal Operating Internal Pressure Loads

3. Normal Operating Thermal Loads

4. Normal Operation Handling Loads

The methodology used to evaluate the effects of these normal loads is addressed in the following paragraphs. Table 8.1-11 summarizes the resulting stresses for normal operating loads.

A. DSC Dead Load Analysis

For the dead load analysis, the most limiting conditions are considered. Both the beam behavior and shell bending behavior of the DSC seated on the HSM support rails are evaluated. Conservatively considering the DSC to be supported at the ends, and distributing the DSC bounding weight of 70,000 pounds along its length, the maximum beam bending stresses in the DSC shell are derived. The analysis of the DSC cylindrical shell acting as a simply supported beam results in a maximum membrane stress intensity of 0.2 ksi which is insignificant compared to the allowable of 22.4 ksi.

For evaluation of local shell bending stresses, it is assumed that the total dead weight of the DSC, less the weight of the shield plugs, is uniformly supported by the continuous DSC support rails. The geometric boundary conditions assumed in this analysis are depicted in Figure 8.1-6.

The correlation from Bednar [8.3] is used in the evaluation of this condition as follows:

$$S_{bx} = 1.75 \sqrt{Rt} \frac{f_3}{t^2}$$ Reference 8.3, p. 193

Where:

S_{bx} = Local Shell Bending Stress Intensity = 4.8 Ksi

t = 0.55 in., minimum acceptable DSC Shell Thickness

R = 33.62 in., DSC Outside Radius

f_3 = 191 lb./in., weight of loaded DSC less shielded end plugs per unit length for each support rail

The DSC shell component vertical dead weight stresses are calculated from the DSC 75g bottom end drop analysis results discussed in Section 8.2.5. The stress results from the 75g bottom end drop linear elastic static analysis are factored by 1/75 to obtain the DSC shell component vertical dead weight stresses.

The horizontal dead weight stresses in the DSC, shield plugs, closure plates, and shell stresses at the top and bottom ends of the DSC, are calculated by ratioing the results from the 0° orientation DSC 75g horizontal side drop linear elastic static analysis results discussed in Section 8.2.5.2.A by 1/75.

The dead weight stresses in these components while inside the HSM are analyzed using the same analytical model. The boundary conditions are modified to support the DSC shell at the locations of the DSC support rails. A linear elastic analysis is performed for the 1g dead weight load.

The controlling calculated dead weight stresses from the analyses described above are tabulated in Table 8.1-11.

B. DSC Normal Operating Design Basis Pressure Analysis

For evaluation of DSC stresses due to design basis normal operating internal pressures, an analytical model is developed using the ANSYS computer program. The DSC shell, the closure plates, and the shield plugs are included in the analytical model, as shown in Figure 8.1-7. Even though the normal and off-normal operating pressure is 0 psig, a bounding internal pressure of 15 psig is applied to the model as a uniform internal pressure loading and the DSC stresses calculated. Two loading distribution cases are considered; one with the inner closure plates pressurized and one with the outer closure plates pressurized. The resulting maximum stress intensities are reported in Table 8.1-11 and Table 8.1-12.

C. DSC Normal Operating Thermal Stress Analysis

The thermal analysis of the DSC is presented in Section 8.1.3. The results of this analysis show that for the range of normal operating ambient temperature conditions, no significant DSC through wall thermal gradients exist. There is also sufficient space provided in the axial direction between the internal basket assembly and the inner surfaces of the DSC shell assembly for free thermal expansion. Similarly, sufficient radial gap is provided between the basket assembly and inside of the DSC shell to permit free thermal expansion. As a result, no thermal stresses are induced in the DSC shell or the basket assembly. This design feature also acts to minimize the effects of thermal cycling and fatigue on the DSC.

For normal operating conditions, a thermal stress analysis of the DSC shell is performed to establish the DSC shell stresses induced by variations in shell temperatures. The 87°F ambient case DSC shell temperature varies, as shown in Figure 8.1-5. The maximum DSC shell thermal gradient results from the 103°F ambient off-normal conditions are described in Section 8.1.3. The thermal stresses due to these temperature variations bound those due to the normal operating events and are conservatively used for the normal operating thermal analysis. The thermal bending and membrane stresses for the off-normal case shell gradients are evaluated using the three-dimensional ANSYS model of the DSC shell shown in Figure 8.1-7. The three-dimensional analytical model includes the full length DSC shell and cover plates with the temperature distribution imposed on the DSC. The analysis results for this case are included in the formulation of normal operating load combination results in Section 8.3.3.

D. DSC Operational Handling Load Analysis

The applied normal operating force from the hydraulic ram, specified in Section 8.1.1.1, is applied to the DSC assembly at the grapple ring location. The three-dimensional ANSYS finite element model shown in Figure 8.1-7 is used to calculate the stresses in the DSC shell assembly. A uniform pressure load is applied to the center of the DSC bottom cover plate over an area approximately equal the contact area of the ram grapple assembly to evaluate the DSC insertion loading condition. A uniform pressure load is applied to the inner surface of the DSC grapple ring plate to evaluate the DSC retrieval loading condition.

In addition to the uniformly distributed load assumption, the DSC bottom cover plate and grapple ring stresses for the DSC retrieval non-uniform load distribution of the ram grapple are analyzed using the 1/4 symmetry ANSYS model shown in Figure 8.1-8. The load is applied to the grapple ring plate nodes corresponding to the contact area between the ram grapple arms and the grapple ring plate. The edges of the DSC bottom cover plate are conservatively modeled as pinned. The analysis results show that the load transferred to the DSC shell is uniformly distributed by the bottom cover plate. Therefore, the results obtained using the three-dimensional model with a uniform pressure load applied to the grapple ring are valid for all the DSC shell components except the bottom cover plate and the grapple ring plate for the DSC retrieval condition.

The maximum stress intensities from these analyses are tabulated in Table 8.1-11.

E. Evaluation of the Results

The maximum calculated DSC shell stress intensities for the normal operating load conditions are shown in Table 8.1-11. The calculated stress intensities for each load case are combined in accordance with the load combinations described in Table 3.2-5. The resulting stress intensities for the controlling load combinations are reported in Section 8.3 and compared to the ASME Code allowable stress intensities.

8.1.1.3 DSC Internal Basket Analysis

The DSC internal basket assembly is a non-structural component, which is classified as not important to safety. As discussed in Section 3.3, it is not required to maintain subcriticality of the stored TMI-2 canisters. As such, the basket structure is not required to meet any structural limits. For information purposes only, the results of an analysis for an 8g dead load case, simulating worst case transfer loads, is provided to demonstrate the level of stresses in the basket and show it has no adverse effect on the DSC shell. The applied loading is shown in Figure 8.1-10. Differential thermal expansion effects are negligibly small due to the very small temperature gradients and the geometry of the basket assembly.

A. DSC Internal Basket Dead Weight Analysis

The basket dead weight stresses are calculated for the horizontal storage orientation inside the HSM.

The basket dead load stress intensities are calculated using the ANSYS spacer disc analytical model shown in Figure 8.1-9. The model boundary conditions are modified to reflect the support conditions provided by the transfer cask and DSC support rails. Linear elastic static analyses are performed. The applied loading is shown in Figure 8.1-10.

B. DSC Internal Basket Thermal Stress Analysis

The effects of axial and radial thermal expansion are evaluated for the DSC internal basket components to ensure that adequate space exists in the cavity of the DSC for free thermal expansion. To verify that adequate provision for free axial expansion of the TMI-2 canisters and other internal components of the basket are included, the differential expansion of each DSC component is calculated. The TMI-2 canisters are assumed to be at their maximum calculated accident temperature (Table 8.1-10) of 219°F (104°C) and the DSC shell is conservatively assumed to be at its long term average normal operating temperature (45°F ambient air) of 95°F (Table 8.1-9). Calculated results for varying ambient temperatures show similar results as the ΔT between the TMI-2 canisters and DSC does not change appreciably. The length of the TMI-2 canister when hot is:

$$L_{HC} = (1 + \alpha_s \Delta T) L_T$$

Where for the design basis TMI-2 canister:

L_{HC} = Hot length of TMI-2 canister, in.

α_s = Stainless steel coefficient of thermal expansion is 9.08 $x10^{-6}$in./in.°F at 200°F

ΔT = 219° - 70° (stress-free temperature) = 149°F

L_T = Length of TMI-2 canister at room temperature (70°F)

= 150 in.

Therefore:

L_{HC} = 150.20 in.

The length of the DSC cavity at room temperature is 151.00 inches. The minimum length of the DSC cavity (L_C) at 95°F is:

$$L_{CH} = L_C \alpha_C \Delta T + L_C$$

Where:

L_C = 151.00 in., DSC cavity at 70°F

ΔT = 95° - 70° = 25°F

α_C = 5.42×10^{-6} in./in.°F at 70°F (SA 516, Gr. 70 Plate)

Therefore:

L_{CH} = 151.02 in.

The minimum axial clearance between the end of the TMI-2 canisters and the inner surface of the shield plug assembly for the long term base case ambient conditions (45°F) and the associated normal operating spent fuel temperature is 0.83 inch. Similarly, assuming that each spacer disc is uniformly heated to the maximum core debris temperature of 219°F and the DSC shell remains at 95°F, the radial gap will be reduced from 0.19 inches to 0.17 inches. Thus, adequate clearance has been provided between the TMI-2 canisters, the DSC shell, and internal basket assembly to permit free thermal expansion of all components for the maximum differential temperatures expected.

8.1.1.4 DSC Support Structure Analysis

The general description of the DSC support structure inside the HSM is provided in previous sections. The DSC support structure is shown in Figures 4.2-1 and 4.2-2. The DSC support rails are supported by the HSM front and rear walls. The DSC support structure design uses welded connections, and allows thermal growth relative to the HSM. Normal operating condition loads on the DSC support structure consist of the DSC dead weight, the support structure dead weight, and the DSC operational handling loads. The normal operating frictional loads are reacted by the support rails, which are bolted to embedments located in the HSM front wall. Because of the dimensions of the HSM internal cavity, the DSC support rails only carry the DSC dead load during insertion and withdrawal operations. During storage conditions, the DSC closure plates transfer the loads to the front and back HSM walls while the DSC shell acts as a rigid beam.

A linear elastic model of the assembly is utilized to evaluate axial, shear, and bending stresses in the DSC support structure members. The geometry for the analytical model is shown in Figure 8.1-14.

A. DSC Support Structure Dead Weight Analysis

For the dead weight analysis, the weight of the DSC and contents is conservatively applied to the support rails as a uniformly distributed load. The dead weight of the DSC support structure is also included in this analysis.

B. DSC Support Structure Operational Handling Analysis

For the NUHOMS®-12T system operational handling loads, a sliding force of 70,000 pounds is applied axially to the DSC support rails (35,000 lb/rail) to account for the sliding friction between the DSC shell and the support rails. This force is combined with the worst case of the normal condition loading of a 40,000 lb. (20,000 lbs/rail) point load or a uniformly distributed load representing the weight of the DSC and contents.

C. DSC Support Structure Thermal Analysis

The DSC support structure is a simple frame structure that permits free thermal expansion relative to the HSM. The connection details permit free thermal expansion of the DSC support structure relative to the HSM, eliminating any significant thermal stresses.

D. Evaluation of DSC Support Structure Results

The maximum calculated DSC support structure deflections for normal and off-normal operating loads are shown in Table 8.1-14. Specific information on the DSC support structure seismic loads can be found in Section 8.2.3. Additional details of the DSC support structure analysis are presented in Section 8.3.

8.1.1.5 HSM Loads Analysis

To qualify the design for the TMI-2 ISFSI, a single free-standing HSM is evaluated. The HSM structural analyses include evaluation of normal operating, off-normal, and postulated accident loads for the HSM. The frame and shear wall action of the HSM floor, walls, and roof slab are the primary structural system for transverse loads. The structural analysis of an individual module provides a conservative methodology for evaluating the response of the HSM structural elements under various static and dynamic loads for any HSM array configured in accordance with Section 4.1.1.

The HSM side walls and roof slab thicknesses are established on the basis of radiological shielding requirements. As such, all other thickness requirements such as the minimum barrier thickness requirements for tornado generated missiles specified by NUREG-0800, Section 3.5.3 [8.4] are bounded. The ultimate strength method is used to evaluate stresses in the HSM reinforced concrete walls, roof, and floor. The HSM reinforcement is designed to meet the minimum flexural and shear reinforcement requirements of ACI 349 [8.5]. The available design strength exceeds that required for the factored design loads specified in Section 3.2. The reinforcement layout for the prefabricated HSMs is shown on Figure 8.1-16 and the Appendix A licensing drawings. HSM construction details such as construction joints and reinforcing bar splices will be detailed on the construction drawings.

For all normal, off-normal, and environmental load cases except the thermal load cases, the reinforced concrete free-standing HSM module is evaluated using the analytical model shown in Figure 8.1-13. The DSC support structure model shown in Figure 8.1-14 is included in the model. The concrete structure is modeled using four layers of three-dimensional brick elements. The reinforced concrete

pocket on the south wall is modeled using three layers of brick elements. The composite steel and concrete door on the north wall is modeled using brick elements with equivalent properties. The DSC and the support structure are modeled using beam elements and lumped mass elements. The three dimensional ANSYS finite element model has 2991 nodes and 1517 brick elements. The load inputs for this analysis are described in Sections 8.2.2 through 8.2.4. The various normal operating mechanical loads are applied to the analytical model and the HSM internal forces and moments calculated by performing a linear elastic finite element anlaysis.

For the thermal load analysis the three-dimensional model shown in Figure 8.1-15 is used. This analytical model does not include the DSC support structure or the HSM door. The model utilizes non-linear three dimensional brick elements with concrete cracking capability. This allows modeling the self relieving nature of thermal stress due to cracking. The analysis shows that a single HSM provides the governing case for load combinations containing tornado wind and missile loads and seismic load conditions. The postulated response investigated for each of these cases is the potential for sliding or overturning of a single free-standing HSM which envelopes that of an HSM array. The analysis also shows that thermal loads control the reinforcement requirements for the HSM walls, roof and floor. The load inputs for this analysis are described in Section 8.1.1.5, Paragraph C, Section 8.1.2.2, Paragraph A, and Section 8.2.10.2.

A description of the individual loads and load analyses are provided in the following sections.

A. HSM Dead Load and Live Load Analyses

The dead weight of the HSM plus the loaded DSC and the DSC support structure weights are applied to the analytical model shown in Figure 8.1-13. The loads applied to the analytical model include the dead weight of the loaded DSC and DSC support structure. The resulting calculated maximum dead load shears and moments are tabulated in Table 8.1-15. A live load of 130 psf is applied to the HSM roof to conservatively envelope all postulated live loads, including snow and ice. The resulting calculated maximum live load shears and moments are tabulated in Table 8.1-15.

B. Concrete Creep and Shrinkage Analyses

ACI 349 Section 9.2.2 states that "where the effects of... creep or shrinkage may be significant, they shall be included with the dead load...". Since creep is mainly dependent on elastic strain due to dead loads, the loading contribution from creep is minimal as the dead loads are small in relation to the capacity of the HSM frame and shear walls formed by the walls, roof and floor. The creep strain is conservatively calculated using the ultimate creep strain value suggested by Wang and Salmon [8.6].

$$\varepsilon'_c = C_u \varepsilon_c$$

Where:

ε'_c = Creep strain in./in.

C_u = Ultimate creep strain or ratio of creep to initial strain from dead weight
= 2.35

ε_c = Initial strain from dead weight
= 3E-5 in./in. (approximate value)

Therefore:

ε'_c = 4.65E-5 in./in.

Shrinkage of the HSM concrete is conservatively calculated using an ultimate shrinkage strain value suggested by Wang and Salmon [8.6]. Additionally, since shrinkage is significantly affected by the surface area to volume ratio, the ultimate shrinkage strain value is reduced according to the method recommended by Fintel [8.7]. The combined shrinkage strain is:

$$\varepsilon_S = \varepsilon_{sh\mu}\alpha$$

Where:

εs = Shrinkage strain (in./in.)

ε_{sh_μ} = Ultimate shrinkage strain = 8E-4 in./in.

α = Volume to surface area reduction = 0.5 (conservative)

Therefore:

εs = 4E-4 in./in.

For determination of moments and shears in the HSM due to creep and shrinkage, the total strain is converted to an axial change in length across the roof of a prefabricated HSM.

$$\Delta L = L(\varepsilon_S + \varepsilon'_c)$$

Where:

ΔL = Axial length change (in.)

L = Length from center to center of HSM walls
= 99 in.

ε_s = 4E-4 in./in.

ε'_c = 4.65E-5 in./in.

The resulting change in length of the HSM roof slab, $\Delta L = 0.044$ inch.

Shortening due to creep and shrinkage occurs gradually over a period of time, and the effects are lessened by plastic creep flow and microcracking of the members. Ambient humidity also acts to reduce the effects of creep and shrinkage. The PCI Design Handbook [8.8] suggests that the calculated creep and shrinkage shortening values be reduced by a factor of three to five for design. Also, creep and shrinkage forces act opposite to those of thermal expansion forces for the HSM. Hence, it is conservative to neglect creep and shrinkage effects. Therefore, creep and shrinkage are not considered further for the HSM design.

C. HSM Thermal Loads Analysis

To evaluate the effects of thermal loads on the HSM, heat transfer analyses for a range of normal ambient temperatures are performed and the limiting thermal gradients and temperature values at various locations in the HSM determined. A more detailed description of the heat transfer analyses is provided in Section 8.1.3. Structural analyses of the HSM for the maximum calculated floor, wall and roof temperature loads listed in Table 8.1-8 and Table 8.1-9 are performed for the HSM using the analytical models shown in Figure 8.1-15. The results of these analyses are summarized in Table 8.1-15. The basis for the HSM thermal analysis is discussed further in the following paragraphs.

ACI 349, Appendix A, provides a general methodology for designing reinforced concrete structures subjected to thermal loads. The commentary to this Appendix, Section A.3.3, defines a range of approaches utilized in the analysis of thermal loads. One approach accounts for the self-relieving nature of the thermal loads (relief is obtained by the occurrence of thermal cracking when the concrete modulus of rupture is reached). For the thermal analysis of the HSM for normal operating conditions, the thermal loads are calculated for the cracked cross section properties of the HSM walls, roof and floor.

To account for the seasonal effects of ambient temperature fluctuations on the outside surface of the HSM, ambient temperatures of -20°F (winter) to 87°F (summer) are considered in the heat transfer analysis for normal operating conditions. Analyses are performed for ambient temperatures of 45°F and 87°F to determine the limiting design conditions for the HSM. For the HSM roof slab, the results of the HSM heat transfer analysis for normal operating conditions for a life time average ambient temperature of 45°F and with solar heat flux effects included are shown in Figure 8.1-3. The maximum temperature and gradients for the roof slab and side walls are shown in Table 8.1-8. The

results demonstrate that the concrete temperatures are within the ACI 349, Section A.4.1 acceptance temperature for local areas of 200°F.

For conservatism and consistency with the philosophy of ACI 349, Section A.4.3, the strength properties of the concrete and reinforcing steel used in the HSM structural analysis are taken at the postulated temperature range for each load case. For all normal operating load cases the concrete and reinforcing properties are assumed to be equal to the specified values (f'_c = 5000 psi for concrete and f_y = 60,000 psi for rebar).

Table 8.1-8 shows that the maximum HSM temperature for the lifetime average ambient temperature of 45°F does not exceed the ACI limit of 200°F for local area temperatures.

The design criteria utilized are adequate to ensure that the NUHOMS®-12T HSM will perform its intended safety function for all design conditions.

D. Radiation Effects on HSM Concrete

As described in Reference 8.9, the accumulated neutron flux over the 50 year service life of the HSM for five year cooled intact fuel (which envelopes the TMI-2 fuel) is estimated to be 1.7E14 neutrons/cm^2. From the study by Hilsdorf, Kropp, and Koch [8.10], the compressive strength and modulus of elasticity of concrete is not affected by a neutron flux of this magnitude.

As described in Reference 8.9, the gamma energy flux deposited in the HSM concrete for five year cooled intact fuel (which envelopes the TMI-2 fuel) is 1.7 E9 MeV/cm^2-sec. or 3.0 E-4 watt/cm^2. According to ANSI/ANS-6.4-1977 [8.11], the temperature rise in concrete due to this level of radiation is negligible. Thus, radiation effects on concrete strength are not evaluated further for the HSM design.

E. HSM Design Analysis

The mechanical design loads (dead load, live load, wind, etc.) were applied to the analytical model shown in Figure 8.1-13, and the thermal loads were applied to the analytical model shown in Figure 8.2-15. In both cases, the design forces and moments are calculated. The results of these analyses are summarized in Table 8.1-15 for the normal operating and off-normal loads.

The ultimate axial force, moment and shear capacities of a typical 12 inch wide section of the HSM walls, roof, or floor are computed using the following relationships:

Ultimate Tension Capacity: $P_{tu} = \phi P_t = \phi A_{st} f_y$

Ultimate Compression Capacity: $P_{cu} = \phi P_n = 0.8\phi[0.85 f_c (A_g - A_{sc}) + f_y A_{sc}]$

Ultimate Moment Capacity: $M_u = \phi M_n = \phi\ A_s\ f_y\ (d-a/2)$

where $a = (A_s\ f_y)/(0.85 f_c\ b)$

Ultimate In-Plane Shear Capacity: $V_{ui} = \phi V_i = \phi\ A_{sc}(2\sqrt{f_c} + \rho_n f_y)$

Ultimate Out-Plane Shear Capacity: $V_{uo} = \phi V_c = \phi\ 2\ \sqrt{f_c}\ (bd)$

The thicker front and rear wall sections qualify as deep flexure members and the allowable out-of plane shear capacity may be calculated in accordance with Section 11.8.6 of ACI using the formula:

$V_{uo} = \phi^* V_c = \phi(3.5-2.5\ M_u/V_u\ d)\ (1.9\sqrt{f_c} + 2500\ \rho_w V_u d / M_u\ )\ b\ d$

but not to exceed $6\ \sqrt{}\ f_c\ b\ d$ and $(3.5-2.5\ M_u/V_u\ d)$ not to exceed 2.5

V_u and M_u are shear force and moments at factored loads

Where:

ϕ = Strength reduction factor (Table 3.2-3)

f_y = 60,000 psi, Rebar design strength at 150°F

f_c = 5,000 psi, Design compressive strength of concrete at 150°F

A_s = Area of tensile reinforcing steel (see Appendix A drawings)

b = 12" width section

d = depth of the section minus rebar cover (see Appendix A drawings)

A_{st} = Area of axial tension reinforcement = 2^*A_s

A_{sc} = Area of axial compression reinforcement = 2^*A_s

A_g = Gross area of concrete = (b*T)

$\rho_n = (2^*A_s)/(b^*T)$

T = Depth of the section including the rebar cover

$\rho_w = A_s/(bd)$

The computed ultimate capacities are tabulated below:

Component	P_{tu} kips/ft	P_{cu} kips/ft	M_u kip-in/ft	V_{ui} kips/ft	V_{uo} kips/ft
Roof	128	817	1427	159	33
Floor	102	745	1046	131	31
Side Walls	102	541	1046	131	31
Front Wall	128	931	1683	164	101
Back Wall	161	1121	2576	203	145

8.1.1.6 HSM Door Analyses

The access opening for transferring the DSC into and out of the HSM is protected by a steel door with a core of concrete shielding material. The door is recessed into the HSM front wall as shown in Figure 4.2-3.

For normal system operation, the door assembly is only subjected to its own dead weight which is transmitted by bearing directly into the HSM front wall, and handling loads resulting from installation and removal of the door during DSC transfer operations.

The concrete bearing strength required to support a bearing load on the front wall concrete for a weight of 5900 pounds is a small fraction of the ACI 349 (Section 10.15) permissible concrete bearing strength of $\phi[0.85\ f_c'A_1] = 0.7\ [0.85 \times 5 \times 6 \times 80.63] = 1440$ kips. The embedded anchors for the HSM door are designed in accordance with ACI 349, Appendix B. The governing design load combination for the HSM door embedded anchors is the dead load plus seismic load combination. The dead load consists of the weight of the door. The seismic load consists of the longitudinal seismic accelerations acting on the door itself (the DSC seismic loads are transferred to the DSC support structure rails.) The seismic loads produce very small shear and tension loads in the anchors.

8.1.1.7 DSC Seismic Retainer

The details of the DSC seismic retainer are shown on the drawings in Appendix A. Additional details are provided in Section 8.2.3.2.

8.1.1.8 MP187 Cask Analysis

Any NRC-approved transfer cask may be utilized to transfer a loaded DSC to the TMI-2 ISFSI provided it meets the requirements for size, weight, and radiological protection required for the NUHOMS®-12T DSCs.

The MP187 cask when used in the 10 CFR Part 72 on-site transfer mode, has been fully evaluated for normal operating condition loads which meet or exceed the loads expected at INL, and the results reported in the SMUD SAR [8.12]. These evaluations have demonstrated that the MP187 cask has adequate margins to safely perform all required operations for the transfer of a loaded DSC. As the MP187 is fabricated from austenitic stainless steel, exposure to the -20°F minimum normal operating temperature will not have any effect on the cask's ability to protect the NUHOMS®-12T DSCs.

8.1.2 Off-Normal Load Structural Analysis

Table 8.1-12 shows the off-normal operating loads for which the NUHOMS®-12T safety-related components are designed. This section describes the design basis off-normal events for the

NUHOMS®-12T system and presents analyses that demonstrate the adequacy of the design safety features of a NUHOMS®-12T system.

8.1.2.1 Jammed DSC During Transfer

The interfacing dimensions of the top end of the MP187 cask and the HSM access opening sleeve are specified so that docking of the cask with the HSM is not possible should gross misalignments between the cask and HSM exist. Furthermore, beveled lead-ins are provided on the ends of the cask, DSC, and DSC support rails to minimize the possibility of a jammed DSC during transfer. Nevertheless, it is postulated that if the cask is not accurately aligned with respect to the HSM, the DSC binds or becomes jammed during transfer operations. Based on the dimensions of the DSC, cask, and HSM, the maximum misalignment of the sliding surfaces is limited by operating procedures to 1/8 inch or less. Assuming a worst case misalignment in positioning and docking the cask with the HSM access opening, the maximum possible misalignment which would permit transfer of the DSC to occur is 1/4 inch. Although unlikely, any greater misalignment may cause axial sticking and/or a rotation of the DSC to occur which may result in a binding condition.

A. Detection of the Event

When a jam of the DSC occurs during transfer the hydraulic pressure in the ram begins to increase. The maximum normal operating ram push/pull forces are limited automatically by features in the ram system design to a maximum load equal to 70,000 lbs..

B. Axial Sticking of the DSC

The off-normal handling load event postulated to occur assumes that the leading edge of the DSC becomes jammed against some immovable feature because of gross misalignment of the cask. As the DSC motion is prevented, the hydraulic pressure increases, thereby increasing the force on the DSC until the system pressure limit is reached. To overcome potentially higher resistance loads due to binding of the DSC in either the cask or the HSM, the 70,000 lb. maximum ram force exceeds the weight of the loaded DSC. This force corresponds to a coefficient of friction of one and is the design basis for the hydraulic ram system. This postulated loading condition is illustrated in Figure 8.1-11. The resulting ram load acting on the DSC grapple ring assembly and bottom cover plate are analyzed in the paragraphs which follow.

The DSC bottom cover plate and the grapple ring assembly are subjected to a maximum force of 70,000 pounds. The method of analysis is as described in Sections 8.1.1.1 and 8.1.1.2. The maximum bending stress intensity calculated for the DSC bottom cover plate, as listed in Table 8.1-11 is well within the ASME Code allowable limit.

It is conservatively assumed that the force created by the jammed DSC condition produces a force-couple of magnitude F x R, where: F is the imposed force of 70,000 pounds and R is 33.63 inches, the outside radius of the DSC shell. Thus, the DSC shell stress is:

$$S_{mx} = \frac{M}{S} 2$$

Where:

M = 2354 in.-kip, Bending moment

S = 2165 $in.^3$, DSC section modulus

Therefore:

S_{mx} = 1.09 ksi

This magnitude of stress is negligible when compared to the allowable membrane stress intensity.

For a jammed DSC, the 70,000 pound ram load is postulated to be reacted by the DSC support rails inside the HSM at the most critical location. At the same time, a concentrated force of one half of the DSC weight is assumed to act vertically at mid-span of the DSC support rail member. The results of this analysis are reported in Table 8.1-13.

C. Binding of the DSC

If axial alignment within system operating specifications is not achieved, it may be possible to pinch the DSC shell as shown in Figure 8.1-12. The pinching force acting on the DSC shell and the cask inner liner is directly proportional to the angle of rotation. The maximum possible inclination angle established by various conservative geometric and operational assumptions is less than one degree. If this angle is conservatively assumed to be one degree, then the pinching force is taken as the product of the maximum ram loading of 70,000 pounds and the sine of the angle, or 1,225 pounds. This force is distributed around the circumference of the DSC shell and either the cask inner shell or HSM sleeve as a cosine distribution.

The 1,225 pound load is conservatively assumed to be applied as a point load at a location away from the ends of the cask or DSC. The resulting maximum stresses are given by Table 30, Case 8a of Roark [8.13] as:

Membrane stress:

$$\sigma = \frac{0.4P}{t^2}$$

Bending stress:

$$\sigma' = \frac{2.4P}{t^2}$$

Therefore, the maximum stress is:

$$\sigma + \sigma' = \frac{2.8P}{t^2}$$

For the DSC shell, t_{min} = 0.55 inch. Substituting for t and P equal to 1,225 pounds, the maximum extreme fiber stresses in the DSC shell is 11.3 ksi. This is well within the ASME Code Service Level C allowable of 34.6 ksi for an off-normal jammed DSC event or the normal or Service Level A allowable of 23.1 ksi.

The tangential component of ram loading under the assumed condition is less than the force of the jammed condition calculated previously in Paragraph B and is not considered further. The stresses on the DSC are given in Table 8.1-12, and for the DSC support assembly inside the HSM for the jammed condition are reported in Table 8.1-13.

D. Consequences of Jammed DSC

In both scenarios for a jammed DSC, the DSC shell stress is much less than the material yield strength and ASME Code allowables. Therefore, no permanent deformation of the DSC shell or cask inner liner will occur and there is no potential for breach of the DSC confinement boundary or potential for release of radioactive material.

E. Corrective Action

In both cases, the required corrective action is to reverse the direction of the ram force being applied to the DSC, and return the DSC to its previous position. Since no permanent deformation of the DSC or MP187 cask inner shell occurs, return of the DSC to its previous position is unimpeded. The cask alignment is then rechecked, and the cask repositioned as necessary before attempts at transfer are renewed.

8.1.2.2 Off-Normal Thermal Load Analysis

Off-normal ambient temperatures of -50°F (extreme winter) and 103°F (extreme summer) are extremes for the INL site. Handling or transporting a DSC containing TMI-2 Canisters will not be performed when DSC temperature is less than 20°F or when the ambient air temperature is less than 0°F. The MP187 is designed for operation at -20°F. The system components affected by the postulated extreme ambient temperatures are the cask and DSC during transfer operations at the ISFSI site, and the HSM during storage of a DSC.

The thermal stresses in the various NUHOMS®-12T system components due to the off-normal temperatures are calculated in the same manner as described for the normal operating thermal loads. A description of these methods is provided in Sections 8.1.1.2 for the DSC shell and 8.1.1.3 for the DSC internals.

A. HSM Off-Normal Thermal Load Analysis

As described in Section 8.1.3.1, the HSM steady state temperatures are calculated for the off-normal extreme ambient temperature of 103°F. The resulting maximum HSM concrete temperatures and gradients for the roof and side walls are shown in Table 8.1-8. The short duration peak concrete temperatures easily meet the ACI 349 limit of 350°F. Since the ultimate shear and moment capacities for each module concrete section are assumed to be the same for off-normal and accident conditions, the maximum calculated shear forces and bending moments resulting from either case are conservatively used for design. The DSC support assembly is free to expand/contract with changing temperatures and, therefore, the changes in temperature have minimal effect on the DSC support structure.

B. DSC Off-Normal Thermal Stress Analysis

The off-normal thermal gradients and maximum temperatures for -50°F and 103°F ambient air are developed for the DSC resting in the cavity of the MP187 cask as described in Section 8.1.3.3. The maximum off-normal calculated surface temperature for the DSC shell is given in Table 8.1-9.

The off-normal thermal gradients and maximum temperatures are also developed for the DSC resting in the HSM, as described in Section 8.1.3.2. The maximum off-normal surface temperature calculated for the DSC shell is given in Table 8.1-9.

8.1.3 Thermal Hydraulic Analysis

This section of the SAR describes the thermal analysis of the NUHOMS®-12T HSM and DSC. The analytical models of the HSM and the DSC are described and the calculation results summarized. The thermophysical properties of the NUHOMS®-12T system components used in the thermal analysis are listed in Table 8.1-6 and Table 8.1-7. The following evaluations are performed for the NUHOMS®-12T system:

1. Thermal Analysis of the HSM
2. Thermal Analysis of the DSC in the HSM
3. Thermal Analysis of the DSC in the Transfer Cask

The NUHOMS®-12T components are evaluated for a range of design basis ambient temperatures as follows:

A. Normal Operating Conditions: The system components are evaluated for ambient temperatures in the range of -20°F to 87°F. The normal operating seasonal daily ambient temperatures fluctuate from a low of -20°F (winter) to a high of 87°F (summer) [8.14]. The thermal analyses are carried out for a sufficient duration to establish steady state conditions in the NUHOMS®-12T components. For the evaluation of thermal cycling and material properties, fluctuations in the ambient temperature from winter to summer conditions are assumed to occur once per year for the HSM. The lifetime average ambient temperature for the 50 year service life is taken as 45°F. The "stress-free" temperature for material properties is assumed to be 70°F.

B. Off Normal and Accident Conditions: The system components are evaluated for the extreme ambient temperatures of -50°F (winter day) and 103°F (summer day) [8.14]. Should these extreme conditions ever occur, they would be expected to last for a short duration of time (a few hours per day for 2 to 3 days in a row). Nevertheless, the thermal analyses are performed for a sufficient duration to cause a steady-state temperature distribution in the NUHOMS®-12T system components.

8.1.3.1 Thermal Hydraulics of the HSM

A. Principles of HSM Cooling System

The HSM is cooled by radiation, natural convection, and heat conduction through the HSM ceiling and walls. The HSM roof and side walls are the primary concrete surfaces conducting heat to the outside environment. For analytical purposes, an HSM centered in a group of HSMs, each loaded with a DSC, is assumed. For the thermal analyses of an HSM at the end of a multiple module array, an end shield wall is added to the side wall and the outer surface is exposed to the prevailing ambient conditions. The ISFSI basemat is in contact with soil, which is assumed to be at a constant temperature of 65°F (summer) and 45°F (winter) at a combined depth of 10.5 feet [8.14]. Air infiltration from the HSM access opening door and HEPA filter door is conservatively neglected.

In the HSM HEATING 7 model, Boundary Type 1 (surface-to-boundary) is used to describe the natural circulation heat transfer between the HSM outer surfaces and the adjacent ambient air. The DSC temperatures from the HSM models are used as constant temperature boundary conditions to determine the temperature distributions for the DSC internals and the TMI-2 canister regions. These calculations are described in the following paragraphs.

B. Computer Program

The HEATING 7 computer program is used for the heat transfer analysis of the HSM and DSC. The HEATING 7 program is known as "The HEATING Program," where HEATING is an acronym for "Heat Engineering and Transfer In Nine Geometries." HEATING 7 is designed to be a functional module within the SCALE system of computer programs [8.15] for performing standardized computer analysis for licensing evaluations of nuclear spent fuel systems. Thus, its features are designed to perform thermal analyses on problems arising in licensing evaluations of shipping and storage of spent fuel containers, and its input format is designed to be compatible with that of other functional modules

within the SCALE system. HEATING 7 is used in the previous NUHOMS® design for thermal analysis of the DSC, HSM, and casks that were reviewed and approved by the USNRC for 10 CFR Part 71 and 10 CFR Part 72 requirements. HEATING 7 may also be used as a stand-alone heat transfer code. The SCALE system was developed by Oak Ridge National Laboratory for the U. S. NRC Transportation Branch.

C. Thermal Model of the HSM

The HEATING 7 thermal model of the HSM is depicted in Figure 8.1-1. The three-dimensional model represents the symmetric right half of an HSM and DSC. As shown in Table 3.1-1, the design basis heat load of 860 W/DSC is used for the NUHOMS®-12T HSM design. This heat load is applied as a volumetric heat density of 9.60E-5 Btu/min-in^3 over the fueled portion of the TMI-2 canister. The heat rejection through the TMI-2 canister ends and the DSC shield plugs and cover plates are included.

The HEATING 7 analytical model of the HSM consists of a typical HSM cross-section. In addition, symmetry or an insulated boundary is assumed along the vertical centerline of the HSM shown in Figure 8.1-1. The HEATING 7 model includes regions for the concrete front, rear, and side walls, roof slab, floor, and basemat of the HSM. The soil below the ISFSI basemat is modeled as a seven foot thick region with a constant temperature boundary at the edge of this region. Sufficient nodal refinement is used in the HSM analytical model to obtain accurate temperature distributions through the thickness of the HSM walls, roof, and floor slab.

The thermal analysis of a typical HSM is performed for a loaded DSC located in the interior of a multiple module array with a DSC present in the two adjacent HSMs. The HSM roof and side walls are modeled, the outer surfaces of which are assumed to be exposed to the prevailing ambient conditions. For summer ambient conditions, a solar heat flux of 67 Btu/hr.-ft.^{2} for normal conditions, and 105 Btu/hr.-ft.^{2} for off-normal and accident conditions, is conservatively applied to the roof surface [8.14]. Solar heat loads are conservatively neglected for the HSM thermal analysis for winter ambient conditions for normal, off-normal and accident conditions.

The DSC cylindrical shell is approximated in the model by equivalent rectangular regions with the thickness and properties of the carbon steel DSC shell. The approximation using rectangular regions is necessary since HEATING 7 restricts the user to one geometry type in the same analytical model. The analytical model also includes regions to model the air gaps between the DSC and the HSM where heat transfer is mainly due to radiation.

The outer surface of the DSC shell dissipates heat to the HSM through radiation. The air surrounding the DSC is modeled as a gap filled with gas (air) with radiation heat transfer only, thus providing a mechanism for heat transfer from all HSM interior surfaces and the DSC outer surface. Any closed cavity convection occurring in the HSM cavity air surrounding the DSC shell is conservatively neglected.

With these temperatures and the equations for the heat transfer coefficients described below, the HEATING 7 program calculates the temperatures of the DSC exterior surface and the HSM interior and exterior surfaces.

The fuel debris decay heat is removed from the DSC outer surface through radiation. Horizontal surfaces with convection on their upper surfaces, such as the HSM roof outer surface, are assumed to be cooled by natural convection with a heat transfer coefficient of h_{plate}.

The HSM concrete walls are assumed to be cooled by air with a heat transfer coefficient of h_{wall}. Radiation heat transfer is modeled between the DSC outer surface and the HSM concrete walls and ceiling, and between the DSC outer surface and the HSM floor. The external surface of the HSM roof is assumed to be cooled by external air with a heat transfer coefficient of h_{plate}, and by radiation heat transfer to ambient air. The formulas used for the calculation of the heat transfer coefficients for natural convection are as follows [all in Btu/(hr. ft.^{2} °F)] [8.16]:

$$H_{plate} = 0.22\ (\Delta T)^{1/3}$$

$$H_{wall} = 0.19\ (\Delta T)^{1/3}$$

The heat transfer coefficients are updated by HEATING 7 following each iteration using the resulting average temperature of the corresponding surface node. A sufficient number of iterations are performed until the temperatures differ by less than 0.001% from the previous temperature calculated in two consecutive iterations indicating that stable convergence is achieved. The effective thermal conductivity of LICON (low density concrete) material, which is a part of the TMI-2 fuel debris canister is calculated for the material composition of 11 weight percent (w/o) glass bubbles, 60 w/o cement and 29 w/o water. Note that small differences in the weight percentage of the LICON constituents has negligible impact on the thermal analysis results of the core debris and canisters. The effective thermal conductivity of LICON is calculated to be 0.726 Btu/hr.-ft.°F. The remaining thermal-hydraulic parameters used in the HSM heat transfer calculations are given in Table 8.1-6 and Table 8.1-7.

The results of the HEATING 7 analysis for the HSM are in the form of temperature distribution profiles. Figure 8.1-2 shows an example of the HEATING 7 results for the HSM. The resulting temperature profile shows the steady state temperature distribution on the outer surface of the DSC, and at various locations throughout the HSM.

The calculated HSM wall and roof temperature gradients are used in the reinforced concrete structural analysis for long term thermal loads which occur during normal operating conditions, and the short term thermal loads occurring during off-normal and postulated accident conditions. The HSM thermal analysis results are also used to obtain steady state temperature distributions for the outer surface of the DSC for the range of design basis ambient conditions. These steady state surface temperatures are used as a constant temperature boundary condition for the DSC model, described in Section 8.1.3.2.

D. Description of the Cases Evaluated for the HSM

The HSM thermal analyses are performed for the design basis ambient air temperatures. These include a total of three cases with ambient air at the following temperatures:

1. 45°F (lifetime average), 87°F (summer daily high), and -20°F (winter daily low) for normal operating conditions which can be expected to occur for long periods of time,

2. 103°F (extreme summer maximum) and -50°F (extreme winter minimum) for off-normal conditions which can be expected to occur for short periods of time (a few hours per day for 2 to 3 days at a time), and

3. 103°F daily high and -50°F daily low extreme ambient temperatures with the gap between the modules blocked, and DSC HEPA filter vents blocked for sufficient duration to reach steady state conditions. This design basis condition is designated as an accident condition assumed to occur once in the service life of an HSM.

The results of these calculations are summarized in Table 8.1-8.

8.1.3.2 Thermal Analyses of the DSC Inside the HSM

For the DSC thermal analyses, the internal basket assembly of the DSC is modeled in detail. A worst case, two-dimensional slice of the DSC and TMI-2 canister cross section is modeled. Heat transfer effects along the axis of the DSC (third dimension) are conservatively neglected. The DSC is assumed to be cooled through radiation with the DSC shell surface specified as a constant temperature boundary condition equal to that calculated in the HSM thermal analysis. The fuel region inside the DSC is modeled as a heat source equal to 1.9 times the conservative decay heat power of 41.9 W/TMI-2 canister. The peaking factor of 1.9 is based on Reference 8.17. For calculating the maximum debris temperature, all 12 TMI-2 canisters inside the DSC are conservatively assumed to contain this decay heat power.

The steady state outer surface temperatures for the DSC resting inside the HSM are calculated in the HSM thermal analysis, described in Section 8.1.3.1. The results for each HSM analysis case are used to obtain maximum DSC surface temperatures for each region in the analytical model representing the DSC cylindrical shell. These surface temperatures are used as boundary conditions for the DSC thermal analysis and are assumed to remain constant.

8.1.3.2.1 NUHOMS®-12T DSC Inside HSM

A. Thermal Model of the NUHOMS®-12T DSC

The HEATING 7 computer program is used to perform the thermal analysis of the DSC internal basket assembly and TMI-2 canister regions. The analytical model of the DSC is shown in Figure 8.1-4 with the individual region numbers indicated. The model includes regions for the fuel debris, boral region with stainless steel skin, which surrounds the fuel debris, LICON, TMI-2 fuel canister shell, and the DSC shell. The gaps between the TMI-2 canisters and DSC shell are assumed to be filled with air.

The heat generated by the debris in each TMI-2 canister is assumed to be transferred by conduction to the TMI-2 canister shell regions. For the narrow gaps between adjacent canisters, heat transfer is assumed to occur through conduction and radiation. The TMI-2 canisters are open to the DSC atmosphere because the Hanson couplings on them may be removed or blocked open. The DSC cavity is vented to the atmosphere through HEPA filters. For the thermal analysis, any convection to the air inside the TMI-2 canisters or DSC is conservatively neglected. For the space between the horizontal and vertical surfaces of the outer TMI-2 canister and the DSC shell, heat is assumed to be transferred through conduction and radiation only. Heat transfer through the DSC shell is achieved by conduction.

The base case decay heat power of 80W for each TMI-2 canister is assumed to be uniformly distributed over the fuel regions inside the TMI-2 canister cavity. The resulting volumetric heat density is 3.982E-4 Btu/min.-in.^{3}. The thermal properties from Table 8.1-6 and Table 8.1-7 are used in the HEATING 7 model of the DSC.

Figure 8.1-5 shows the resulting temperature distribution inside the DSC for the 87°F ambient case.

The resulting calculated temperature profiles for the DSC are used for the evaluation of TMI-2 fuel debris and other DSC internal component temperatures. The results are summarized in Table 8.1-10.

B. Evaluation of NUHOMS®-12T DSC inside the HSM

From the 87°F ambient temperature profile in Figure 8.1-5 for the DSC, it can be observed that the maximum temperatures occur for the fuel regions in the center-most TMI-2 canister just above the horizontal center line of the DSC. The maximum temperature occurs slightly above the midplane because the lower half of the DSC shell is at a lower temperature than the upper half.

For variations in ambient air temperatures for normal operating conditions, the maximum calculated fuel debris temperature is 174°F (79°C) for the 87°F ambient air case. The maximum calculated fuel debris temperature is less than 174°F (79°C) for the 45°F and -20°F ambient air cases. Therefore, the maximum fuel debris temperature for 87°F ambient is well below the design basis fuel debris storage temperature limit of 724°F (384°C) defined in Section 3.3.7.1 for long term dry storage. For extreme ambient conditions, or short term operating conditions, the maximum fuel debris temperature is 191°F (88°C). This value is well below the short term fuel debris temperature limit of 1058°F (570°C) defined in Section 3.3.7.1.

These temperatures are well within the filter tested temperature range of -194^{o}C to 140^o C. The temperatures are also within the operating range for both the metallic seals and the elastomerics used in the filter assembly. The limiting case is the elastomerics used in the filter assembly that has a normal operating range for a static seal between -50^{o}F and 250^{o}F with the capability of going beyond these limits for short periods.

8.1.3.3 Thermal Analysis of the NUHOMS®-12T DSC Inside the MP187 Cask

A. NUHOMS®-12T DSC in Cask During Transfer Operation

The design basis heat load for the MP187 cask for 10 CFR Part 72 conditions is 13.5kW [8.12]. The design basis heat load in the NUHOMS®-12T DSC is 0.86kW. Therefore, the thermal analysis for the NUHOMS®-12T DSC in the MP187 cask is bounded by the results presented in the MP187 10 CFR Part 71 SAR [8.18] and 10 CFR Part 72 SAR [8.12].

8.1.4 Storage with Detected Leakage of Vent and Purge Port Seals

A Limiting Condition for Operation (LCO) during storage operations at the TMI-2 ISFSI is maintenance of the DSC vent and purge housing seal leak rate below 1E-02 standard cc/s. Compliance with the LCO is demonstrated through periodic performance of a leak check of the vent and purge housing double metallic seals on each DSC containing TMI-2 canisters

The basis for verifying the integrity of the DSC is the need to maintain confinement of the radioactive material stored in each DSC. The vent and purge housing seals make up part of the DSC confinement barrier. Failure of the confinement barrier is considered in the accident analysis discussed in Section 8.2. Verification of the vent and purge housing seal integrity ensures that the HEPA filtered vent system is the only vent path for the DSC. The required action to reseat or replace the vent and purge housing seals within seven days of a failed leak test recognizes the low motive force available to transport radioactive material through the leaking vent and purge seals.

If the seals cannot pass the leak test after being reseated or replaced, continued storage with increased radioactive contamination surveys and standard contamination control practices would be implemented.

8.1.4.1 Hydrogen Venting Analysis

Leakage of the vent port seals would not adversely affect the ability of the vent system to allow hydrogen to diffuse through the HEPA filters.

8.1.4.2 Confinement Analysis

Particulate radioactive material release through leaking double metallic seals would be expected to be negligible without a significant motive force. The only motive forces for release through leaking double metallic seals are diffusion, temperature gradients, and atmospheric pressure changes, all of which are quite small. For a release of radioactive material from within a DSC to occur, the radioactive material would have to be so fine that it can pass through a canister seal leak, become airborne and migrate to the DSC seal area, then pass through leaking double metallic seals with a significant motive force to sustain it. Without HEPA filter blockage, most of any motive force would be dissipated through the HEPA filters rather than acting to pass radioactive material through the seals.

Even if the double metallic seals were completely missing, the gaps between the vent and purge filter housings and the DSC lid are so small that it would be difficult for particulate radioactive material to pass though without significant motive force. The worst case would be all the particulate radioactive material that could potentially be released from the DSC during normal operation is released unfiltered through the leaking double metallic seals. If such a case is assumed, the release is estimated to be 0.1 Ci/y [8.45].

The worst case release rate from a single DSC due to leaking double metallic seals (0.1 Ci/y of particulate radioactivity) would result in a Total Effective Dose Equivalent (TEDE) rate at the INL site boundary of 0.17 mrem/y. The TEDE rate at the INTEC fence would be 130 mrem/y based on the ratio of the Table 7.6-1 TEDE values for 100 and 13,700 meter distances [8.45].

8.1.4.3 Continued Storage Analysis

Neither of the two intended functions of the DSC vent system will be compromised with leaking DSC vent or purge housing double metallic seals. Leaking seals will not disrupt the diffusion path for hydrogen. It can be concluded from the calculations that any particulate radioactive material release through leaking double metallic seals would be negligible without a significant motive force. The worst case would be if all the particulate radioactive material that could potentially be released from the DSC during normal operation were released unfiltered through the leaking double metallic seals. Such a release would be estimated to be only 0.1 Ci/y. The resulting dose rate at the INL site boundary would be 0.17 mrem/y; well below the 100 mrem/y limit in 10 CFR 20.1301. The resulting dose rate at the INTEC fence would be 130 mrem/y; well below the 500 mrem/y limit in 10 CFR 20.1502.

Table 8.1-1
NUHOMS®-12T Normal Operating Loading Identification

Load Type	Affected Component			
	DSC Shell Assembly	DSC Internals	DSC Support Structure	Reinforced Concrete HSM
Dead Weight	X	X	X	X
Internal Pressure	X			
Normal Thermal	X		X	X
Normal Handling	X		X	X
Live Loads				X

Table 8.1-2
NUHOMS®-12T Off-Normal Operating Loading Identification

Load Type	Affected Component		
	DSC Shell Assembly	DSC Support Structure	Reinforced Concrete HSM
Dead Weight	X	X	X
Internal Pressure	X		
Off-Normal Thermal	X	X	X
Off-Normal Handling	X	X	X

Table 8.1-3
Mechanical Properties of Materials

Material	Tempera-ture (°F)	Stress Properties[1] (ksi)			Elastic Modulus[1] (x1.0E3 ksi) (E)	Mean Coefficient of Thermal Expansion[1] (μ in./in.-°F)
		Stress Intensity (S_m)	Yield Strength (S_y)	Ultimate Strength (S_u)		
Carbon Steel ASME SA36	70	19.3	36.0	58.0	29.5	5.53
	100	19.3	36.0	-	29.3	5.53
	200	19.3	32.8	-	28.8	5.89
	300	19.3	31.8	-	28.3	6.26
Carbon Steel Plate ASME SA516 Grade 70	70	23.3	38.0	70.0	29.5	5.53
	100	23.3	38.0	70.0	29.3	5.53
	200	23.1	34.6	70.0	28.8	5.89
	300	22.5	33.7	70.0	28.3	6.26

Material	Temperature (°F)	28 Day Compressive Strength (ksi)	Modulus of Elasticity (1.0E3 ksi)
Concrete Normal Wt.[2] 5000 psi Strength	100	5.0	4.03
	200	5.0	4.03
	300	4.8	3.30

Material	Temperature (°F)	Yield Strength (ksi)	Modulus of Elasticity (1.0E3 ksi)
Reinforcing Steel[2] ASTM A615 Grade 60	100	60.0	29.0
	200	57.0	28.4
	300	54.0	27.8

Table 8.1-3
Mechanical Properties of Materials
(continued)

Material	Temperature (°F)	Allowable Stress Values for Class 2[1] Components (S) (ksi)	Yield Strength[1] (ksi)
Structural Bolting Material ASTM A325	100	20.2	81.0
	200	20.2	73.9
	400	20.2	69.3

Material	Temperature (°F)	Yield Stress[1] (ksi)	Normal Condition Allowables		
			F_{tb}[3, 5] (ksi)	F_{vb}[4, 5] (ksi)	SI[6] (ksi)
Filter Housing Bolts SA 193 Grade B8 Normal Conditions	100	30	20.0	12.0	27.0
	200	25.8	17.2	10.3	23.2
	300	23.3	15.5	9.3	21.0

Material	Temperature (°F)	Yield Stress[1, 7] (ksi)	0.6 S_y	Accident Condition Allowables	
				F_{tb}[5, 8] (ksi)	F_{vb}[5, 9] (ksi)
Filter Housing Bolts SA 193 Grade B8 Accident Conditions	100	30	18.0	30	18.0
	200	25.8	15.5	25.8	15.5
	300	23.3	14.0	23.3	14.0

Table 8.1-3
Mechanical Properties of Materials
(concluded)

Notes:

(1) Steel data and thermal expansion coefficients are obtained from ASME Boiler and Pressure Vessel Code, Section II, Part D [8.19].

(2) Concrete and reinforcing steel data were obtained from Handbook of Concrete Engineering, by Mark Fintel. [8.7]

(3) Allowable tensile stress $F_{tb} = (2/3)S_y$

(4) Allowable shear stress $F_{vb} = (0.6)\ (2/3)S_y$

(5) Tension and shear stresses must be combined using the following interaction equation:

$$\left(\frac{f_{tb}}{F_{tb}}\right)^2 + \left(\frac{f_{vb}}{F_{vb}}\right)^2 \leq 1.0$$

(6) Stress intensity from the combined tensile, shear and residual torsion loads must be less than the allowable stress intensity: $SI = 1.35(2/3)S_y$

(7) Yield stress values from [8.19]. Note that S_u is 75 ksi at all temperatures of interest.

(8) Allowable tensile stress F_{tb} is the smaller of $0.7S_u$ or S_y. Where: $0.7S_u = 0.7(75\ ksi) = 52.5\ ksi$.

(9) Allowable shear stress F_{vb} is the smaller of $0.42S_u$ or $0.6S_y$. Where: $0.42S_u = 0.42(75\ ksi) = 31.5\ ksi$.

Table 8.1-4
Estimated NUHOMS®-12T Component Weights

	Component Description	Calculated Weight (Pounds)
1.	Dry Shielded Canister Shell Assembly	12,300
2.	DSC Top Shield Plug Assembly	4,700
3.	DSC Internal Basket Assembly	4,800
4.	DSC Top Cover Plate Assembly	1,600
5.	12 heaviest TMI-2 Canisters	35,000
6.	Total Dry DSC Loaded Weight	58,400
7.	MP187 Cask Empty Weight (include. internal spacers)	159,400
8.	MP187 Cask Max. Loaded Weight	217,800
9.	HSM Single Module Weight (empty)	272,000

Table 8.1-5
NUHOMS®-12T DSC Operating and Accident Pressures

Case	Ambient Air Temperature (°F)	Normal and Off-Normal Condition Pressure (1) (psia)	Accident Condition Pressure(2,3) (psia)	Design Basis Pressure (psia)
1	45	<26.1	<26.1	29.7
2	87	<26.1	<26.1	29.7
3	103	<26.1	26.1	29.7
4	DSC in Cask with ambient air @ 87°	<29.7	<29.7	29.7

(1) Even though the normal and off-normal operating pressure is 0 psig, a 11.4 psig pressure is assumed for Case 1, 2, and 3 and a 15.0 psig pressure is assumed for Case 4. Atmosphere pressure is conservatively assumed to be 14.7 psia.

(2) Assumes HEPA filters are blocked, the gap between adjacent HSMs is blocked, and this condition is not discovered for twelve months.

(3) For a postulated accident involving hydrogen burn, a pressure spike of 194 psig lasting a few milliseconds is also considered for the TMI-2 canister.

Table 8.1-6
Thermophysical Properties of Materials

Material	Effective Thermal Conduct. (k) (Btu/hr-ft-°F)	Emissivity (ε) Fraction
Carbon Steel/ Stainless Steel	Table 8.1-7 [8.19]	0.587 [8.20]
Concrete	Table 8.1-7 [8.43]	0.9 [8.16]
Soil	0.5 [8.44]	--
LICON	0.726 (Section 8.1.3.1.C)	--
UO_2 Debris	4.623 [8.21]	--

Table 8.1-7
Temperature Dependent Thermophysical Properties

	Temperature (°F)	Thermal Conductivity (Btu/hr-ft.-°F)
Carbon Steel	70	23.62
	100	23.90
	150	24.19
	200	24.41
	300	24.41
	400	24.19
	500	23.69
Concrete	-50	1.10
	100	1.17
	200	1.14
	300	1.11
	400	1.08
	500	1.04
Stainless Steel	70	8.57
	100	8.71
	150	9.00
	200	9.29
	250	9.58
	300	9.79
	350	10.08
	400	10.37
	450	10.58
	500	10.87
Air [8.16]	0	0.0133
	32	0.0140
	100	0.0154
	200	0.0174
	300	0.0193
	400	0.0212
	500	0.0231

Table 8.1-8
Thermal Load Case Definitions for NUHOMS®-12T HSM Structural Analysis(1)

Thermal Condition	Case No.	Ambient Temp. (°F)	Maximum Inner Surface Temperature (°F)			Maximum Outer Surface Temperature (°F)			Maximum Thermal Gradient(2) (°F)		
			Roof	Wall	Floor	Roof	Wall	Floor(3)	Roof	Wall	Floor(3)
Normal Operating (T_o)	1	45	90.8	74.5	77.2	87.6	54.2	69.5	3.2	20.3	7.7
	2	87	128.7	114.6	115.4	125.5	94.9	107.1	3.2	19.7	8.3
	3	-20	4.0	3.9	9.9	-13.3	-11.7	4.3	17.3	15.6	5.6
Off-Normal (T_a)	1	103	152.5	133.4	133.5	155.4	111.4	124.2	2.9	22.0	9.3
	2(2)	-50	-25.1	-25.0	-16.8	-42.7	-40.9	-22.0	17.6	15.9	5.2
Accident (T_a)	1	103	174.9	178.6	167.6	159.4	173.8	157.5	15.5	4.8	10.1
	2(2)	-50	-11.6	9.7	16.4	-38.3	3.2	13.0	26.7	6.5	3.4

(1) The maximum concrete temperature for normal operating condition is 129°F, which is significantly below the ACI 349 temperature limit of 200°F. Similarly, the maximum concrete temperature for accident conditions in 179°F, which is also significantly below the ACI 349 temperature limit of 350°F.

(2) Based on maximum gradient at any cross-section.

(3) The floor outside temperature and maximum gradient are reported for the two-foot thick HSM floor.

Table 8.1-8
Thermal Load Case Definitions for NUHOMS®-12T HSM Structural Analysis[1]
(cont)

Ambient Temperature[4] (°F)	Front Wall Gradient[5] (°F)	Back Wall Gradient[5] (°F)	Coordinates for the max thermal gradient (in.)
103[6]	10.9	-	(37.5, -34.5, 187.5 to 218)
103[6]	-	12.9	(37.5, -90, 0 to 36)
-50	8.7	-	(0, 34.5, 187.5 to 218)
-50	-	14.8	(0, 34.5, 0 to 36)

(4) These off-normal cases will bound the normal operating cases. The -50°F case will bound the -20°F case, which is the other case without solar insolation, because the outside surface temperature is raised 30°F while the inside surface temperature would be raised by a lower amount. The 103°F will bound the 87 and 45°F cases since the solar insolation is significantly higher (105 vs. 67 Btu/hr-ft^2)

(5) The front and back wall do not include the regions from x = 37.5 to x = 61.5 in. These regions are considered part of the side wall.

(6) These gradients are from higher outside surface temperatures to lower inside surface temperatures due to the combination of low decay heat and high solar insolation. The maximum gradients for this case from a higher inside surface to a lower outside surface is 6.1 and 11.2 °F for the front and back wall respectively.

Table 8.1-8
Thermal Load Case Definitions for NUHOMS®-12T HSM Structural Analysis
(concluded)

Normal Conditions

1. Interior module with 45°F ambient temperature, 24 inch side walls open to ambient, solar heat flux of 67.0 Btu/hr-ft^2

2. Interior module with 87°F ambient temperature, 24 inch side walls open to ambient, solar heat flux of 67.0 Btu/hr-ft^2

3. Interior module with -20°F ambient temperature, 24 inch side walls open to ambient, solar heat flux neglected

Off-Normal Conditions

1. Interior module with 103°F ambient temperature, 24 inch side walls open to ambient, solar heat flux of 105 Btu/hr-ft^2

2. Interior module with -50°F ambient temperature, 24 inch side walls open to ambient, neglect solar heat flux

Accident Conditions

1. Interior module with 103°F ambient temperature, the gap between HSMs is blocked, solar heat flux of 105 Btu/hr-ft^2

2. Interior module with -50°F ambient temperature, the gap between HSMs is blocked, neglect solar heat flux

Table 8.1-9
NUHOMS®-12T DSC Thermal Analysis Results Summary(1)

Thermal Conditions	Case	Ambient Temperature (°F)	Maximum DSC Outer Surface Temperature (°F)		
			Bottom	Side	Top
Normal	1	45	94.4	94.7	97.8
	2	87	130.3	131.0	134.2
	3	-20	29.1	28.2	28.1
Off-Normal	1	103	148.5	149.7	154.4
	2	-50	4.8	3.8	3.7
Accident	1	103	180.8	183.8	183.5
	2	-50	28.1	26.2	23.3

(1) See Table 8.1-8 for concrete temperatures and definitions of these cases.

Table 8.1-10 [1,2]

NUHOMS® DSC Thermal Analysis Results Summary

Thermal Conditions	Case	Ambient Temperature (°F)	Maximum Fuel Debris Temperature (°F/°C)	Fuel Debris Acceptance Criteria[3] (°F/°C)
Normal	1	45	<174/79	724/384
	2	87	174/79	724/384
	3	-20	<174/79	724/384
Off-Normal	1	103	191/88	1058/570
	2	-50	<191/88	1058/570
Accident	1	103	219/104	1058/570
	2	-50	<219/104	1058/570
(DSC in cask with internal vacuum)	1	100[3]	<289/143	1058/570

(1) See Table 8.1-8 for concrete temperatures and definitions of these cases.

(2) See Table 8.1-9 for DSC Shell temperatures.

(3) These temperature limits are based on intact fuel. The TMI-2 debris has been subjected to temperatures greater than these and the cladding is degraded. As such, the typical fuel temperature limits are not applicable with respect to cladding damage. These limits are used here for consistency.

Table 8.1-11
Maximum NUHOMS®-12T DSC Stresses for Normal Loads

DSC Components	Stress Type	Stress Intensity (ksi)(1)			
		Dead Weight	Internal Pressure(2)	Thermal(3)	Normal Handling
DSC Shell	Primary Membrane	2.5	10.5	---	3.3
	Membrane + Bending	5.3	17.8	---	9.6
	Primary + Secondary	5.3	17.8	1.6	15.0
Top Shield Plug	Primary Membrane	0.6	4.4	---	0.3
	Membrane + Bending	1.3	6.2	---	0.3
	Primary + Secondary	1.3	6.2	0.2	0.3
Top Cover Plate	Primary Membrane	1.2	8.0	---	0.3
	Membrane + Bending	1.7	12.0	---	0.3
	Primary + Secondary	1.7	12.0	0.5	0.3
Inner Bottom Cover Plate	Primary Membrane	0.8	0.7	---	0.3
	Membrane + Bending	1.3	1.0	---	0.3
	Primary + Secondary	1.3	1.0	0.3	0.7
Outer Bottom Cover Plate	Primary Membrane	0.3	3.6	---	2.0
	Membrane + Bending	0.5	7.1	---	10.3
	Primary + Secondary	0.5	7.1	0.3	13.4

(1) Values shown are maximum irrespective of location.
(2) Even though the normal operating pressure is 0 psig, a bounding 15 psig pressure load is applied.
(3) All thermal stresses are classified as secondary. All stresses from deadweight and pressure loads are classified as primary membrane or bending.

Table 8.1-12
Maximum NUHOMS®-12T DSC Stresses for Off-Normal Loads

DSC Components	Stress Type	Stress Intensity (ksi)(1)		
		Internal Pressure(2)	Thermal	Off-Normal Handling
DSC Shell	Primary Membrane	10.5	N/A	1.9
	Membrane + Bending	17.8	N/A	13.0
	Primary + Secondary	17.8	1.6	30.0
Top Shield Plug	Primary Membrane	4.4	N/A	0.0
	Membrane + Bending	6.2	N/A	0.0
	Primary + Secondary	6.2	0.2	0.2
Top Cover Plate	Primary Membrane	8.0	N/A	0.1
	Membrane + Bending	12.0	N/A	0.1
	Primary + Secondary	12.0	0.5	0.6
Inner Bottom Cover Plate	Primary Membrane	0.7	N/A	0.0
	Membrane + Bending	1.0	N/A	0.3
	Primary + Secondary	1.0	0.3	1.3
Outer Bottom Cover Plate	Primary Membrane	3.6	N/A	4.0
	Membrane + Bending	7.1	N/A	20.6
	Primary + Secondary	7.1	0.3	26.8

(1) Values shown are maximum irrespective of location.
(2) Even though the off-normal operating pressure is 0 psig, a bounding 15 psig pressure load is applied.

Table 8.1-13
Maximum DSC Support Structure Stresses for Normal and Off-Normal Loads

Component	Load Type	Calculated Stress	
		Axial (ksi)	Shear (ksi)
Support Rail	Dead Weight	0.00	0.9
	Normal DSC Handling Loads	1.42	3.40
	Off-Normal DSC Handling Loads	2.84	4.00
Cross Beam	Dead Weight	0.13	0.02
	Normal DSC Handling Loads	1.20	0.00
	Off-Normal DSC Handling Loads	1.70	0.04

Table 8.1-14
Maximum DSC Support Structure Vertical Displacements for Normal and Off-Normal Loads

Components	Load Type	Maximum Vertical Displacements (in.)
Support Rails	Dead Weight $DW_s + DW_c$	0.004
	Normal DSC Handling Loads $DW_s + HL_n$	0.047
	Off-Normal DSC Handling Loads $DW_s + DW_c + HL_o$	0.094

Table 8.1-15
Maximum NUHOMS®-12T HSM Reinforced Concrete Bending Moments and Shear Forces for Normal and Off-Normal Loads

Structural Section	Force Component	HSM Internal Forces (kip/ft., in.-k/ft.)(1)			
		Dead Weight	Live Loads	Normal (2,3) Thermal	Off-Normal (4) Thermal
Floor Slab	Shear	0.57	0.1	6.9	6.9
	Moment	33.7	3.3	357.2	357.2
Side Wall	Shear	0.26	0.1	9.3	9.3
	Moment	17.5	2.9	582.4	582.4
Front Wall	Shear	9.6	2.9	42.6	42.6
	Moment	175.0	36.1	791.5	791.5
Rear Wall	Shear	1.1	0.5	33.0	33.0
	Moment	128.2	12.1	532.6	532.6
Roof Slab	Shear	0.45	0.2	3.2	3.2
	Moment	33.3	10.8	430.2	430.2

(1) Values shown are maximums irrespective of location.

(2) Maximum moments are based on cracked section properties.

(3) See Table 8.1-8 for concrete temperatures and definitions of these cases.

(4) Worst case internal loads are used for normal, off-normal and accident conditions. Normal thermal results are bounded by off-normal thermal results. Therefore, off-normal results are tabulated both for normal and off-normal cases.

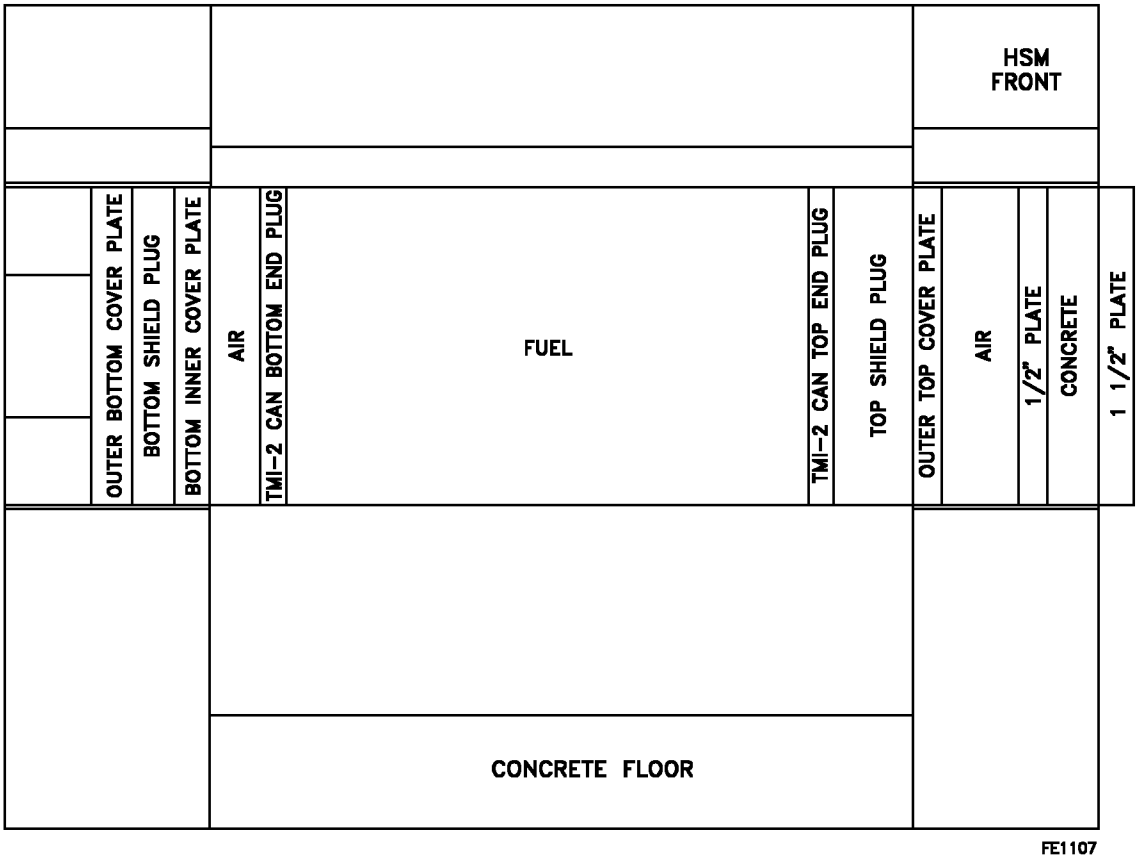

Figure 8.1-1
HEATING 7 Model of NUHOMS®-12T DSC Used in HSM

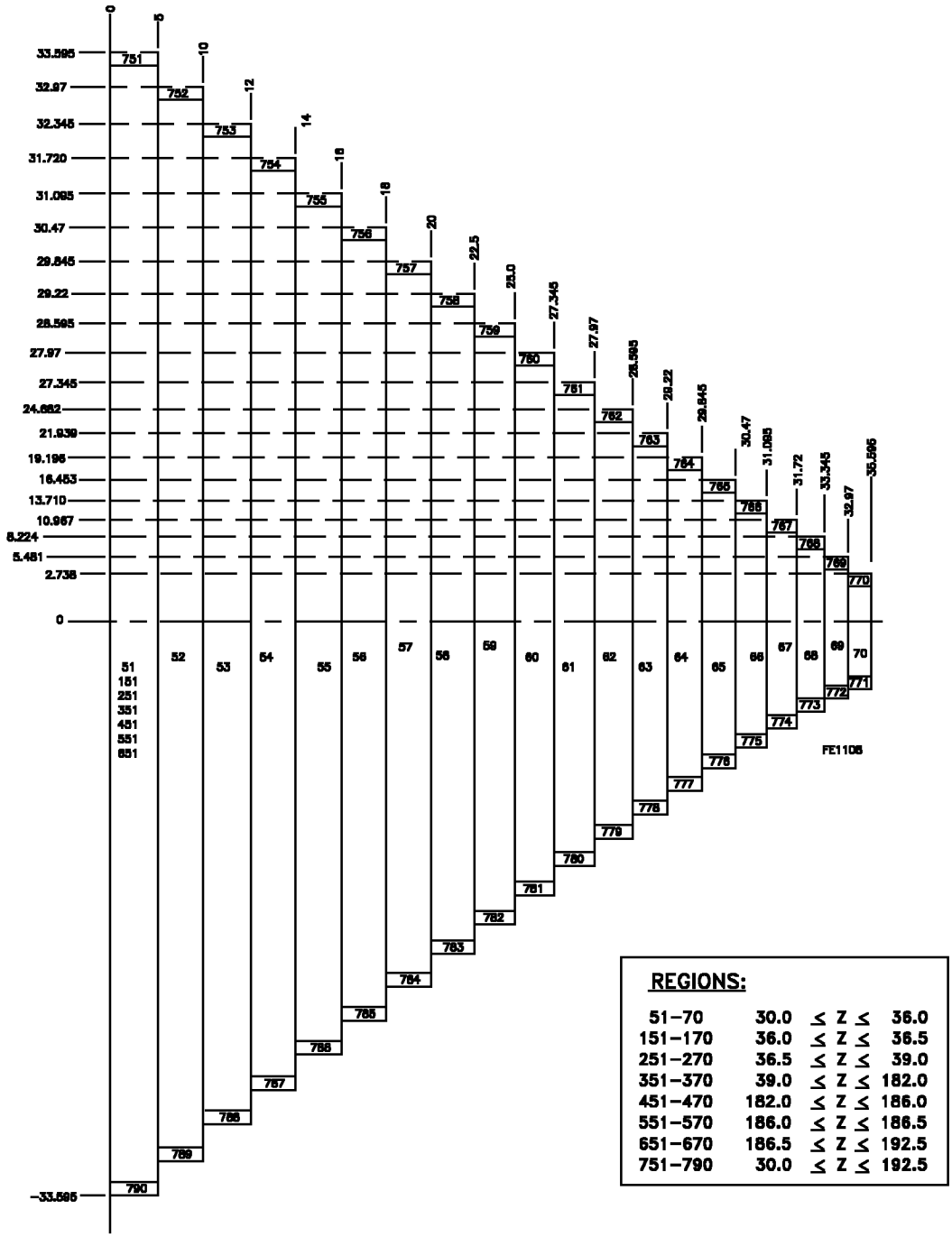

Figure 8.1-1
HEATING 7 Model of NUHOMS®-12T DSC Used in HSM
(Concluded)

TMI-4D7 HSM 45 F AMB,0.86kW/DSC,non-insulated side, solar Thu Aug 8 08:28:01 1996

Steady-State Temperature Distribution at Time 0.0000E+00

Z = 1.1050E+02

64	72.00	87.56	87.50	87.33	87.22	87.10	86.95	86.78	86.65	86.60	86.33	86.03	85.72	85.63	85.53
63	71.75	87.55	87.49	87.30	87.20	87.07	86.92	86.74	86.60	86.55	86.28	85.97	85.64	85.55	85.45
62	65.31	87.33	87.22	86.88	86.68	86.45	86.17	85.86	85.59	85.50	84.99	84.42	83.83	83.66	83.48
61	58.88	87.49	87.34	86.87	86.59	86.26	85.86	85.41	85.03	84.90	84.17	83.34	82.48	82.24	81.99
60	52.44	88.21	88.02	87.46	87.11	86.70	86.20	85.63	85.14	84.97	84.02	82.92	81.77	81.45	81.11
59	46.00	89.58	89.39	88.79	88.42	87.97	87.42	86.77	86.21	86.00	84.85	83.45	81.91	81.46	81.01
58	44.00	90.14	89.96	89.38	89.01	88.57	88.03	87.39	86.83	86.62	85.45	83.98	82.22	81.71	81.19
57	42.00	90.77	90.60	90.04	89.70	89.27	88.75	88.14	87.59	87.39	86.25	84.77	82.75	82.04	81.40
56	38.25	93.76	93.58	92.87	92.41	91.86	91.19	90.40	89.69	89.44	87.96	86.07	83.82	83.15	82.45
55	34.50	96.98	96.86	96.06	95.50	94.84	94.09	93.23	92.47	92.20	90.62	88.55	86.02	85.23	84.41
54	33.59	97.77	97.72	96.91	96.29	95.62	94.86	93.99	93.25	92.97	91.43	89.37	86.79	85.97	85.11
53	32.97	97.79	97.73	97.51	96.85	96.16	95.40	94.54	93.80	93.54	92.02	89.99	87.38	86.55	85.66
52	32.34	97.85	97.75	97.52	97.41	96.71	95.95	95.10	94.38	94.12	92.65	90.66	88.03	87.18	86.25
51	31.72	97.91	97.81	97.54	97.41	97.27	96.52	95.68	94.96	94.71	93.31	91.38	88.75	87.87	86.91
50	31.09	97.98	97.87	97.60	97.42	97.27	97.09	96.27	95.56	95.33	94.00	92.16	89.55	88.63	87.63
49	30.47	98.04	97.94	97.66	97.48	97.27	97.08	96.87	96.14	95.97	94.73	93.00	90.43	89.48	88.42
48	30.00	98.08	97.98	97.70	97.52	97.32	97.08	96.87	96.55	96.47	95.29	93.67	91.18	90.18	89.07
47	29.84	98.09	98.00	97.71	97.54	97.33	97.09	96.87	96.68	96.64	95.48	93.90	91.44	90.43	89.29
46	29.22	98.15	98.05	97.77	97.59	97.38	97.14	96.87	96.68	96.61	96.27	94.87	92.58	91.49	90.25
45	28.59	98.21	98.11	97.82	97.65	97.44	97.20	96.92	96.71	96.61	96.26	95.91	93.93	92.69	91.28
44	27.97	98.26	98.16	97.87	97.70	97.49	97.25	96.98	96.75	96.67	96.27	95.90	95.58	94.05	92.37
43	27.34	98.31	98.21	97.92	97.75	97.54	97.30	97.03	96.80	96.73	96.32	95.90	95.58	95.54	93.44
42	24.68	98.50	98.41	98.11	97.94	97.73	97.49	97.22	97.00	96.92	96.50	96.04	95.55	95.50	95.46
41	21.94	98.67	98.57	98.27	98.10	97.89	97.65	97.38	97.16	97.08	96.65	96.17	95.65	95.50	95.45
40	19.20	98.80	98.70	98.40	98.23	98.02	97.78	97.51	97.28	97.20	96.77	96.28	95.76	95.61	95.46
39	16.45	98.89	98.79	98.50	98.32	98.11	97.87	97.60	97.37	97.29	96.86	96.37	95.86	95.71	95.56
38	15.00	98.93	98.83	98.53	98.36	98.15	97.91	97.63	97.41	97.33	96.90	96.41	95.90	95.76	95.62
37	13.71	98.95	98.85	98.55	98.38	98.17	97.93	97.66	97.43	97.35	96.92	96.44	95.93	95.79	95.64
36	10.97	98.97	98.88	98.58	98.40	98.20	97.96	97.68	97.46	97.38	96.95	96.47	95.97	95.83	95.69
35	8.22	98.96	98.86	98.57	98.39	98.19	97.95	97.68	97.45	97.37	96.95	96.48	95.99	95.85	95.70
34	7.50	98.95	98.85	98.56	98.38	98.18	97.94	97.67	97.45	97.37	96.94	96.47	95.98	95.85	95.70
33	5.48	98.91	98.81	98.52	98.34	98.14	97.90	97.63	97.41	97.33	96.91	96.45	95.96	95.83	95.69
32	2.74	98.83	98.73	98.43	98.26	98.06	97.82	97.55	97.33	97.26	96.84	96.38	95.90	95.77	95.63
31	.00	98.71	98.61	98.31	98.14	97.94	97.70	97.44	97.22	97.14	96.73	96.27	95.80	95.67	95.54
30	-2.74	98.55	98.45	98.16	97.99	97.78	97.55	97.28	97.06	96.99	96.58	96.12	95.65	95.52	95.39
29	-5.48	98.35	98.26	97.96	97.79	97.59	97.35	97.09	96.87	96.79	96.38	95.92	95.45	95.32	95.18
28	-7.50	98.19	98.09	97.80	97.62	97.42	97.19	96.92	96.70	96.63	96.21	95.75	95.28	95.14	95.01
27	-8.22	98.12	98.02	97.73	97.56	97.36	97.12	96.86	96.64	96.56	96.15	95.69	95.21	95.08	94.94
26	-10.97	97.85	97.76	97.46	97.29	97.09	96.85	96.59	96.37	96.29	95.87	95.41	94.93	94.79	94.65
25	-13.71	97.55	97.45	97.16	96.98	96.78	96.55	96.28	96.06	95.98	95.56	95.09	94.61	94.47	94.33
24	-15.00	97.39	97.29	97.00	96.83	96.62	96.39	96.12	95.90	95.82	95.40	94.94	94.45	94.31	94.17
23	-16.45	97.21	97.11	96.81	96.64	96.44	96.20	95.93	95.71	95.64	95.22	94.75	94.25	94.11	93.97
22	-19.20	96.83	96.73	96.43	96.26	96.05	95.82	95.55	95.33	95.26	94.84	94.37	93.87	93.73	93.58
21	-21.94	96.41	96.31	96.01	95.84	95.64	95.40	95.13	94.91	94.84	94.43	93.97	93.47	93.33	93.29
20	-24.68	95.96	95.86	95.56	95.38	95.18	94.94	94.67	94.45	94.38	93.98	93.55	93.09	93.05	93.02
19	-27.34	95.48	95.38	95.08	94.91	94.69	94.45	94.18	93.96	93.88	93.49	93.11	92.88	92.85	90.23
18	-27.97	95.37	95.26	94.97	94.79	94.58	94.33	94.06	93.84	93.75	93.36	93.07	92.86	90.84	88.73
17	-28.59	95.25	95.14	94.85	94.67	94.46	94.21	93.93	93.73	93.61	93.33	93.06	90.51	88.92	87.15
16	-28.62	95.24	95.14	94.84	94.66	94.45	94.20	93.93	93.72	93.61	93.33	92.98	90.41	88.83	87.08
15	-29.22	95.13	95.02	94.73	94.55	94.33	94.08	93.80	93.64	93.59	93.32	91.46	88.54	87.16	85.62
14	-29.84	95.01	94.90	94.61	94.43	94.21	93.96	93.77	93.62	93.60	92.05	89.95	86.81	85.56	84.16
13	-30.47	94.88	94.77	94.49	94.30	94.08	93.93	93.76	92.73	92.50	90.81	88.52	85.26	84.08	82.79
12	-31.09	94.76	94.65	94.37	94.18	94.05	93.91	92.77	91.76	91.44	89.61	87.16	83.84	82.71	81.49

.00	5.00	10.00	12.00	14.00	16.00	18.00	19.50	20.00	22.50	25.00	27.34	27.97	28.59
1	2	3	4	5	6	7	8	9	10	11	12	13	14

Figure 8.1-2
HSM HEATING 7 Results for 45°F Ambient

TMI-4D7 HSM 45 F AMB,0.86kW/DSC,non-insulated side, solar Thu Aug 8 08:28:01 1996

Steady-State Temperature Distribution at Time 0.0000E+00

Z = 1.1050E+02

64	72.00	85.44	85.34	85.24	85.14	85.04	84.93	84.82	84.71	84.54	83.93	82.99	81.83	80.32	76.89
63	71.75	85.35	85.25	85.15	85.05	84.94	84.83	84.71	84.60	84.42	83.80	82.83	81.63	80.07	76.53
62	65.31	83.30	83.12	82.94	82.74	82.55	82.35	82.14	81.93	81.62	80.51	78.82	76.81	74.35	69.42
61	58.88	81.73	81.47	81.21	80.94	80.66	80.38	80.09	79.80	79.37	77.85	75.64	73.16	70.32	65.19
60	52.44	80.78	80.43	80.08	79.72	79.35	78.98	78.61	78.23	77.68	75.78	73.18	70.45	67.51	62.54
59	46.00	80.55	80.08	79.60	79.12	78.63	78.14	77.64	77.13	76.40	73.93	71.05	68.30	65.45	60.79
58	44.00	80.66	80.13	79.60	79.07	78.53	77.98	77.43	76.87	76.04	73.12	70.32	67.68	64.92	60.37
57	42.00	80.79	80.20	79.63	79.06	78.49	77.91	77.32	76.72	75.78	72.00	69.55	67.10	64.44	60.01
56	38.25	81.72	80.97	80.19	79.39	78.56	77.70	76.81	75.89	74.49	69.25	68.12	66.15	63.71	59.46
55	34.50	83.53	82.62	81.67	80.67	79.64	78.57	77.46	76.32	74.59	68.31	67.44	65.62	63.26	59.10
54	33.59	84.20	83.24	82.23	81.19	80.10	78.97	77.81	76.61	74.81	68.28	67.40	65.57	63.20	59.04
53	32.97	84.71	83.71	82.67	81.59	80.46	79.30	78.10	76.86	75.01	68.31	67.40	65.54	63.16	59.00
52	32.34	85.27	84.24	83.15	82.03	80.86	79.66	78.42	77.14	75.23	68.37	67.42	65.53	63.14	58.97
51	31.72	85.89	84.81	83.68	82.51	81.30	80.05	78.77	77.46	75.50	68.48	67.47	65.54	63.12	58.94
50	31.09	86.56	85.43	84.25	83.02	81.76	80.47	79.15	77.80	75.79	68.63	67.54	65.55	63.11	58.92
49	30.47	87.29	86.09	84.85	83.57	82.26	80.93	79.56	78.17	76.12	68.83	67.63	65.58	63.10	58.90
48	30.00	87.88	86.63	85.33	84.00	82.65	81.28	79.89	78.47	76.38	69.01	67.71	65.61	63.11	58.89
47	29.84	88.08	86.81	85.49	84.15	82.79	81.40	80.00	78.57	76.47	69.08	67.74	65.62	63.11	58.88
46	29.22	88.92	87.55	86.16	84.75	83.33	81.89	80.45	78.99	76.85	69.39	67.88	65.67	63.11	58.87
45	28.59	89.81	88.33	86.84	85.36	83.88	82.40	80.91	79.42	77.25	69.76	68.03	65.72	63.13	58.86
44	27.97	90.71	89.09	87.51	85.96	84.42	82.90	81.38	79.86	77.66	70.22	68.19	65.79	63.15	58.86
43	27.34	91.57	89.82	88.16	86.54	84.96	83.39	81.85	80.30	78.08	70.76	68.36	65.86	63.17	58.85
42	24.68	93.72	92.00	90.30	88.62	86.96	85.32	83.70	82.09	79.79	72.43	69.14	66.21	63.31	58.87
41	21.94	95.42	93.72	92.02	90.32	88.62	86.94	85.25	83.58	81.17	73.36	69.77	66.56	63.49	58.92
40	19.20	95.41	95.38	93.63	91.87	90.11	88.35	86.59	84.83	82.29	73.91	70.22	66.86	63.65	58.98
39	16.45	95.41	95.36	95.32	93.41	91.54	89.68	87.83	85.97	83.27	74.24	70.54	67.08	63.79	59.03
38	15.00	95.47	95.33	95.30	93.84	92.15	90.35	88.48	86.58	83.79	74.37	70.66	67.17	63.84	59.05
37	13.71	95.49	95.34	95.27	95.24	93.21	91.21	89.21	87.20	84.28	74.45	70.74	67.23	63.88	59.06
36	10.97	95.54	95.38	95.23	95.17	95.14	92.97	90.78	88.58	85.37	74.56	70.85	67.31	63.93	59.07
35	8.22	95.56	95.41	95.25	95.09	95.05	94.99	92.52	90.08	86.56	74.59	70.88	67.33	63.93	59.05
34	7.50	95.56	95.42	95.27	95.13	95.00	94.97	92.81	90.46	86.91	74.59	70.88	67.33	63.92	59.04
33	5.48	95.55	95.40	95.25	95.10	94.94	94.88	94.84	92.10	88.09	74.56	70.84	67.28	63.87	58.99
32	2.74	95.50	95.35	95.21	95.06	94.91	94.76	94.70	94.66	89.74	74.46	70.74	67.17	63.76	58.90
31	.00	95.40	95.27	95.13	94.99	94.85	94.71	94.57	94.54	89.82	74.29	70.56	67.00	63.60	58.76
30	-2.74	95.25	95.11	94.97	94.83	94.68	94.53	94.48	94.46	89.48	74.05	70.31	66.75	63.37	58.58
29	-5.48	95.05	94.91	94.76	94.62	94.46	94.41	94.39	91.59	87.49	73.73	69.97	66.43	63.07	58.34
28	-7.50	94.87	94.73	94.59	94.46	94.34	94.31	92.10	89.69	86.05	73.43	69.67	66.13	62.80	58.14
27	-8.22	94.80	94.65	94.51	94.35	94.31	94.29	91.73	89.22	85.59	73.31	69.55	66.02	62.70	58.06
26	-10.97	94.51	94.36	94.21	94.17	94.15	91.89	89.61	87.32	83.99	72.80	69.02	65.51	62.25	57.72
25	-13.71	94.19	94.04	93.99	93.97	91.83	89.72	87.61	85.50	82.43	72.17	68.36	64.90	61.71	57.32
24	-15.00	94.04	93.90	93.88	92.33	90.55	88.64	86.66	84.65	81.70	71.81	68.00	64.57	61.42	57.11
23	-16.45	93.82	93.78	93.77	91.71	89.71	87.72	85.74	83.76	80.90	71.37	67.55	64.16	61.08	56.86
22	-19.20	93.54	93.52	91.61	89.69	87.77	85.86	83.95	82.05	79.31	70.37	66.55	63.28	60.34	56.34
21	-21.94	93.27	91.35	89.44	87.54	85.66	83.79	81.93	80.09	77.46	69.04	65.31	62.23	59.51	55.77
20	-24.68	90.98	88.97	87.00	85.07	83.18	81.32	79.50	77.70	75.16	67.18	63.75	61.03	58.59	55.17
19	-27.34	87.92	85.80	83.81	81.90	80.06	78.26	76.50	74.76	72.28	64.35	61.91			
18	-27.97	86.68	84.71	82.82	80.99	79.20	77.44	75.71	74.00	71.54	63.48	61.47	59.43	57.42	54.41
17	-28.59	85.34	83.54	81.77	80.02	78.29	76.59	74.90	73.22	70.80	62.70	61.02	59.13	57.20	54.27
16	-28.62	85.28	83.49	81.72	79.97	78.25	76.55	74.86	73.18	70.76	62.66	61.00	59.11	57.19	54.26
15	-29.22	84.00	82.35	80.68	79.02	77.37	75.72	74.08	72.43	70.05	61.99	60.58	58.82	56.98	54.12
14	-29.84	82.68	81.15	79.59	78.01	76.43	74.84	73.25	71.64	69.31	61.34	60.15	58.52	56.75	53.98
13	-30.47	81.41	79.98	78.51	77.01	75.49	73.96	72.42	70.86	68.58	60.75	59.72	58.21	56.53	53.84
12	-31.09	80.20	78.85	77.45	76.02	74.57	73.09	71.60	70.09	67.87	60.20	59.31	57.92	56.31	53.70

29.22	29.84	30.47	31.09	31.72	32.34	32.97	33.59	34.50	37.50	41.50	45.50	49.50	55.50
15	16	17	18	19	20	21	22	23	24	25	26	27	28

Figure 8.1-2
HSM HEATING 7 Results for 45°F Ambient
(Continued)

TMI-4D7 HSM 45 F AMB,0.86kW/DSC,non-insulated side, solar Thu Aug 8 08:28:01 1996

Steady-State Temperature Distribution at Time 0.0000E+00

Z = 1.1050E+02

64	72.00	69.74
63	71.75	69.16
62	65.31	61.96
61	58.88	58.66
60	52.44	56.80
59	46.00	55.62
58	44.00	55.34
57	42.00	55.10
56	38.25	54.74
55	34.50	54.50
54	33.59	54.46
53	32.97	54.43
52	32.34	54.41
51	31.72	54.39
50	31.09	54.37
49	30.47	54.36
48	30.00	54.34
47	29.84	54.34
46	29.22	54.33
45	28.59	54.32
44	27.97	54.31
43	27.34	54.31
42	24.68	54.30
41	21.94	54.31
40	19.20	54.34
39	16.45	54.36
38	15.00	54.36
37	13.71	54.37
36	10.97	54.37
35	8.22	54.35
34	7.50	54.34
33	5.48	54.31
32	2.74	54.24
31	.00	54.15
30	-2.74	54.03
29	-5.48	53.88
28	-7.50	53.75
27	-8.22	53.69
26	-10.97	53.47
25	-13.71	53.21
24	-15.00	53.08
23	-16.45	52.92
22	-19.20	52.59
21	-21.94	52.24
20	-24.68	51.86
19	-27.34	51.48
18	-27.97	51.39
17	-28.59	51.30
16	-28.62	51.29
15	-29.22	51.21
14	-29.84	51.12
13	-30.47	51.03
12	-31.09	50.95

61.50

29

TMI-4D7 HSM 45 F AMB,0.86kW/DSC,non-insulated side, solar Thu Aug 8 08:28:01 1996

Steady-State Temperature Distribution at Time 0.0000E+00

Z = 1.1050E+02

11	-31.72	94.63	94.52	94.24	94.14	94.03	93.00	91.81	90.77	90.42	88.44	85.86	82.52	81.43	80.27
10	-32.34	94.50	94.38	94.19	94.12	93.17	92.10	90.86	89.79	89.41	87.32	84.63	81.28	80.23	79.10
9	-32.97	94.38	94.34	94.17	93.29	92.33	91.22	89.93	88.82	88.43	86.23	83.45	80.11	79.08	78.00
8	-33.59	94.35	94.32	93.31	92.47	91.49	90.36	89.02	87.88	87.47	85.17	82.32	78.99	77.99	76.94
7	-34.50	93.48	93.25	92.11	91.30	90.32	89.14	87.75	86.55	86.12	83.70	80.76	77.46	76.49	75.48
6	-56.25	77.29	76.89	75.64	74.90	74.01	72.98	71.80	70.82	70.47	68.60	66.48	64.30	63.68	63.05
5	-78.00	77.18	76.96	76.26	75.81	75.26	74.59	73.76	73.03	72.76	71.21	69.23	66.84	66.13	65.43
4	-90.00	69.51	69.29	68.64	68.25	67.78	67.23	66.61	66.09	65.90	64.91	63.81	62.69	62.38	62.07
3	-102.00	64.46	64.30	63.82	63.54	63.22	62.84	62.42	62.08	61.96	61.32	60.63	59.94	59.75	59.55
2	-120.00	60.56	60.45	60.14	59.96	59.75	59.50	59.23	59.01	58.93	58.51	58.05	57.59	57.46	57.32
1	-204.00	65.00	65.00	65.00	65.00	65.00	65.00	65.00	65.00	65.00	65.00	65.00	65.00	65.00	65.00

.00	5.00	10.00	12.00	14.00	16.00	18.00	19.50	20.00	22.50	25.00	27.34	27.97	28.59
1	2	3	4	5	6	7	8	9	10	11	12	13	14

Figure 8.1-2
HSM HEATING 7 Results for 45°F Ambient
(Continued)

```
TMI-4D7 HSM 45 F AMB,0.86kW/DSC,non-insulated side, solar                                                    Thu Aug  8 08:28:01 1996
                                    Steady-State Temperature Distribution at Time 0.0000E+00
                                                          Z     =  1.1050E+02
    11  -31.72 |   79.04   77.75   76.42   75.05   73.66   72.24   70.79   69.33   67.17   59.69   58.92   57.63   56.10   53.56
    10  -32.34 |   77.93   76.69   75.42   74.11   72.77   71.40   70.01   68.59   66.49   59.20   58.53   57.34   55.89   53.42
     9  -32.97 |   76.86   75.68   74.46   73.20   71.91   70.59   69.24   67.86   65.83   58.75   58.16   57.06   55.68   53.29
     8  -33.59 |   75.84   74.70   73.53   72.31   71.07   69.79   68.49   67.16   65.20   58.31   57.80   56.79   55.48   53.16
     7  -34.50 |   74.43   73.35   72.24   71.09   69.91   68.69   67.45   66.19   64.31   57.72   57.30   56.41   55.19   52.97
     6  -56.25 |   62.41   61.76   61.10   60.42   59.73   59.03   58.32   57.60   56.54   52.88   52.67   52.21   51.55   50.25
     5  -78.00 |   64.75   64.09   63.44   62.81   62.18   61.56   60.96   60.35   59.49   56.65   55.29   53.98   52.71   50.86
     4  -90.00 |   61.76   61.45   61.13   60.82   60.50   60.19   59.88   59.57   59.12   57.70   56.00   54.46   53.03   51.03
     3 -102.00 |   59.36   59.16   58.96   58.76   58.56   58.36   58.16   57.95   57.65   56.65   55.32   54.00   52.69   50.78
     2 -120.00 |   57.19   57.05   56.91   56.77   56.63   56.49   56.34   56.19   55.97   55.21   54.14   53.00   51.79   49.85
     1 -204.00 |   65.00   65.00   65.00   65.00   65.00   65.00   65.00   65.00   65.00   65.00   65.00   65.00   65.00   65.00
               +-------------------------------------------------------------------------------------------------------------------
                   29.22   29.84   30.47   31.09   31.72   32.34   32.97   33.59   34.50   37.50   41.50   45.50   49.50   55.50
                      15      16      17      18      19      20      21      22      23      24      25      26      27      28
TMI-4D7 HSM 45 F AMB,0.86kW/DSC,non-insulated side, solar                                                    Thu Aug  8 08:28:01 1996
                                    Steady-State Temperature Distribution at Time 0.0000E+00
                                                          Z     =  1.1050E+02
    11  -31.72 |   50.86
    10  -32.34 |   50.77
9  -32.97 |   50.69
     8  -33.59 |   50.61
     7  -34.50 |   50.49
     6  -56.25 |   48.69
     5  -78.00 |   49.04
     4  -90.00 |   49.13
     3 -102.00 |   48.95
     2 -120.00 |   47.74
     1 -204.00 |   65.00
               +--------
                   61.50
                      29
```

Figure 8.1-2
HSM HEATING 7 Results for 45°F Ambient
(Concluded)

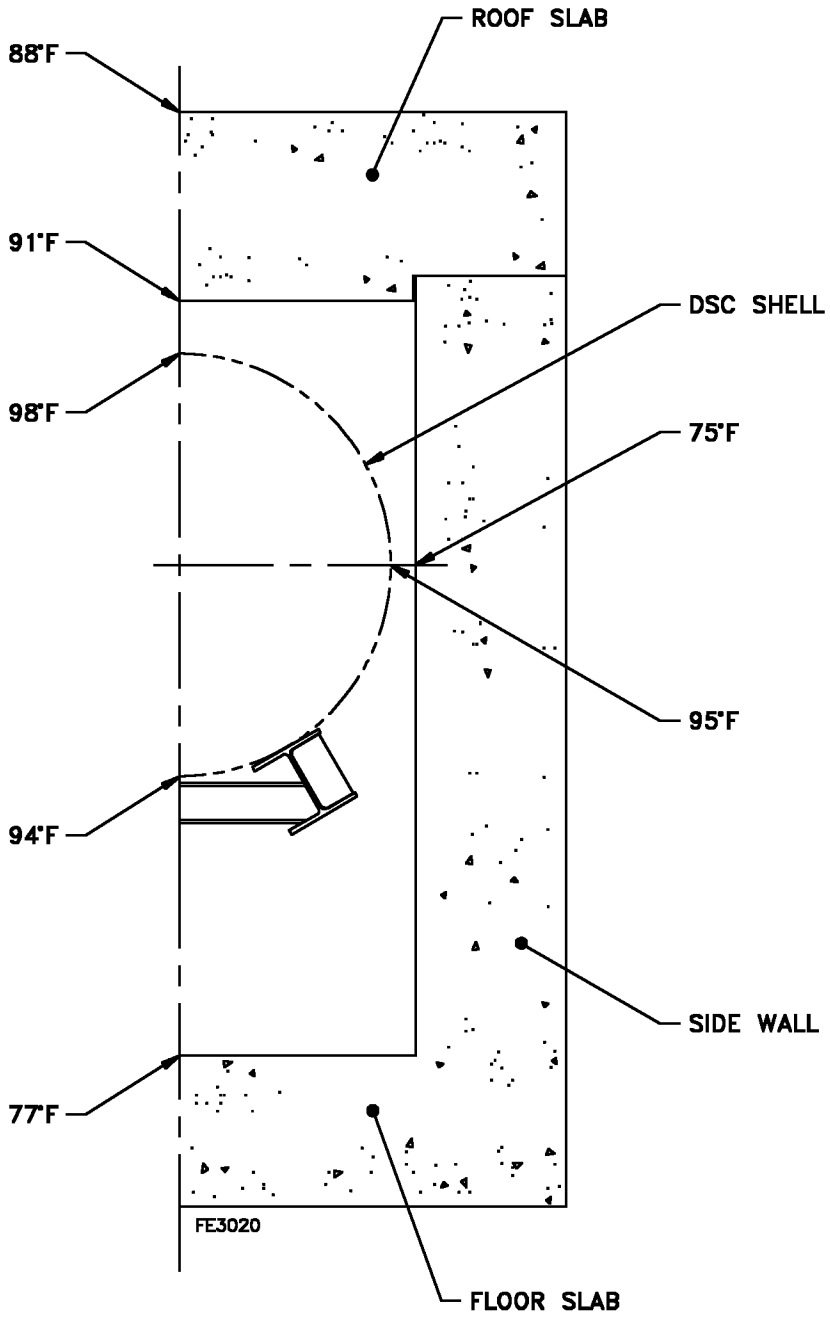

Figure 8.1-3
NUHOMS®-12T HSM Temperature Distribution for 45°F Ambient

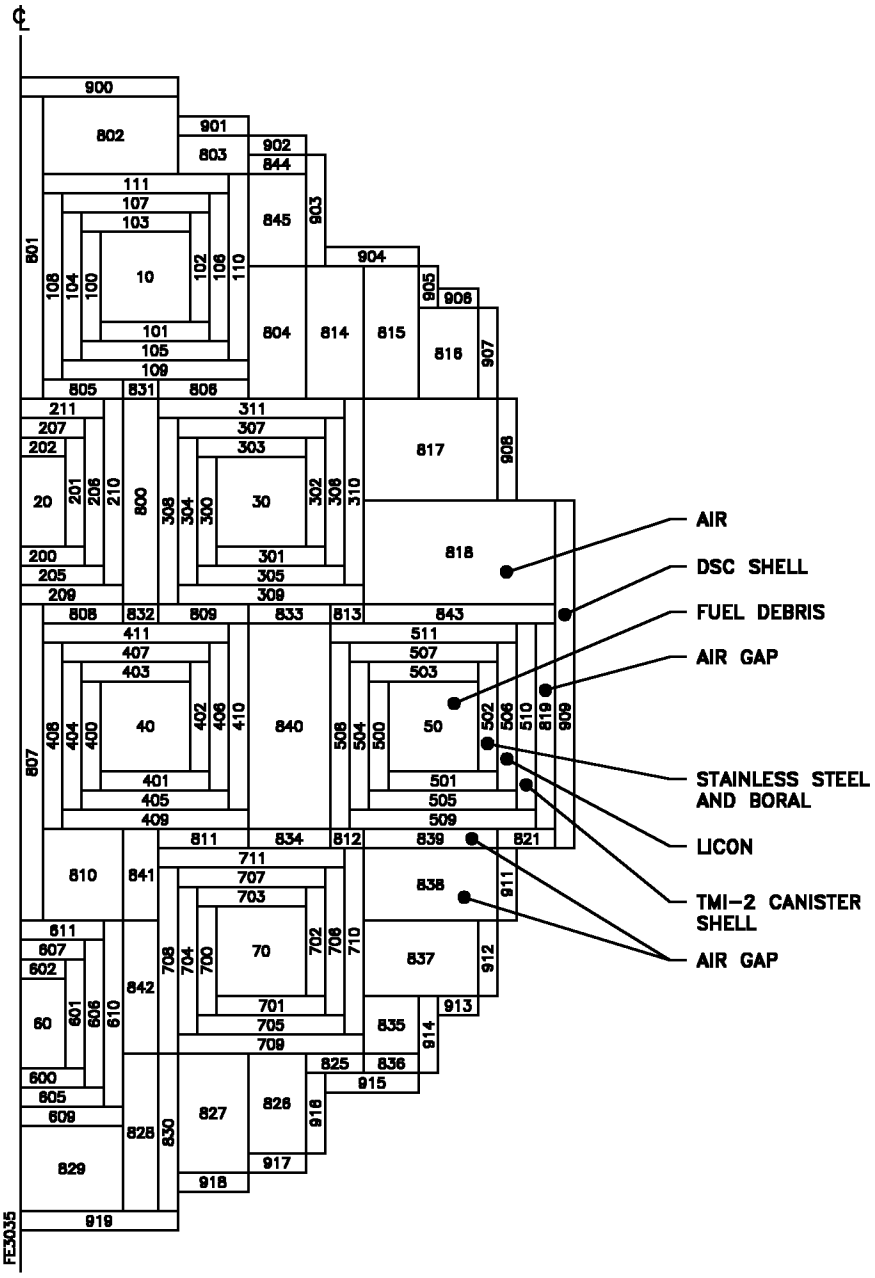

Figure 8.1-4
HEATING 7 Model of NUHOMS®-12T DSC

TMI-2 Fuel Debris Can TMI87.inp, normal at 87F case, horiz with air Thu Aug 8 15:19:10 1996

Steady-State Temperature Distribution at Time 0.0000E+00

59	33.62	134.20	134.20	134.20	134.20	134.20	134.20	134.20	134.20	134.20	134.20	134.20				
58	33.00	134.25	134.25	134.24	134.24	134.24	134.24	134.24	134.24	134.24	134.24	134.24				
57	31.85	143.09	143.32	143.34	143.30	143.27	143.11	143.04	142.18	141.85	135.94	134.20	134.20	134.20	134.20	
56	31.23	147.75	148.25	148.30	148.24	148.20	148.00	147.91	146.90	146.51	138.74	134.25	134.24	134.24	134.24	
55	30.41	153.49	154.76	154.85	154.71	154.67	154.46	154.38	153.60	153.35	149.00	148.17	147.16	147.07	146.58	
54	29.49	159.00	162.54	162.54	162.04	161.98	161.81	161.77	161.56	161.53	161.35	161.34	161.30	161.30	161.36	
53	29.24	160.00	162.58	162.56	162.06	162.00	161.83	161.79	161.58	161.55	161.37	161.35	161.31	161.31	161.37	
52	27.59	162.85	163.54	163.55	164.57	164.66	164.78	164.80	164.87	164.87	164.80	164.79	164.64	164.61	164.36	
51	27.33	163.14	163.68	163.68	164.69	164.71	164.82	164.84	164.91	164.91	164.84	164.83	164.69	164.66	164.42	
50	26.48	163.84	164.10	164.10	164.99	165.01	165.09	165.11	165.18	165.19	165.12	165.11	164.97	164.94	164.73	
49	25.86	164.25	164.38	164.38	165.20	165.21	165.28	165.30	165.37	165.37	165.31	165.30	165.16	165.13	164.93	
48	21.41	165.75	165.77	165.77	166.23	166.24	166.29	166.30	166.33	166.33	166.26	166.25	166.13	166.11	165.96	
47	21.30	165.78	165.80	165.80	166.25	166.26	166.31	166.32	166.35	166.35	166.28	166.26	166.15	166.12	165.97	
46	18.33	166.58	166.39	166.39	166.53	166.54	166.56	166.56	166.55	166.55	166.44	166.42	166.29	166.27	166.13	
45	18.08	166.72	166.43	166.43	166.54	166.54	166.56	166.56	166.55	166.55	166.44	166.42	166.29	166.27	166.12	
44	16.43	168.04	166.72	166.72	166.85	166.86	166.87	166.86	166.76	166.73	166.35	166.31	166.08	166.04	165.83	
43	16.17	168.54	166.74	166.73	166.85	166.86	166.87	166.87	166.76	166.74	166.35	166.31	166.07	166.04	165.83	
42	16.03	168.87	169.02	169.08	169.33	169.36	169.43	169.45	169.51	169.50	165.65	165.64	165.36	165.32	165.00	
41	15.78	168.89	169.04	169.09	169.34	169.37	169.44	169.45	169.52	169.52	165.64	165.64	165.36	165.32	165.00	
40	14.13	171.18	171.16	171.16	171.06	171.04	170.93	170.87	169.87	169.87	165.79	165.79	165.44	165.43	165.31	
39	13.88	171.21	171.19	171.18	171.09	171.06	170.96	170.95	169.92	169.92	165.81	165.81	165.44	165.43	165.31	
38	9.44	171.81	171.79	171.78	171.67	171.64	171.55	171.53	170.48	170.48	165.97	165.97	165.55	165.55	165.45	
37	4.88	171.71	171.69	171.68	171.58	171.55	171.46	171.45	170.55	170.54	165.79	165.79	165.39	165.38	165.25	
36	4.62	171.70	171.67	171.67	171.56	171.54	171.44	171.32	170.54	170.54	165.77	165.76	165.39	165.38	165.24	
35	2.97	170.71	170.73	170.73	170.71	170.70	170.66	170.64	170.51	170.51	165.58	165.58	165.25	165.20	164.82	
34	2.72	170.71	170.72	170.73	170.71	170.70	170.66	170.64	170.51	170.50	165.58	165.57	165.25	165.20	164.82	
33	1.97	169.45	168.36	168.35	168.33	168.31	168.25	168.23	167.99	167.95	167.40	167.32	166.82	166.74	166.19	
32	1.72	169.16	168.35	168.35	168.33	168.31	168.25	168.22	167.99	167.95	167.40	167.33	166.83	166.74	166.19	
31	.07	168.44	168.32	168.32	168.44	168.45	168.45	168.45	168.36	168.34	168.03	167.98	167.65	167.59	167.21	
30	.00	168.42	168.31	168.31	168.44	168.45	168.45	168.45	168.36	168.34	168.03	167.99	167.65	167.59	167.21	
29	-.19	168.36	168.31	168.31	168.45	168.45	168.46	168.45	168.37	168.34	168.04	167.99	167.66	167.60	167.23	
28	-9.19	167.60	167.64	167.64	167.94	167.94	167.96	167.96	167.87	167.85	167.53	167.48	167.12	167.06	166.65	
27	-9.44	167.53	167.60	167.60	167.90	167.92	167.94	167.94	167.86	167.83	167.51	167.46	167.10	167.04	166.61	
26	-11.09	166.98	167.30	167.29	167.08	167.05	166.92	166.88	166.60	166.55	165.88	165.79	165.23	165.14	164.63	
25	-11.34	166.83	167.29	167.29	167.08	167.04	166.92	166.88	166.60	166.55	165.88	165.78	165.22	165.13	164.62	
24	-11.40	166.79	167.21	167.21	167.00	166.96	166.83	166.78	166.43	166.34	164.92	164.83	164.31	164.23	163.74	
23	-11.96	166.34	166.52	166.51	166.27	166.21	165.94	165.83	164.76	164.36	155.38	155.36	155.32	155.30	155.05	
22	-12.21	166.12	166.22	166.21	165.95	165.88	165.56	165.43	164.12	163.66	155.35	155.35	155.32	155.29	155.05	
21	-13.86	164.54	164.48	164.44	164.04	163.93	163.46	163.28	161.56	161.14	155.06	155.06	154.62	154.58	154.45	
20	-14.12	164.30	164.23	164.20	163.79	163.68	163.21	163.03	161.33	160.92	155.02	155.02	154.58	154.57	154.45	
19	-16.64	162.24	162.18	162.15	161.96	161.92	161.76	161.71	161.32	161.30	154.70	154.70	154.36	154.35	154.28	
18	-16.89	162.24	162.17	162.15	161.95	161.92	161.76	161.71	161.31	161.30	154.67	154.67	154.33	154.33	154.25	
17	-18.55	161.96	161.93	161.92	161.81	161.79	161.70	161.67	160.95	160.95	154.42	154.42	154.11	154.11	154.05	
16	-18.80	161.96	161.93	161.92	161.81	161.79	161.70	161.69	160.90	160.90	154.37	154.37	154.07	154.07	154.01	
15	-23.11	161.60	161.57	161.56	161.43	161.41	161.31	161.29	160.13	160.13	153.14	153.14	153.17	153.17	153.12	
14	-23.37	161.56	161.53	161.51	161.39	161.37	161.26	161.25	160.08	160.07	153.03	153.03	153.10	153.14	153.09	
13	-25.02	161.25	161.22	161.20	161.08	161.05	160.94	160.93	159.73	159.72	152.20	152.18	151.49	151.40	150.93	
12	-25.27	161.19	161.16	161.15	161.02	161.00	160.89	160.87	159.67	159.67	152.18	152.16	151.49	151.39	150.92	
11	-25.86	161.06	161.03	161.01	160.89	160.86	160.75	160.73	159.53	159.53	152.15	151.76	150.17	149.98	149.04	
10	-26.48	160.90	160.87	160.86	160.73	160.70	160.59	160.57	159.35	159.35	151.64	151.09	148.69	148.40	147.03	
9	-27.80	160.53	160.50	160.49	160.36	160.33	160.20	160.18	158.88	158.88	149.42	148.67	145.14	144.71	142.72	
8	-28.05	160.49	160.46	160.45	160.32	160.29	160.14	159.87	158.77	158.77	148.80	148.02	144.35	143.91	141.87	
7	-29.70	157.52	157.53	157.53	157.58	157.60	157.67	157.69	157.99	158.00	143.34	142.31	138.46	138.02	136.18	
		.00	1.46	1.71	3.36	3.62	4.50	4.75	6.41	6.66	8.96	9.21	10.87	11.12	12.62	
		1	2	3	4	5	6	7	8	9	10	11	12	13	14	

Figure 8.1-5
NUHOMS®-12T DSC Internal Temperature Distribution for 87°F Ambient

TMI-2 Fuel Debris Can TMI87.inp, normal at 87F case,horiz with air Thu Aug 8 15:19:10 1996
Steady-State Temperature Distribution at Time 0.0000E+00

59	33.62														
58	33.00														
57	31.85	134.20	134.20	134.20											
56	31.23	134.24	134.22	134.20	134.20										
55	30.41	146.19	139.87	134.22	134.20	134.20									
54	29.49	161.38	161.65	161.62	134.20	134.20									
53	29.24	161.39	161.68	161.69	134.20	134.20									
52	27.59	164.03	162.74	162.73	134.20	134.20									
51	27.33	164.39	162.88	162.88	134.20	134.20									
50	26.48	164.71	163.33	163.32	134.20	134.20	134.20	134.20	134.20						
49	25.86	164.92	163.62	163.61	134.25	134.24	134.23	134.21	134.18	134.20					
48	21.41	165.94	165.06	165.06	148.42	147.77	143.76	143.11	132.57	132.54	131.00				
47	21.30	165.96	165.09	165.08	148.73	148.08	144.04	143.39	132.57	132.54	131.00	131.00			
46	18.33	166.11	165.49	165.49	155.84	155.35	152.03	151.45	140.66	139.20	131.00	131.00			
45	18.08	166.09	165.51	165.51	156.47	156.00	152.85	152.28	141.22	139.67	131.00	131.00			
44	16.43	165.80	165.58	165.58	160.58	160.33	158.68	158.30	144.31	142.34	131.00	131.00			
43	16.17	165.80	165.58	165.56	161.22	161.00	159.72	159.53	144.70	142.68	131.00	131.00			
42	16.03	164.93	164.45	164.36	161.58	161.38	160.30	160.27	144.91	142.87	131.00	131.00	131.00		
41	15.78	164.93	164.45	164.36	161.58	161.39	160.30	160.28	145.24	143.17	131.23	131.02	131.00		
40	14.13	165.27	164.99	164.94	163.18	163.03	160.06	160.05	146.73	144.68	131.71	131.09	131.00		
39	13.88	165.28	165.00	164.95	163.20	163.15	160.04	160.02	146.90	144.86	131.76	131.09	131.00		
38	9.44	165.42	165.17	165.13	163.53	163.48	159.92	159.91	147.80	145.82	131.93	131.11	131.00	131.01	131.01
37	4.88	165.22	164.93	164.87	163.08	163.04	159.83	159.82	146.40	144.53	134.60	134.14	131.43	131.02	131.01
36	4.62	165.21	164.92	164.86	163.06	162.90	159.84	159.83	146.09	144.24	134.67	134.22	131.45	131.02	131.01
35	2.97	164.75	164.20	164.11	161.22	161.04	159.97	159.95	143.40	141.82	135.00	134.58	131.60	131.02	131.01
34	2.72	164.75	164.20	164.10	161.21	161.03	159.97	159.92	142.75	141.35	135.08	134.67	131.75	131.02	131.01
33	1.97	166.08	165.32	165.30	144.35	144.28	143.23	143.04	140.33	139.81	135.34	135.01	132.65	132.50	131.04
32	1.72	166.08	165.31	165.29	144.30	144.28	143.22	143.03	140.33	139.82	135.34	135.01	132.62	132.55	131.04
31	.07	167.10	164.92	164.91	144.43	144.42	142.17	142.05	140.67	140.37	137.53	137.26	131.99	131.96	131.02
30	.00	167.13	164.91	164.89	144.44	144.43	142.14	142.05	140.67	140.37	137.53	137.33	131.97	131.94	131.02
29	-.19	167.20	164.87	164.86	144.45	144.44	142.07	142.04	140.67	140.38	137.56	137.48	131.92	131.89	131.02
28	-9.19	166.62	164.05	164.04	144.03	144.02	141.87	141.84	140.55	140.26	137.51	137.43	131.93	131.91	131.02
27	-9.44	166.48	164.03	164.02	143.99	143.98	141.94	141.84	140.54	140.25	137.48	137.23	132.01	131.99	131.02
26	-11.09	164.54	163.93	163.92	143.62	143.60	142.58	142.41	140.01	139.54	135.32	135.00	132.76	132.69	131.04
25	-11.34	164.53	163.93	163.89	143.64	143.59	142.58	142.41	140.01	139.54	135.31	135.00	132.79	132.70	131.03
24	-11.40	163.65	163.07	163.00	144.42	144.34	143.35	143.19	140.07	139.55	135.12	134.67	132.57	131.10	131.01
23	-11.96	155.00	154.48	154.38	151.82	151.68	150.86	150.82	140.65	139.70	133.33	131.33	131.29	131.01	131.00
22	-12.21	154.99	154.48	154.38	151.83	151.69	150.85	150.84	140.84	139.76	132.79	131.33	131.29		
21	-13.86	154.42	154.17	154.13	152.70	152.59	150.58	150.57	141.33	140.00	131.84	131.27	131.24		
20	-14.12	154.42	154.17	154.13	152.71	152.67	150.54	150.53	141.34	140.00	131.75	131.25	131.22		
19	-16.64	154.25	154.06	154.02	152.76	152.73	150.23	150.22	140.81	139.42	131.10	131.00	131.00		
18	-16.89	154.23	154.04	154.00	152.75	152.72	150.19	150.18	140.68	139.29	131.17	131.16			
17	-18.55	154.03	153.85	153.81	152.60	152.56	149.94	149.93	139.53	138.18	131.71	131.70			
16	-18.80	153.99	153.81	153.78	152.56	152.53	149.90	149.89	139.26	137.93	131.75	131.75			
15	-23.11	153.10	152.92	152.88	151.56	151.52	148.89	148.88	130.68	130.66	131.00	131.00			
14	-23.37	153.08	152.88	152.85	151.52	151.36	148.81	148.80	130.67	130.66	131.00				
13	-25.02	150.85	150.37	150.30	148.70	148.64	148.31	148.30	130.47	130.45					
12	-25.27	150.84	150.36	150.29	148.69	148.63	148.29	148.25	130.42	130.41					
11	-25.86	148.89	147.86	147.61	131.39	131.35	131.20	131.15	130.30	130.30					
10	-26.48	146.80	145.32	145.01	131.30	131.31	131.18	131.14	130.30						
9	-27.80	142.40	140.41	140.08	130.97	130.97									
8	-28.05	141.54	139.49	139.15	130.91	130.91									
7	-29.70	135.86	133.62	133.23	130.48	130.48									
		12.87	14.52	14.77	20.12	20.38	22.02	22.27	25.86	26.48	31.27	31.53	33.18	33.43	33.44
		15	16	17	18	19	20	21	22	23	24	25	26	27	28

Figure 8.1-5
NUHOMS®-12T DSC Internal Temperature Distribution for 87°F Ambient
(Continued)

TMI-2 Fuel Debris Can TMI87.inp, normal at 87F case,horiz with air Thu Aug 8 15:19:10 1996
Steady-State Temperature Distribution at Time 0.0000E+00

```
   59   33.62 |
   58   33.00 |
   57   31.85 |
   56   31.23 |
   55   30.41 |
   54   29.49 |
   53   29.24 |
   52   27.59 |
   51   27.33 |
   50   26.48 |
   49   25.86 |
   48   21.41 |
   47   21.30 |
   46   18.33 |
   45   18.08 |
   44   16.43 |
   43   16.17 |
   42   16.03 |
   41   15.78 |
   40   14.13 |
   39   13.88 |
   38    9.44 |  131.00
   37    4.88 |  131.00
   36    4.62 |  131.00
   35    2.97 |  131.00
   34    2.72 |  131.00
   33    1.97 |  131.00
   32    1.72 |  131.00
   31     .07 |  131.00
   30     .00 |  131.00
   29    -.19 |  131.00
   28   -9.19 |  131.00
   27   -9.44 |  131.00
   26  -11.09 |  131.00
   25  -11.34 |  131.00
   24  -11.40 |  131.00
   23  -11.96 |  131.00
   22  -12.21 |
   21  -13.86 |
   20  -14.12 |
   19  -16.64 |
   18  -16.89 |
   17  -18.55 |
   16  -18.80 |
   15  -23.11 |
   14  -23.37 |
   13  -25.02 |
   12  -25.27 |
   11  -25.86 |
   10  -26.48 |
    9  -27.80 |
    8  -28.05 |
    7  -29.70 |
           +---------
               33.62
                  29
```

Figure 8.1-5
NUHOMS®-12T DSC Internal Temperature Distribution for 87°F Ambient
(Continued)

```
TMI-2 Fuel Debris Can TMI87.inp, normal at 87F case,horiz with air                                  Thu Aug  8 15:19:10 1996
                                Steady-State Temperature Distribution at Time 0.0000E+00

     6  -29.95 |  157.51  157.52  157.52  157.57  157.58  157.65  157.68  157.96  157.96  142.08  141.00  137.40  137.00  135.32
     5  -30.41 |  154.01  154.00  154.00  153.97  153.95  153.89  153.86  153.31  152.85  139.45  138.23  135.36  135.06  133.77
     4  -31.23 |  147.72  147.68  147.67  147.49  147.43  147.19  147.07  145.76  145.20  134.33  131.54  131.41  131.37  131.05
     3  -31.85 |  142.88  142.82  142.80  142.53  142.45  142.13  142.00  140.60  140.15  132.64  131.52  131.39  131.36  131.03
     2  -33.00 |  133.96  133.87  133.83  133.45  133.37  133.04  132.93  132.08  131.92  130.46  130.30
     1  -33.62 |  133.95  133.85  133.81  133.43  133.35  133.02  132.91  132.06  131.91  130.46  130.30
                +-------------------------------------------------------------------------------------------------------------
                     .00    1.46    1.71    3.36    3.62    4.50    4.75    6.41    6.66    8.96    9.21   10.87   11.12   12.62
                       1       2       3       4       5       6       7       8       9      10      11      12      13      14
```

```
TMI-2 Fuel Debris Can TMI87.inp, normal at 87F case,horiz with air                                  Thu Aug  8 15:19:10 1996
                                Steady-State Temperature Distribution at Time 0.0000E+00

     6  -29.95 |  135.02  132.78  132.24  130.42  130.42
     5  -30.41 |  133.51  131.37  130.34  130.30  130.30
     4  -31.23 |  130.98  130.41  130.30  130.30
     3  -31.85 |  130.96  130.40  130.30
     2  -33.00 |
     1  -33.62 |
                +-------------------------------------------------------------------------------------------------------------
                   12.87   14.52   14.77   20.12   20.38   22.02   22.27   25.86   26.48   31.27   31.53   33.18   33.43   33.44
                      15      16      17      18      19      20      21      22      23      24      25      26      27      28
```

```
TMI-2 Fuel Debris Can TMI87.inp, normal at 87F case,horiz with air                                  Thu Aug  8 15:19:10 1996
                                Steady-State Temperature Distribution at Time 0.0000E+00

     6  -29.95 |
     5  -30.41 |
     4  -31.23 |
     3  -31.85 |
     2  -33.00 |
     1  -33.62 |
                +--------
                   33.62
                   29
```

Figure 8.1-5
NUHOMS®-12T DSC Internal Temperature Distribution for 87°F Ambient
(Concluded)

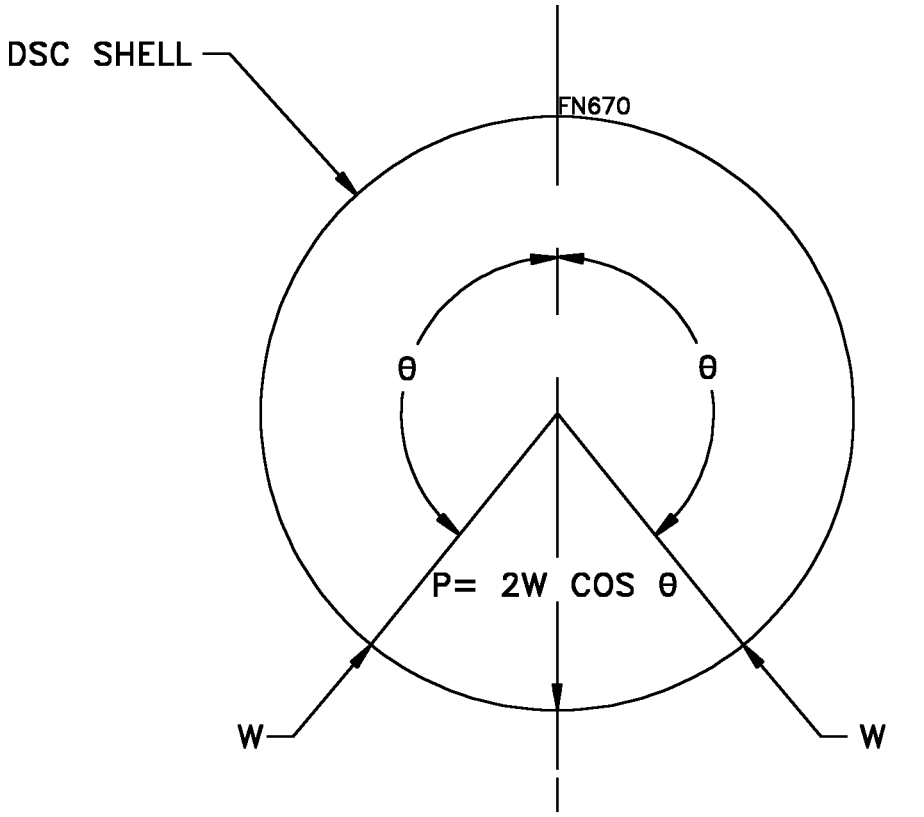

KEY:
P= DEAD WEIGHT OF LOADED DSC.
W= DSC SUPPORT RAIL REACTION.

Figure 8.1-6
DSC Shell Stress Analysis Diagram

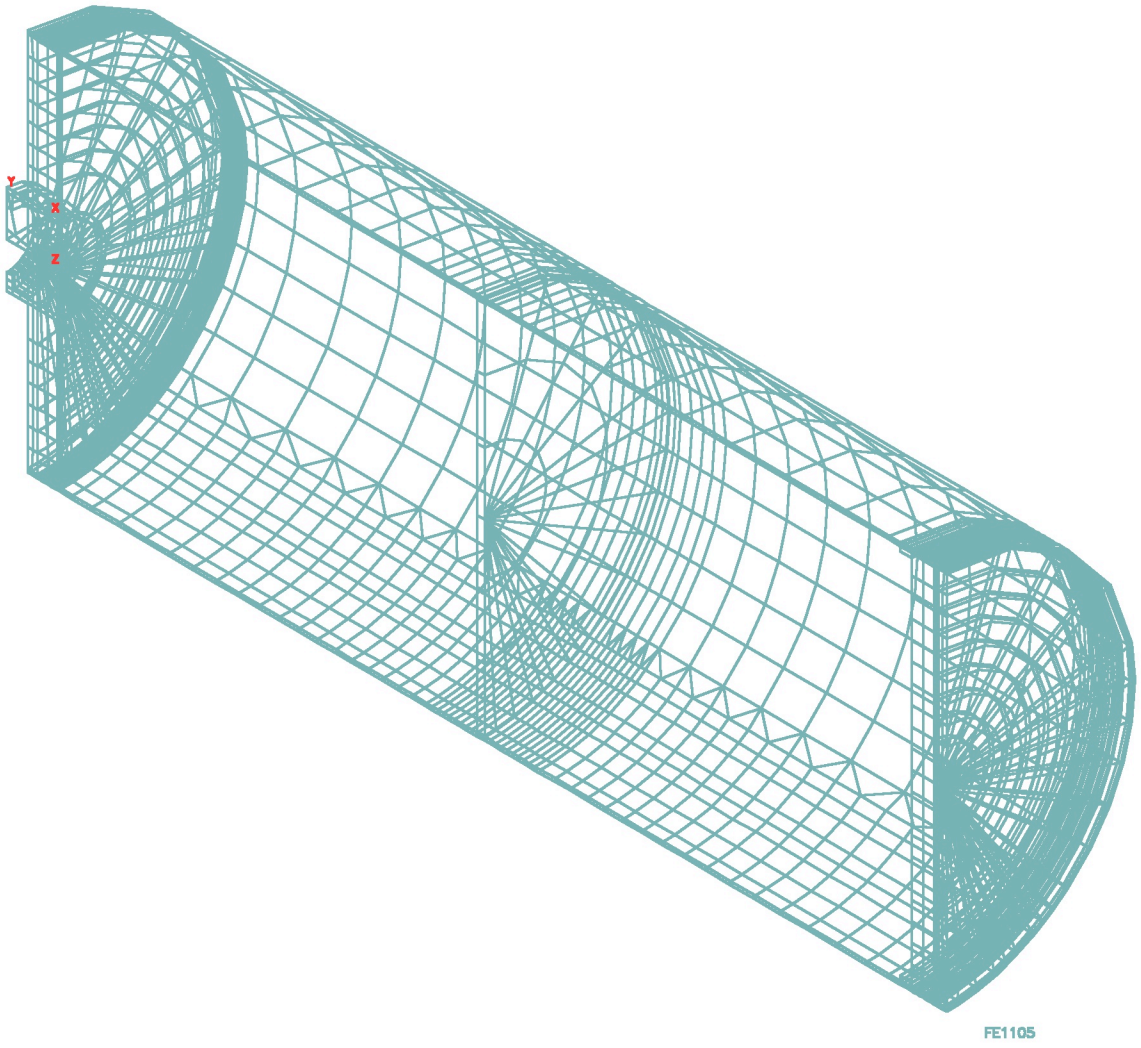

Figure 8.1-7
DSC Shell Axisymmetric Analytical Model

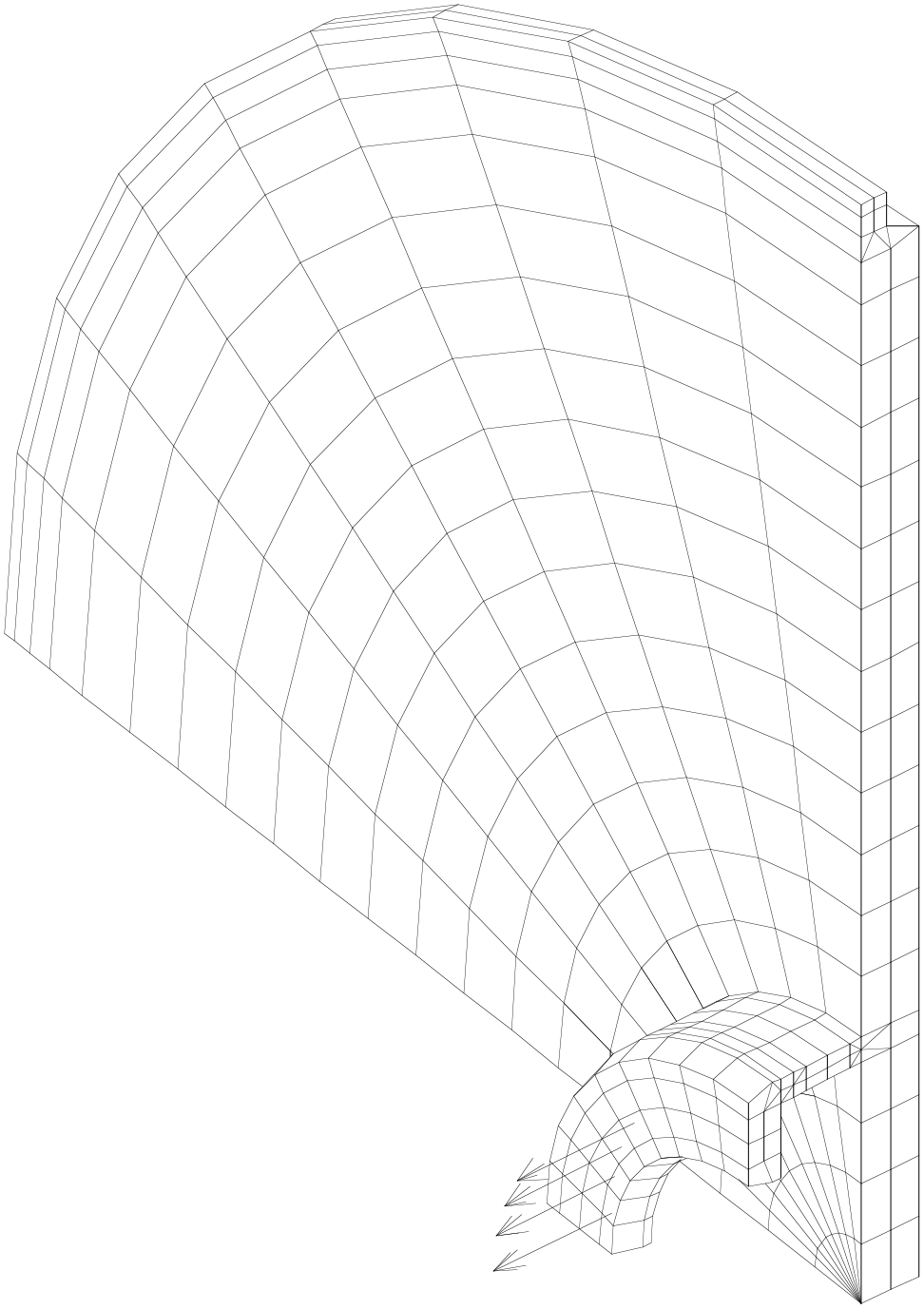

Figure 8.1-8
DSC Bottom Cover Plate/Grapple Ring Analytical Model

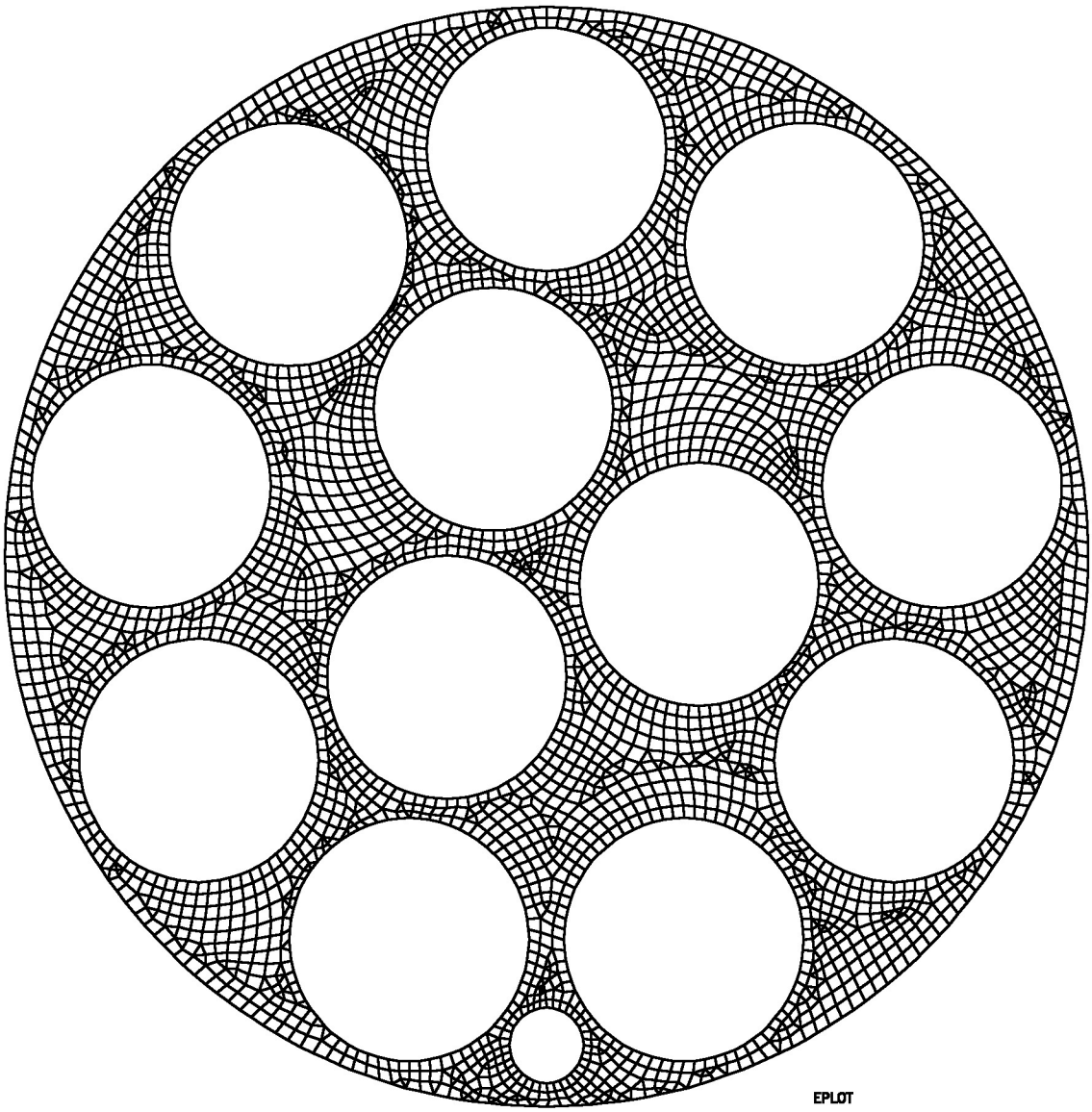

Figure 8.1-9
NUHOMS®-12T DSC Spacer Disc Analytical Model

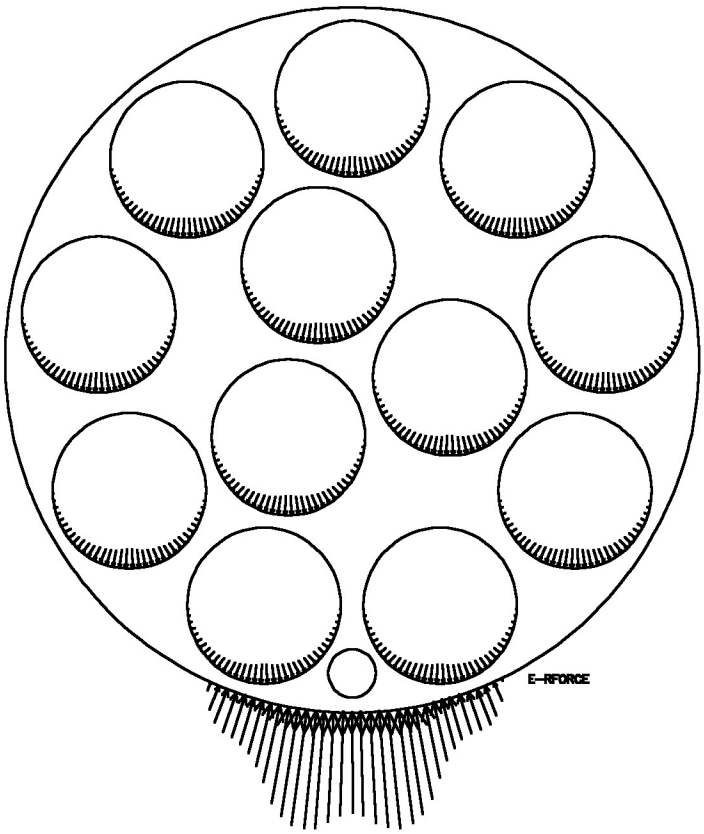

Component	Dead Load		8g Load[2]
F_P, Spacer Disk	495 lb	--	3.96 k
F_F, TMI-2 Canisters	21.78 lb/in	5096 lb[1]	40.77 k
F_{RGS}, Support Rod	1.29 lb/in	151 lb	1.21 k
$F_{Applied}$, Total Applied Load			45.94 k
$F_{Reaction}$, ANSYS Reaction Load			44.30 k
Ratio ($F_{Applied}$/ $F_{Reaction}$)			1.04

(1) Dead load is calculated for 12 heaviest TMI-2 canisters, maximum spacer disc spacing of 19.5 inches.

(2) Represents worst case transportation/transfer loads applied in 0-180 degree plane.

Figure 8.1-10
NUHOMS®-12T DSC Spacer Disc Applied 8g Loading

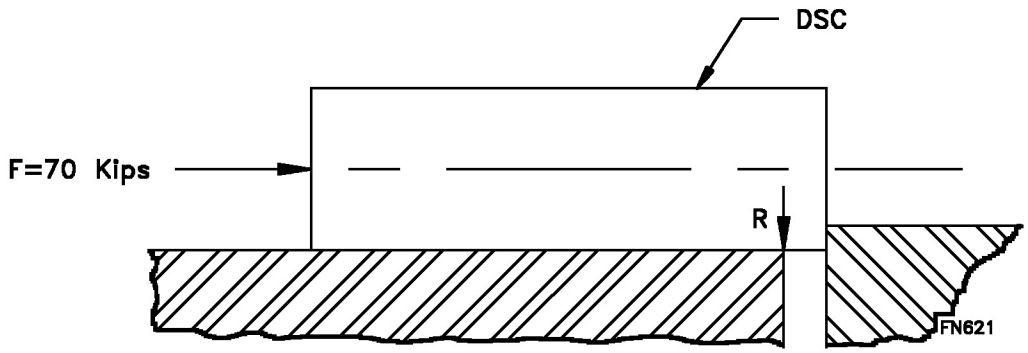

Figure 8.1-11
DSC Axial Jam Condition

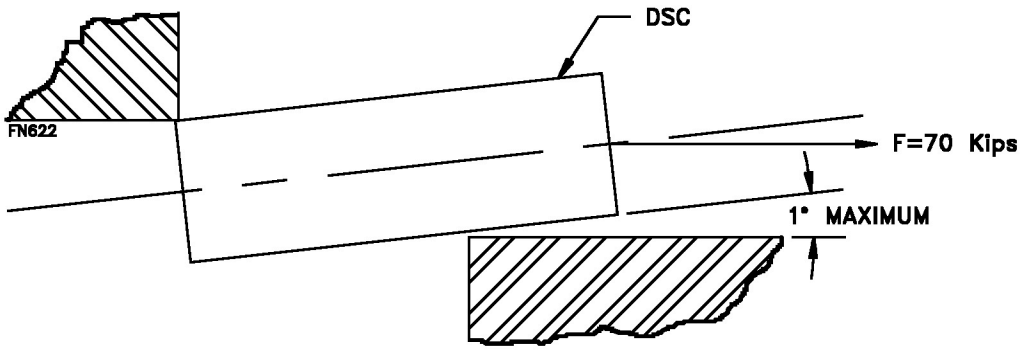

Figure 8.1-12
DSC Binding (Pinching) Condition

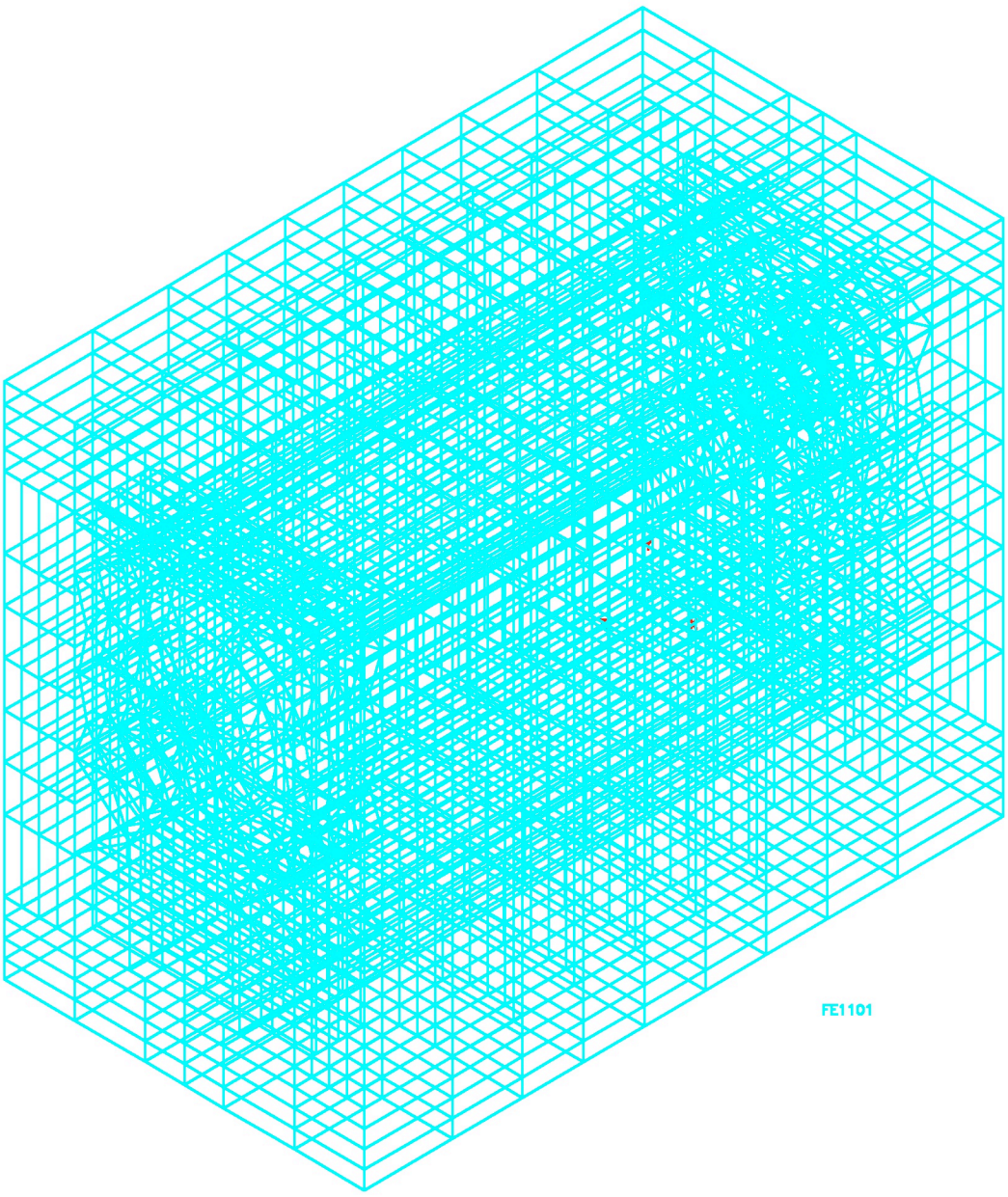

Figure 8.1-13
Prefabricated HSM Analytical Model

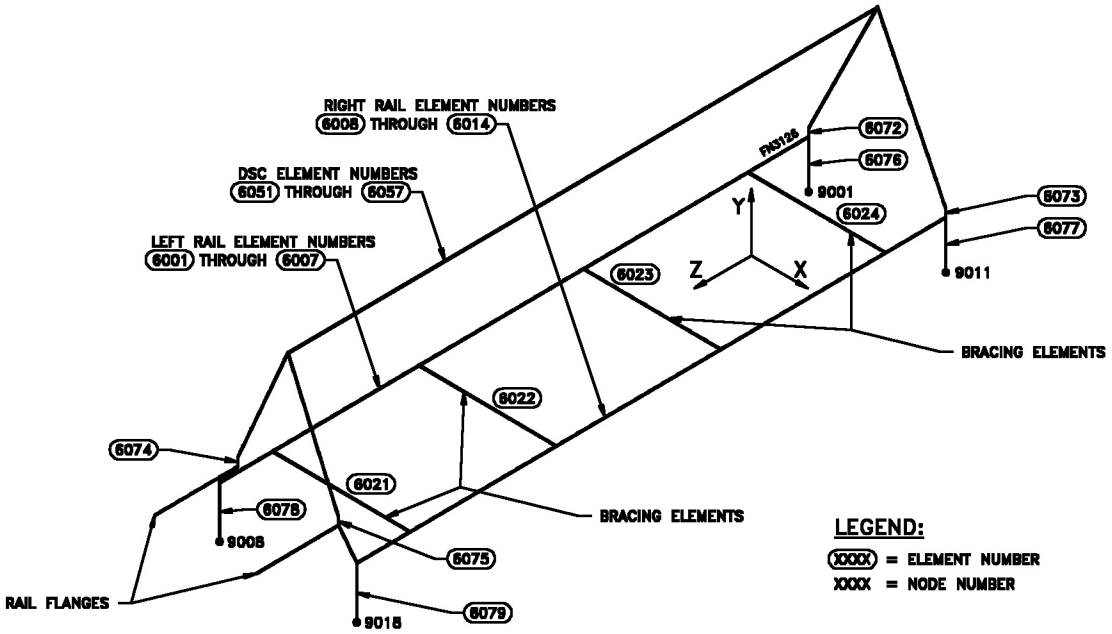

Figure 8.1-14
Analytical Model for DSC Support Structure

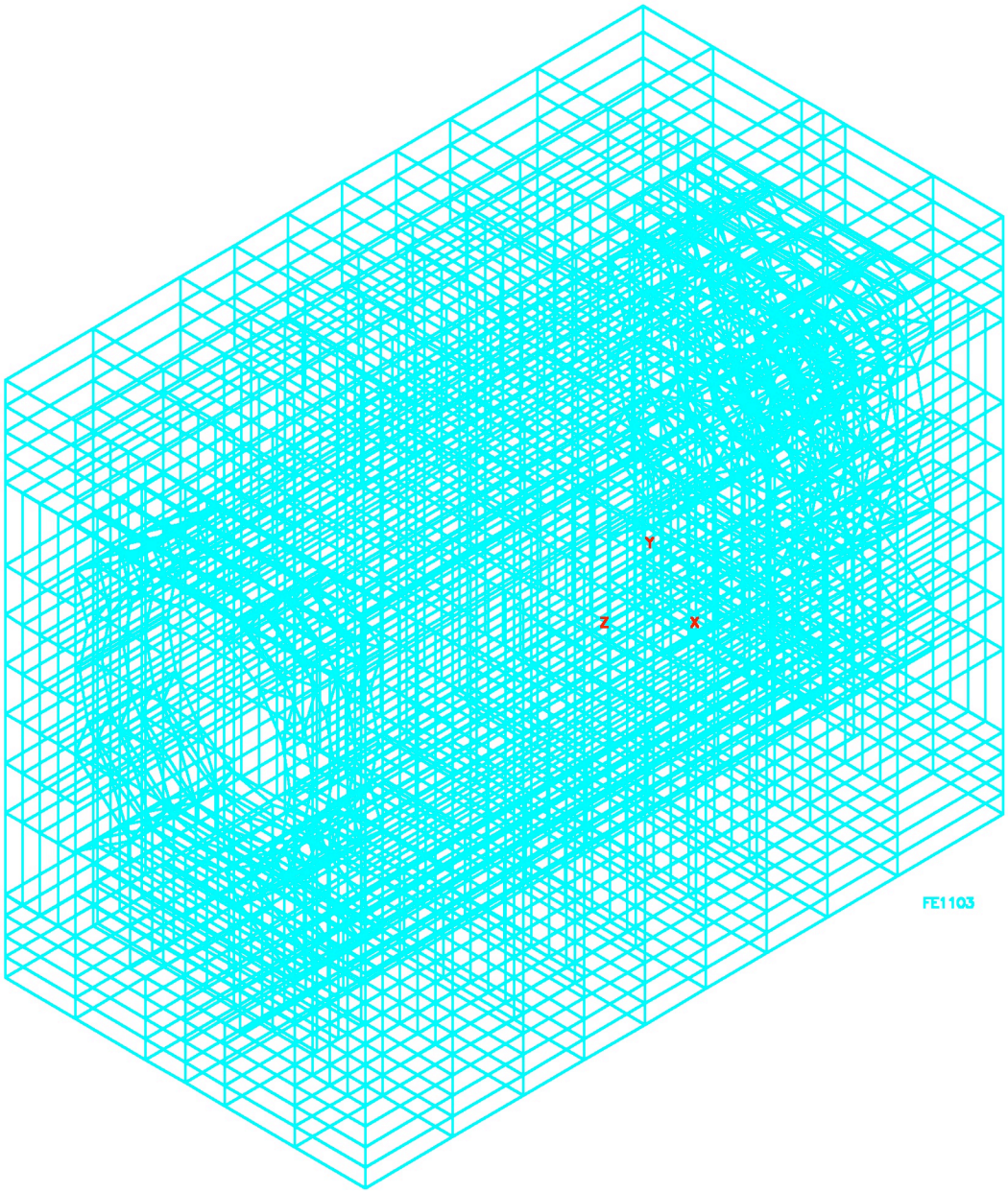

Figure 8.1-15
Analytical Model for HSM Base Unit
Thermal Conditions

Security-Related Information
Figure Withheld Under 10 CFR 2.390.

Figure 8.1-16
Typical HSM Reinforcement

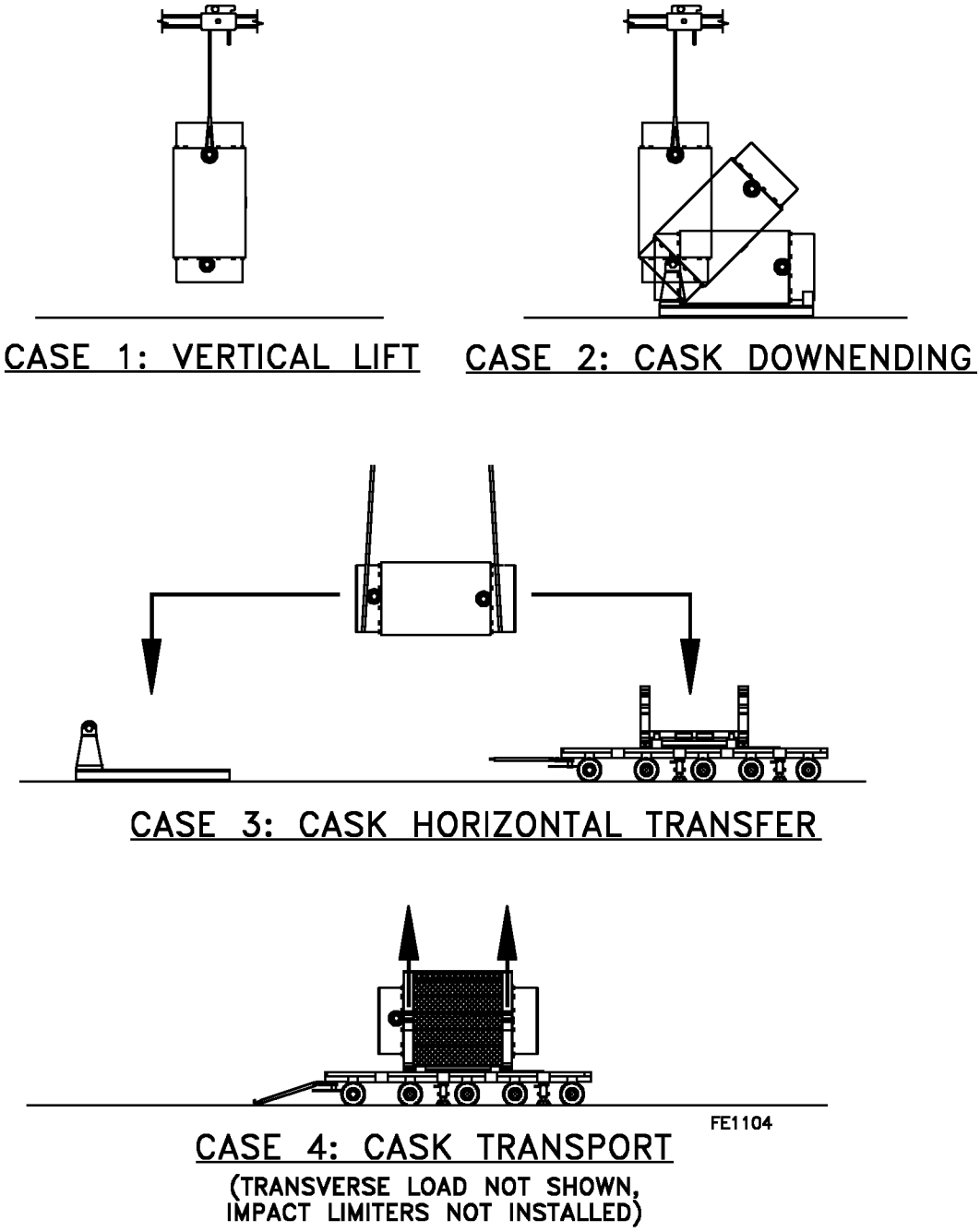

Figure 8.1-17
MP187 Cask Handling Loads

8.2 Accident Analyses for the ISFSI

The design basis accident events specified by ANSI/ANS 57.9-1984, and other credible and non-credible accidents postulated to affect the normal safe operation of the TMI-2 ISFSI are addressed in this section of the SAR. In accordance with 10 CFR Part 72, analyses are provided for a range of hypothetical accidents, including those with the potential to result in an annual dose greater than 25 mrem outside the owner-controlled area. The postulated accidents considered in the analyses and the associated NUHOMS®-12T components affected by each accident condition are shown in Table 8.2-1.

Based on a review of the Safety Analysis Reports of other facility activities within the INTEC site, it has been determined that no credible explosion or fire associated with a co-located INTEC facility could occur that would pose a threat to the ISFSI which either exceeds a vehicular fire related to an ISFSI service vehicle (Section 8.2.9), or exceed the potential impacts of either the wind loading, or airborne missile impact of a tornado scenario (Section 8.2.2). Thus, the impacts of any credible accidents involving fire or explosion at co-located INTEC facilities are bounded by the analysis of the design basis tornado and the combustion of fuel from a ISFSI service vehicle.

In the following sections, each accident condition is analyzed to demonstrate that the applicable requirements of 10 CFR 72.122 are met and that adequate safety margins exist for the TMI-2 ISFSI design. Radiological calculations are performed to confirm that on-site and off-site dose rates are within acceptable limits. The resulting accident condition stresses in the NUHOMS®-12T system components are evaluated and compared with the applicable code limits set forth in Section 3.2. Where appropriate, these accident condition stresses are combined with those of normal operating loads in accordance with the load combination definitions in Tables 3.2-4, 3.2-5, and 3.2-6.

The postulated accident conditions addressed in this SAR section include:

A. Reduced HSM self-shielding.

B. Tornado winds and tornado generated missiles.

C. Design basis earthquake.

D. Design basis flood.

E. Accidental cask drop.

F. Lightning effects.

G. Postulated DSC leakage.

H. DSC Pressurization.

I. On-site fire and explosion hazards.

J. Blockage of gap between adjacent modules.

For each postulated accident condition, the cause, the consequences (structural, thermal, radiological), and the recovery measures are presented.

8.2.1 Reduced HSM Self-Shielding

This postulated accident is the partial loss of self-shielding for the HSM side walls provided by the adjacent HSMs. All other components of the NUHOMS®-12T system are assumed to be functioning normally.

8.2.1.1 Cause of Accident

An array of free-standing prefabricated HSMs is designed to remain intact for all postulated events. In the unlikely event that large settlements of the ISFSI foundation occur, or a seismic event displaces individual HSMs, the resultant shifting of adjacent HSMs may cause the HSMs to separate. Although adequate means are provided to ensure that the spacing of adjacent HSMs is maintained, it is postulated for the sake of this conservative analysis that an HSM in the middle of the array is separated. The HSM now rests against the adjacent HSM side wall, moves forward/backward, and/or projects out from the face of adjacent HSMs. The arrangement will increase the distance between the HSM on the opposite side from the nominal spacing of six inches between HSMs, or result in HSMs staggered in plan from adjacent modules.

8.2.1.2 Accident Analysis

A separation of the HSMs will not result in any structural consequences that will affect the safe operation of the NUHOMS®-12T system. Potential thermal effects of this accident result from the HSM side walls coming in contact with each other or exposure of additional side walls due to the longitudinal displacement. For the thermal accident case considered, the HSMs were analyzed assuming fully insulated boundaries on both side walls, and the accident calculations presented in Section 8.1.3 bound the thermal consequences of this accident for the HSM, DSC, and TMI-2 canister maximum temperatures. The radiological consequences of this accident are described in the paragraph below.

8.2.1.3 Accident Dose Calculations

The off-site radiological effects resulting from a partial loss of adjacent HSM shielding are a very small increase in the air scattered (skyshine), and direct doses between separated HSMs. On-site radiological effects result from an increase in direct radiation during recovery operations and increased skyshine radiation. The calculation of these doses during normal conditions is described in Section 7.3.2.2.

The peak dose rate expected for any surface location of an uncovered interior wall is about 270 mrem per hour. This represents an external dose only, as no radionuclide releases will occur as a result of this event. The actual exposure received by workers during the recovery from this event is dependent on the final configuration of the HSMs. Conservatively assuming two workers spend an hour at the highest dose location, the resultant dose will be 0.54 person-rem. Exposure increases due to the reduced shielding at locations outside the INTEC will be negligible and no increase in exposure at locations beyond the INL controlled area boundary will be observed.

8.2.1.4 Recovery

Recovery from an accident resulting in a partial loss of adjacent HSM shielding requires repositioning of the HSMs. This can be accomplished by using hydraulic jacks or by reinstalling the HSM lifting eyes and repositioning the affected HSMs with a suitable crane. As stated above, an exposure of 0.54 person-rem is conservatively estimated for workers during recovery from this event. Severe foundation settlement requires that the affected HSMs be unloaded and removed from service until foundation repairs are made.

8.2.2 Tornado Winds/Tornado Missile

8.2.2.1 Cause of Accident

In accordance with ANSI-57.9 and 10 CFR 72.122, the TMI-2 ISFSI NUHOMS®-12T HSM is designed for tornado effects, including tornado wind loads. Although not specifically required by ANSI-57.9 and 10 CFR 72.122, the HSM is also designed for tornado missile effects. For this evaluation, the NUHOMS®-12T system is designed to be located on the INL in the State of Idaho. As described in Section 3.2.1, the design basis for this postulated accident is provided by the Region III tornado wind loadings specified by NUREG-0800 [8.] and NRC Regulatory Guide 1.76 [8.22] modified in accordance with References8.23 and 8.24.

8.2.2.2 Accident Analysis

The applicable design parameters for the design basis tornado (DBT) are specified in Section 3.2.1. The tornado wind and tornado missile loads acting on the HSM are detailed in Section 3.2.1.4. The front and rear faces of all modules and the side walls of the end modules of an array resist the tornado wind and missile loads. The pressures used for the stability evaluations of the HSM conservatively used a value of 240 mph rather than apply the Region III tornado wind

speed reduction of 240 mph to 200 mph permitted by References 8.25 and 8.26. The missle impact analysis in Section 8.2.2.8 uses the 200 mph allowed by References 8.23 and 2.24. The tornado loads are assumed to act on a single free-standing HSM. This case conservatively envelopes the effects on an HSM array.

A. Effect of DBT Wind Pressure Loads on HSM

The maximum DBT generated wind loads for a 200 mph maximum wind speed are 99 lb/ft^2 and 62 lb/ft^2 on the windward and leeward walls of an HSM. The exterior side wall and roof are also subjected to a suction load of 87 lb/ft^2. The leeward side of the windward end HSM has no appreciable suction load in an array of HSMs due to the close proximity of the adjacent module. The 62 lb/ft^2 suction load is applicable to the exposed side wall of the leeward end module in the array. In addition, the HSM is subjected to a differential wind pressure load of 1.5 psi (216 psf) suction on the walls and the roof.

The DBT pressures are applied to the HSM as uniformly distributed loads on the walls and roof. The rigidity of the HSM in the transverse direction (frame and shear wall action of a single HSM) is the primary load transfer mechanism assumed in the analysis. The bending moments and shears at critical locations in the HSM walls and roof are calculated by performing an analysis using the ANSYS analytical model of the prefabricated HSM shown in Figure 8.1-13 and Table 8.1-15. The resulting moments and shears are tabulated in Table 8.2-2 and are included in the formulation of HSM load combination results reported in Section 8.3.5.

An analysis is also performed to evaluate the effects of overturning and sliding of a single, free-standing HSM due to a postulated DBT. For the DBT wind overturning analysis, the overturning moment and the resulting stabilizing moments are calculated.

(i) HSM Overturning Analysis

The stabilizing moment (M_{st}) for the windward module plus shield wall in an array is:

$$M_{st} = Wd$$

Where:

W = 302 kips, Weight of HSM plus minimum weight of DSC

d = 61.5 in (5.13 ft), Horizontal distance between center of gravity of HSM to the outer edge of the side wall.

Therefore:

$$M_{st} = 18{,}570 \text{ K-in}$$

and the overturning moment (M_{to}) for the windward module due to DBT wind pressure is:

$$M_{to} = w_1 A_w h/2 + w_3 A_r d$$

Where:

w_1 = (99 – 216 + 62+216) = 161 lb/ft^2, wind load, windward wall

h = 14.5 ft wall height

w_3 = (87 + 216) = 303 lb/ft^2, wind uplift on roof

A_r = 186 ft^2, Roof area

A_w = 263 ft^2, wall area

Therefore:

M_{to} = 7,159 K-in

Since the overturning moment is significantly smaller than the stabilizing moment, the free-standing HSM will not overturn. The resulting factor of safety against overturning effects for DBT wind loads is 2.6.

The (87 + 216) = 303 lb/ft^2 DBT negative pressure acting on the HSM door results in a total load of 12.8 kips, which is reacted by the HSM door embedded anchors. The door embedded anchors have a tensile load capacity that provides a large factor of safety based on this total load.

(ii) HSM Sliding Analysis

To evaluate the potential for sliding of a single, free-standing HSM, the sliding force generated by the postulated DBT wind pressure is compared to the sliding resistance provided by friction between the base of the HSM and the ISFSI basemat.

The force (F_{sl}) required to slide the end module in an array is:

$$F_{sl} = [W - w_3 A_r]\mu$$

Where:

μ = 0.6, coefficient of friction (ACI 349) [8.5]

W, w_3 and A_r are defined above.

Substituting gives:

$$F_{sl} = 147 \text{ kips}$$

The sliding force (F_{hw}) generated by DBT wind pressure for a single HSM is:

$$F_{hw} = w_1 A_w$$

Where: w_1 and A_w are as defined above. Substituting gives:

$$F_{hw} = 43 \text{ kips}$$

Since the horizontal force generated by the postulated DBT is smaller than the force required to slide the end module in an HSM array, the HSM will not slide. The factor of safety against sliding of the HSM due to DBT wind loads is 3.4.

B. HSM Missile Impact Analysis

The side walls and roof slab of the reinforced concrete HSM are 24 and 30 inches thick, respectively. The walls and roof are designed to provide adequate biological shielding and easily meet the minimum acceptable barrier thickness requirements for local damage against tornado generated missiles, as specified for Region III in NUREG-0800, Section 3.5.3, Table 1. To demonstrate the adequacy of the HSM design for tornado missiles, a bounding analysis of the end module in an array is performed. The items evaluated include the resistance to penetration, spalling, scabbing, and perforation for a postulated missile impact. In addition, the tornado missile loads are individually applied to the roof and walls of the HSM analytical model shown in Figure 8.1-13. The resultant tornado missile forces and moments are combined with other loads as required by Table 3.2-4 and the results are reported in Table 8.3-4. For these analyses, a rigid, penetration-resistant missile consisting of a 125 Kg (276 lb), eight inch diameter blunt nosed hardened steel object traveling at 35% of the maximum wind speed (103 fps) is conservatively postulated. The method of analysis is based on the modified National Defense Research Committee (NDRC) formula as recommended in Section 3.5.3 of NUREG-0800.

The doors covering the access openings of the HSM are also evaluated for DBT missile penetration resistance. The HSM front wall access door is constructed of steel plate, and is filled with concrete. The rear door covering the HEPA filter DSC vent area is fabricated from steel plate. Missile impact is resisted by the steel plate. The results of these evaluations indicate that the HSM access and HEPA filter enclosure doors provide sufficient capacity to preclude penetration.

The DBT missile penetration resistance analyses for the HSM are presented in the following paragraphs.

(i) Missile Impact Penetration Resistance Analysis

The modified NDRC formula from Kennedy, Holmes and Narver [8.25] is used to predict the HSM wall penetration depth for a postulated DBT missile.

$$x = \sqrt{4KNWd^{-0.8}\left[\frac{V}{1000}\right]^{1.8}}$$

When: $\frac{x}{d}3 \leq 2.0$

Where:

	x	=	Total penetration depth (in)
	d	=	8 in, Projectile diameter
	K	=	$180/\sqrt{f_c'}$ 4, Concrete penetrability factor
		=	2.55 for f_c' 5= 5000
	N	=	0.84 (blunt nosed), Projectile shape factor
	f_c'	=	5000 psi, Concrete compressive design strength at 150°F
	W	=	Projectile weight = 276 lb
	V	=	Striking velocity = 103 ft/s

Therefore: x = 2.7 inches and $\frac{x}{d} = 0.34$

The perforating thickness, or maximum thickness that the postulated DBT missile will completely penetrate, is calculated using the correlation:

$$\frac{e}{d} = 3.19\left(\frac{x}{d}\right) - 0.718\left(\frac{x}{d}\right)^2 \text{ for } \frac{x}{d} < 1.35$$

Substituting yields:

e = 8.07 in

Therefore, e, the maximum perforation thickness, is conservative.

The minimum thickness necessary to prevent scabbing of material from the rear face of the target is calculated using:

$$\frac{s}{d} = 7.91\left(\frac{x}{d}\right) - 5.06\left(\frac{x}{d}\right)^2 \text{ for } \frac{x}{d} < 0.65$$

Substituting yields:

$$s = 16.9 \text{ in}$$

Where: s = Scabbing thickness (in)

Scabbing effects control the minimum required wall thickness. ACI 349 requirements for nuclear safety related concrete structures require a minimum of 20% additional wall thickness to prevent perforation and scabbing. Therefore, the minimum wall thickness required to provide complete protection for the enveloping DBT missile is:

$$1.2s = 20.3 \text{ in}$$

The specified minimum wall thickness for the HSM side walls is 24 inches. To provide complete protection for the DSC shell, 12-inch thick shield walls are added to the end module exposed side walls in each row (a total of four walls). The addition of these walls provides a minimum concrete thickness of 27 inches behind the DSC (rear wall), 30 inches (front wall), and 36 inches for exposed side walls. Consequently, there is adequate protection against local DBT missile impact damage.

(ii) Local Barrier Impingement Analysis

A composite door comprising a steel plate and concrete is used to cover the HSM front wall access opening. The HSM front wall access and HEPA filter vent doors are analyzed to verify their adequacy for local barrier impingement of a DBT missile. The 276 pound, eight inch diameter missile is used for this calculation as it envelopes effects caused by all other missiles. The minimum thickness of a steel plate that can be perforated by the postulated DBT missile is given in the McDonalds, Mehta, and Minor paper [8.26] as:

$$T = \frac{(0.5 M_m V_s^2)^{2/3}}{672 d_m} 6 = 0.24 \text{ in}$$

Where: T = Perforation thickness (in)

M_m = Mass of missile $= \frac{W}{g} 7 =$ 8.57 slugs

W = Weight = 276 lb

g = 32.2 ft/s^2

V_s = Missile strike velocity = 103 ft/s

d_m = Diameter of missile = 8 in

The specified 1-1/2 inch thick steel HSM access and HEPA filter access rear doors easily exceed the minimum required perforation thickness of (1.25 x 0.24) = 0.3 inches.

(iii) Massive Missile Impact Analysis

The HSM stability and potential damage due to impact of the postulated DBT massive missile consisting of a 3,990 lb. automobile, 20 sq. ft. frontal area traveling at 103 ft/sec., is evaluated. The massive missile is assumed to impact the side wall of an end module in an array. The shield wall is conservatively ignored. Using the principles of conservation of momentum with a coefficient of restitution of zero, the analysis presented below demonstrates that the end module remains stable and the missile energy is dissipated by sliding or slight tipping of the module.

Using conservation of momentum, the missile impact force equals the change in linear (sliding) or angular (overturning) momentum of the HSM. The HSM velocities immediately after impact are:

Sliding: $$V = \frac{m v_i}{M + m}$$

Overturning: $$\omega_A = \frac{m d v_i}{m d^2 + I_A}$$

Where: V = Initial linear velocity of module after impact

v_i = 103 ft/sec., Initial velocity of missile

ω_A = Initial rotational velocity about point A (Figure 8.2-2)

m = 124 slugs, Mass of missile

M = 10,310 slugs, Mass of loaded HSM (single freestanding HSM)

d = 12.5 ft, height of missile center of gravity above basemat

I_A = 1,225,000 slug-ft^2, mass moment of inertia of loaded HSM about point A

Substituting and solving for V and ω_A produces an initial linear velocity of 1.23 ft/sec. and an angular velocity of 0.13 radians/sec.

The actual ratio between HSM sliding and rotation depends on where the missile impacts the shield wall. A low elevation impact produces mainly sliding, while a high elevation impact produces mainly rotation.

For an impact at the bottom of the HSM wall, the kinetic energy imparted to the HSM is absorbed by sliding friction between the concrete of the HSM and the basemat. ACI 349 [8.5] recommends a coefficient of friction of 0.6. Assuming that the missile impulse load results in sliding of the HSM and equating the kinetic energy to the sliding friction gives:

$$(M + m)\ \mu g\ \Delta = \frac{1}{2}(M + m)\ V^2$$

Where:

μ = 0.6, Coefficient of friction

Δ = Linear distance module slides

M, m, g, and V are as defined above

Substituting gives Δ = 0.47 inches

Therefore, a single free-standing module slides a maximum distance of 0.47 inches due to a low elevation tornado missile impact. At the opposite extreme, when the massive missile impacts at the top of the side wall, most of the missile energy is absorbed in rotation of the HSM. Equating the initial kinetic energy of the HSM to the increase in potential energy as the HSM center of gravity rises due to rotation gives:

Loss of Kinetic Energy = Increase in Potential Energy

$$\frac{1}{2}\ I_A \omega_A^2 = Mgd\ [\cos(\beta + \alpha - \frac{\pi}{2}) - \cos\ \beta]$$

Where:

α and β are defined in Figure 8.2-2

M, g, d, I_A, and ω_A are as defined above

Substituting and solving for α shows that the HSM rotates a maximum of 0.41° about the bottom edge opposite the point of impact. Therefore, the HSM provides a stable body as tip over will not occur until the center of gravity rotates past the edge (point A in Figure 8.2-2) to an angle of more than 34.6°.

8.2.2.3 Accident Dose Calculations

Each exposed component of the NUHOMS®-12T system is specifically designed to withstand tornado generated missiles as discussed in the preceding paragraphs. The consequence of reduced shielding effects of adjacent HSMs is presented in Section 8.2.1.

8.2.2.4 Recovery

Following a tornado missile strike, all damaged HSM components will be evaluated for structural adequacy and measured dose rates, and the appropriate repair/replacement program initiated. For a missile strike on an end shield wall, this plan would include the use of temporary shielding until the wall can be repaired or replaced. As noted above, the dose consequences to the INL workers and public are bounded by the reduced shielding analysis presented in Section 8.2.1.

8.2.3 Earthquake

8.2.3.1 Cause of Accident

The design basis seismic acceleration described in Section 3.2.3.1 are assumed to act on the TMI-2 ISFSI system components. For this evaluation, the TMI-2 ISFSI free field site accelerations (zpa's) with design response spectra of NRC Regulatory Guide 1.60 [8.27] are used for the seismic analysis of the NUHOMS®-12T system components. The horizontal and vertical design response spectra are shown in Figure 8.2-3.

8.2.3.2 Accident Analysis

As discussed in Section 3.2.3.2, the peak free field horizontal ground acceleration of 0.36g and the peak vertical ground acceleration of 0.24g are utilized for the seismic analysis of the NUHOMS®-12T components. Based on NRC Regulatory Guide 1.61 [8.28], a damping value of three percent is used for the DSC seismic analysis. Similarly, a damping value of seven percent for miscellaneous steel and concrete is utilized for the HSM. An evaluation of the frequency

content of the loaded HSM is performed to determine the dynamic amplification factors associated with the design basis seismic response spectra for the NUHOMS®-12T HSM and DSC. The dominant structural frequencies calculated are 23.8 Hz in the horizontal direction and 67.8 Hz for the DSC and DSC support steel in the vertical direction, and 36.3 Hz and 67.8 Hz for the HSM in the horizontal and vertical directions, respectively. Table 1 of NRC Regulatory Guide 1.60 requires amplification factors for structural frequencies below 33 Hz, which result in horizontal accelerations of 0.49g for the DSC and 0.36g for the HSM. The dominant vertical frequencies of the DSC and HSM exceed 33 Hz, corresponding to the zero period acceleration of 0.24g in the vertical direction.

A. DSC Seismic Evaluation

As discussed above, the maximum calculated seismic accelerations for the DSC inside the HSM are 0.49g horizontally and 0.24g vertically. A simplified rigid body static analysis using these accelerations shows that the DSC may lift off the support rails inside the HSM. The resulting stresses in the DSC shell due to vertical and horizontal seismic loads are determined and included in the appropriate load combinations. The seismic evaluation of the DSC is described in the paragraphs that follow. The DSC support structure is subjected to the calculated DSC seismic reaction loads as discussed in Paragraph C below.

(i) DSC Natural Frequency Calculation

Two natural frequencies, each associated with a distinct mode of vibration of the DSC, are evaluated. These two modes are the DSC shell cross-sectional ovalling mode, and the mode with the DSC shell bending as a beam.

a. DSC Shell Ovalling Mode

The natural frequency of the DSC shell ovalling mode is determined from the Blevins [8.29] correlation as follows:

$$f = \frac{\lambda_i}{2\pi R}\sqrt{\frac{E}{\mu(1-\upsilon^2)}} \qquad \text{(Table 12-1, Case 3) [8.29]}$$

R = 33.31 in, DSC mean radius

E = 28.8E6 psi, Young's Modulus

ν = 0.3, Poisson's ratio

$$\lambda_i = 0.289 \frac{t}{R} \frac{i(i^2 - 1)}{\sqrt{1 + i^2}}$$

t = 0.55 in, minimum thickness of DSC shell

μ = 0.284/g, steel mass density

The lowest natural frequency corresponds to the case when i = 2.

Hence: λ_2 = 0.0128 sec.

Substituting gives: f = 12.7 Hertz

For conservatism it is assumed that the entire DSC mass is excited by the DSC ovalling mode and the static analysis is performed using this frequency.

b. DSC Beam Bending Mode

The DSC shell is conservatively assumed to be simply supported at the two ends of the DSC. The beam bending mode natural frequency of the DSC was calculated using the following equation:

$$f_i = \frac{\lambda_i^2}{2\pi L^2} \sqrt{\frac{EI}{m}} 8 \qquad \text{(Table 8.1, Case 5) [8.29]}$$

E = 28.8E6 psi, Young's Modulus

I = 65,700 in^4, DSC moment of inertia

L = 163.5 in, Total length of DSC

m = 70,000/163.5g = 428/g lb/in

$\lambda 9$ = $i\pi$; 10 for lowest natural frequency, i = 1

Substituting yields: f_1 = 76.6 Hertz.

The DSC spectral accelerations at this frequency correspond to the zero period acceleration.

(ii) DSC Seismic Stress Analysis

With the DSC resting on the support rails inside the HSM, the stresses induced in the DSC shell are calculated due to the 0.62g horizontal and 0.24g vertical seismic accelerations applied as equivalent static loads. The DSC stresses due to the resulting vertical acceleration are calculated by factoring the dead load analysis results reported in Section 8.1. For the stress evaluation of the DSC shell due to seismic accelerations in the lateral direction, the resulting equivalent static acceleration is conservatively assumed to be resisted by one of the two support rails inside the HSM. The DSC shell stresses obtained from the analyses of vertical and horizontal seismic loads are combined by sum of the squares (SRSS).

As stated in Section 4.2.5.1, an axial retainer is included in the design of the DSC support system inside the HSM to prevent sliding of the DSC in the axial direction during a postulated seismic event. The stresses induced in the DSC shell and bottom cover plate due to the restraining action of this retainer for a horizontal seismic load, applied along the axis of the DSC, are evaluated and found to be negligible.

The stability of the DSC against lifting off one of the support rails during a seismic event is evaluated by performing a rigid body analysis, using the free field 0.36g horizontal and 0.24g vertical accelerations. The horizontal equivalent static acceleration of 0.49g is applied laterally to the center of gravity of the DSC. The point of rigid body rotation of the DSC is assumed to be the center of the support rail. The applied moment acting on the DSC is calculated by summing the overturning moments. The stabilizing moment, acting to oppose the applied moment, is calculated by subtracting the effects of the upward vertical seismic acceleration of 0.24g from the total weight of the DSC and summing moments at the support rail. Since the rigid body applied moment is greater than the stabilizing moment, the DSC may lift off the DSC support structure inside the HSM. However, as shown in the Appendix A drawings, the DSC is embedded within the HSM front and rear walls to ensure that the maximum possible lift off is limited to one inch. Therefore, the DSC will remain seated on the support rails in the HSM at the conclusion of a seismic event. The DSC vent system, including HEPAs, will remain functional during and after the seismic event.

B. HSM Seismic Evaluation

The seismic response of the HSM is performed using equivalent static procedure. The dominant frequency of the HSM concrete structure in the lateral direction 36.3 Hz. The dominant frequency of the concrete structure in the vertical direction is 70.8 Hz. All these frequencies are in the rigid range. Therefore, the seismic evaluation of the HSM concrete structure is performed in the rigid range by applying the rigid range horizontal (0.36g) and vertical (0.24g) accelerations. Seismic loads in the horizontal direction are assumed to be resisted by frame and shear wall action of the HSM. Accordingly, the HSM is modeled with three dimensional brick elements and the horizontal rigid range accelerations are applied to the model in both horizontal directions. Similarly, the vertical rigid range acceleration is applied to account for the vertical seismic effect. The results are included in the load combinations with the appropriate strength reduction factors. The factors used for the HSM are presented in Section 3.2.5. The load

combination results for normal, off-normal, and accident conditions are presented in Section 8.3.5.

An analysis is also performed to establish a conservative rigid body factor of safety against overturning and sliding for a single, free-standing module. This analysis consists of comparing the stabilizing moment produced by the weight of the HSM and DSC, reduced by 24% to account for the upward vertical seismic acceleration, against the overturning moment produced by applying the 0.36g load at the centroid of the HSM and 0.49g at the centroid of the DSC. For sliding of the HSM, the horizontal force of 0.36g acceleration for the HSM and 0.49g for the DSC are compared against the frictional resisting force of the foundation slab. In this manner, the factor of safety against sliding is established. The concrete coefficient of friction is taken as 0.6 as defined in Section 11.7.4.3 of ACI 318-95 [8.30].

The details of the seismic evaluation of the HSM are described in the paragraphs that follow.

(i) HSM Frequency Analysis

To determine the loaded HSM frequency content, the ANSYS [8.31] finite element model shown in Figure 8.1-13 is utilized. The lowest significant horizontal structural frequencies calculated are 23.8 Hz for the DSC with the support structure, and 36.3 Hz for the HSM. The lowest significant vertical mode is 67.9 Hz for both DSC with the support structure HSM. The corresponding spectral accelerations are 0.36g for the HSM, 0.49 for the DSC and DSC support structure in the horizontal direction, and 0.24g for the HSM and DSC in the vertical direction.

(ii) HSM Seismic Response Spectra Analysis

The rigid range accelerations in horizontal and vertical directions are applied to the finite element model in three orthogonal directions and static analysis is performed. The model of the DSC and the DSC support structure is also included in the three dimensional model of the HSM. The resulting forces and moments in the HSM walls, roof and floor of a single HSM are calculated using the linear finite element model shown in Figure 8.1-13 and the computer program ANSYS [8.31]. The three directional rigid mode responses are combined by the square root of the sum of the squares (SRSS) method. The combined maximum moments and shear forces are reported in Table 8.2-2.

(iii) HSM Overturning Due to Seismic

The following conservative analysis is performed to show that a single, free-standing HSM will not overturn due to seismic loads. The HSM stabilizing moment (M_{st}) is:

$$M_{st} = (W_{hsm} + W_{dsc})d = 1703\text{K-ft}$$

Where: W_{hsm} = Weight of HSM = 272 kips

W_{dsc} = Maximum weight of DSC = 60 kips

d = 5.13 ft, Horizontal distance from center line to corner

d_1 = Height of HSM center of gravity = 7.4 ft

d_2 = Height of DSC center line = 8.5 ft

The seismic overturning moment is:

$$M_{ot} = (W_{hsm}a_{v1} + W_{dsc}a_{v2})d + W_{hsm}d_1a_{h1} + W_{dsc}d_2a_{h2} = 1{,}423 \text{ K-ft}$$

Where: M_{ot} = Overturning moment

a_{v1} = 0.24g, HSM vertical seismic acceleration

a_{v2} = 0.24g, DSC vertical seismic acceleration

a_{h1} = 0.36g, HSM horizontal seismic acceleration

a_{h2} = 0.49g, DSC horizontal seismic acceleration

The result of this analysis indicates that a single loaded free-standing HSM will not overturn during a seismic event. The margin of safety against overturning is 1.2.

(iv) HSM Sliding Due to Seismic

To show that a single free-standing HSM will not slide due to the postulated horizontal and vertical seismic accelerations, the following conservative analysis is performed. The friction force resisting sliding (F_{s1}) is:

$$F_{s1} = [W_{hsm}(1-a_{v1}) + W_{dsc}(1-a_{v2})]\mu = 151 \text{ kips}$$

μ = Coefficient of friction between the HSM concrete walls and the floor slab foundation = 0.6

The applied horizontal seismic force (F_{hs}) is:

$$F_{hs} = W_{hsm}a_{h1} + W_{dsc}a_{h2} = 127 \text{ kips}$$

The force required to slide the HSM is larger than the resulting lateral seismic force and therefore, the HSM will not slide. The factor of safety against sliding is 1.19.

C. DSC Support Structure Seismic Evaluation

(i) DSC Support Structure Natural Frequency

The lowest structural frequency of the DSC and the DSC support structure inside the HSM is dominated by the mass of the DSC. The DSC and support structure are included in the HSM analytical model. The lowest significant horizontal and vertical frequencies of the DSC/DSC support structure are 23.8 Hz and 67.9 Hz, respectively.

(ii) DSC Support Structure, Seismic Response Spectra Analysis

The DSC support structure has two flexible modes; 15.22 Hz and 24.13 Hz in two orthogonal horizontal directions. The flexible mode response of the support structure is computed for these two modes and combined with the rigid mode response. For the support frame cross members, the maximum axial stress is 2 ksi and the maximum shear stress is 0.03 ksi.. Similarly, the maximum axial stress in the support rail is 2.9 ksi and the maximum shear strerss is 5.7 ksi. These compare with Code allowables of 13.1 ksi for shear stress and 19.7 ksi axial stress and, as a result, have a considerable design margin.

The effect of concentrated anchor bolt forces is included in the design of the DSC support structure connection details. Similarly, each connection of the support rails is designed for the resulting seismic loads. This condition envelopes all other loading conditions for the individual bolts or structural elements of the DSC support structure.

The stresses in the DSC support structure members due to seismic accelerations are included in the load combination results reported in Section 8.3.7.

(iii) DSC Seismic Retainer Analysis

The DSC seismic retainer detail, located inside the HSM access opening, is shown on the Appendix A drawings. The retainer bears on the end of the DSC and transfers axial seismic loads to the support structure.

The clearance between the DSC seismic retainer and the DSC is designed for the maximum DSC thermal expansion. During normal storage, there is a small (1/4 to 1/2 inch) gap that allows movement of the DSC relative to the HSM. This motion produces a small increase in the DSC axial force due to seismic loads, and has been included in the design of the DSC.

The HSM ANSYS finite element model includes the seismic retainer and the DSC rear stop. The resulting axial forces in the retainer calculated in seismic analysis are combined and applied

to the seismic retainer. The total resulting force excluding the force to overcome friction is 49.1 kips.

This load is transferred to the HSM front and rear walls and is included in the design basis forces and moments. The maximum bending and shear stresses in the seismic retainer are 12.3 ksi and 16.1 ksi which are less than the allowable shear and bending stresses of 18.4 ksi and 39.4 ksi respectively.

8.2.3.3 Accident Dose Calculations

The NUHOMS®-12T system components are conservatively designed and analyzed to withstand the forces generated by a postulated design basis earthquake accident. Hence, there are no dose consequences resulting from an earthquake.

8.2.4 Flood

8.2.4.1 Cause of Accident

As described in Section 3.2.2, the ISFSI base slab is located at, or above, the maximum predicted flood plain elevation. The maximum flood water elevation is well below the bottom of the DSC, which is some 5'-9" above the slab. Therefore, there are no credible flood loads that act on the TMI-2 ISFSI components.

8.2.5 Accidental Cask Drop

This section addresses the structural integrity of the DSC when subjected to postulated cask drop accident conditions. As described in Chapter 3, the DSC basket assembly is not required to maintain subcriticality of the TMI-2 canisters for this application. Therefore, no evaluation of the basket is performed. The structural integrity of the MP187 cask and DSC confinement boundary for all postulated on-site transfer accident drops have been evaluated for bounding loads and the results are described in the SMUD SAR [8.12]. The transportation hypothetical accident conditions are described in the 10 CFR Part 71 SAR [8.18]. This section demonstrates the adequacy of the DSC confinement boundary for postulated 10 CFR Part 72 transfer operation drop accident events.

8.2.5.1 Cause of Accident

A. Cask Handling and Transfer Operation

As described in Section 5.0, all handling operations involving hoisting and movement of the cask and DSC are performed inside the TAN facility. These include utilizing the crane for placement of the DSC into the cavity of the MP187 cask, and placement of the MP187 cask/DSC onto/off of the turning skid/transport skid/trailer.

Once the MP187 cask is loaded onto the transport skid/trailer, and the impact limiters are installed and secured, it is pulled to the TMI-2 ISFSI site by a tractor vehicle using 10 CFR Part 71 transportation regulations. A predetermined route is chosen to minimize the potential hazards that could occur during transport. This movement is performed at low speeds. Safeguards provided in system operating procedures ensure that the system design margins are not compromised. As a result, it is highly unlikely that any plausible incidents leading to a cask drop accident could occur. Similarly, at the ISFSI site, after removing the impact limiters, the transport skid/trailer is aligned with the HSM using hydraulic positioning equipment. The cask is docked with, and secured to, the HSM access opening. The loaded DSC is transferred to/from the HSM using a hydraulic ram system. The hold down mechanisms that securethe cask to the transport skid/trailer remain in place at all times during the DSC transport. As a result, there is no mechanistic way during these operations for a cask drop accident to occur.

B. Cask Drop Accident Scenarios

In spite of the incredible nature of any scenario that could lead to a cask drop accident, a conservative range of drop scenarios during the 10 CFR Part 72 transfer operations are developed and evaluated. These bounding scenarios assure that the integrity of the DSC and TMI-2 canisters are not compromised. Comparison of these scenarios to the 10 CFR Part 71 postulated drop scenarios demonstrate that the MP187 cask maintains structural integrity and the DSC confinement boundary will remain intact. Therefore, there is no potential for a release of radioactive materials to the environment due to a cask drop. The range of 10 CFR Part 72 transfer drop scenarios conservatively selected for design are illustrated in Figure 8.2-1 and include the following cases:

1. A horizontal side drop from a height of 80 inches after the impact limiters have been removed.

2. An oblique corner drop from a height of 80 inches at an angle of 30° to the horizontal, onto the top or bottom corner of the cask after the impact limiters have been removed (two cases).

The height of 80 inches is chosen as this envelopes the maximum vertical height of the cask when secured to the transport skid/trailer assembly. The angle of inclination for the corner drop of 30° represents the maximum possible impact angle that the cask can rotate downward with one end supported horizontally on the transport skid trailer at a height of 80 inches.

C. Cask Drop Accident Load Definitions

Transportation of the MP187 cask and contents from the TAN facility to the TMI-2 ISFSI site will be performed under the rules of 10 CFR Part 71 with the cask impact limiters installed as described in the MP187 cask SAR [8.18]. The impact limiters will be removed once the transportation trailer reaches the TMI-2 ISFSI site. From the time the impact limiters are removed until the DSC is transferred into the HSM, the trailer will be moved a distance of less than 500 feet over compacted gravel, asphalt, and 12 to 30 inch thick concrete surfaces. There

will be no vertical lifts of the cask and the only large horizontal motions are controlled by movement of the tractor/trailer at speeds of 5 mph or less. Once the cask and DSC are located at the chosen HSM, final alignment will be achieved by use of the hydraulically controlled skid positioning system. Neither of these movements create a potential for a cask drop accident.

As described in the SMUD Part 72 SAR [8.12], it is assumed that the cask can slide off the end (corner impact), or side (side impact) by an undefined nonmechanistic failure. These drops would result in a maximum drop height of 80 inches onto an under-reinforced concrete slab. As there are no vertical cask movements considered at the TMI-2 ISFSI there are no potential end impact scenarios.

EPRI Report NP-4830, "The Effects of Target Hardness on the Structural Design of Concrete Storage Pads for Spent Fuel Casks," [8.33] provides expected decelerations for postulated cask side and end drops for typical ISFSIs licensed to 10 CFR Part 72 requirements. The report establishes the maximum expected decelerations for a range of surface conditions and drop heights up to 80 inches. For the MP187 cask weight and dimensions, the expected maximum decelerations for drops onto a 30 inch thick under-reinforced concrete slab are less than 75g for an end drop or a side drop. Corner drops are not explicitly covered in the EPRI report. However, the maximum decelerations for a corner drop are determined to be significantly lower than those for side drops [8.33].

8.2.5.2 Accident Analyses

The 10 CFR Part 72 and 10 CFR Part 71 hypothetical accident condition drop analyses presented in the SMUD Part 72 SAR [8.12] and the MP187 cask SAR [8.18], respectively, provide assurance that the MP187 cask can withstand all postulated impacts without affecting the DSC confinement boundary integrity.

A. NUHOMS®-12T DSC Drop Analyses

The DSC confinement boundary stresses for the postulated Part 72 drops are similar to those reported in the generic NUHOMS® SAR [8.9]. The finite element model shown in Figure 8.1-7 was used to develop the DSC confinement boundary stress intensities reported in Table 8.2-3 for the design basis 75g side (horizontal) and end (vertical) drops.

The basic design of the TMI-2 DSC basket is similar to the NUHOMS® generic DSC basket which has been demonstrated to withstand the design basis 10 CFR Part 72 drop loads without significant deformations [8.9]. The TMI-2 ISFSI basket assembly is not required to maintain geometrical control to ensure subcriticality of the TMI-2 canisters following a drop accident and, therefore, is not analyzed for the hypothetical drop accident decelerations. It is expected that the TMI-2 DSC basket will behave in a similar manner to that described for the NUHOMS® generic basket in the Reference 8.9 postulated drop decelerations. However, in the worst case, the TMI-2 basket structure may yield and the TMI-2 canisters could bear on the DSC shell. The TMI-2 canisters were drop tested to 190g during their design program, as described in Reference 8.34,

and can support the weight of all TMI-2 canister assemblies without affecting any of the criticality assumptions described in Section 3.3. The original drop tests were performed by placing the TMI-2 canisters into pipe sections to simulate the 125-B inner containment vessel. The TMI-2 DSC spacer disc simulates the tube design of the 125-B and will have little effect on the maximum TMI-2 canister stresses. The TMI-2 canister maximum bending stress in the 14 inch diameter, 1/4 inch wall tube for the 75g horizontal drop is less than 2 ksi. This is a very small fraction of the material yield of 30 ksi and the ASME Code Service Level D allowable of 66 ksi at 300^{o}F.

B. MP187 Transfer Cask Drop Analyses

Results for the 10 CFR Part 72 drop analyses for the MP187 cask are reported in Reference 8.12. These analyses envelop those resulting from the drop accident scenarios described above, and clearly demonstrate the acceptability of the MP187 cask and DSC confinement boundary to meet ASME Code requirements.

8.2.5.3 Loss of Neutron Shield

This accident conservatively postulates loss of neutron shield on the MP187 cask.

8.2.5.3.1 Cause of Accident

The reference SMUD Part 72 SAR [8.12] design basis cask drop analyses show that all components of the MP187 maintain their structural integrity for the postulated drop accident events. Complete loss of the neutron shield material is not a credible event. For this conservative analysis, it is assumed that the cask neutron shield is breached as a result of a postulated drop accident, and the shielding effects are lost. The effect on the cask, DSC, and TMI-2 canister temperatures is bounded by the results of the 103°F ambient case described in Section 8.1.3.3.

8.2.5.3.2 Accident Dose for Loss of Neutron Shield

For an MP187 cask containing a design basis NUHOMS®-12T DSC, complete loss of the neutron shield would increase the peak cask surface contact dose from 3.2 mrem/hour to 4.9 mrem/hour. The only potential off-site dose consequences would be additional direct and air scattered radiation. This accident dose rate is well below typical fuel storage and transportation cask dose rates for normal operations. Because the accident dose rate is so low, no significant exposure will be received by workers or members of the public. Following a loss-of-neutron shield event, the canister should be removed from the cask as discussed in Section 8.2.5.4. Conservatively assuming two workers are exposed to the peak cask surface dose rate for eight hours, an additional exposure of 27 person-mrem may be received. No release of radionuclides will occur due to this event.

This does not preclude handling operations for recovery of the cask and its contents. Water bags, or other neutron absorbing material could be wrapped around the cask to reduce the surface dose to an acceptable limit for recovery operations, thus minimizing exposure of personnel in the vicinity. The actual local dose rate, recovery time, operations needed to retrieve the cask, and the required actions to be performed following the event, depend upon the severity of the event and the resultant cask and trailer/skid damage.

The INL site boundary is approximately eight miles from the ISFSI and there would be no measurable increase above background levels regardless of how long it took to recover from the accidental loss of the neutron shield.

8.2.5.4 Recovery

For drop heights of less than 15 inches, the cask will be loaded back onto the transfer skid/trailer and moved to the HSM. The DSC will then be transferred to the HSM in the normal manner described previously. For drop heights greater than 15 inches, the cask and contents will be returned to the TAN Hot Shop, or other appropriate facility. There, the DSC will be inspected for damage, the DSC opened and the TMI-2 canisters removed for inspection, as necessary. Removal of the DSC cover plate and shield plug assembly are described in Section 5.0.

Following recovery of the cask and unloading of the DSC, the cask will be inspected, repaired, and tested, as appropriate, prior to reuse.

8.2.6 Lightning

8.2.6.1 Postulated Cause of Event

As described in Reference 8.35, a lightning risk assessment has been conducted for the ISFSI in accordance with the Lightning Protection Code, NFPA 780. This risk assessment calculated a "moderate risk" factor for the TMI-2 ISFSI site. Although the effects of a lightning strike are not significant, a lightning protection system is provided to further reduce the risk.

8.2.6.2 Analysis of Effects and Consequences

Should lightning strike in the vicinity of the HSM, the normal storage operations of the HSM will not be affected. The current discharged by the lightning will follow the low impedance path offered by an early streamer emission system attached to the light support poles surrounding the ISFSI. As an added safety factor, the HSMs would not be damaged by the heat or mechanical forces generated by any current passing through the higher impedance concrete. Since the HSMs require no equipment for their continued operation, any resulting current surge from a lightning strike would not affect the normal operation of the HSM.

Since no off-normal condition will develop as a result of a lightning strike in the vicinity of the HSM, no corrective action would be necessary. Also, there are no radiological consequences of a lightning strike at the ISFSI.

8.2.7 DSC Leakage

The DSC shell is designed as a confinement boundary to prevent leakage of contaminated materials. The analyses of normal, off-normal, and accident conditions have shown that no credible conditions can breach the DSC shell or fail the double seal welds at each end of the DSC. For the TMI-2 ISFSI, the DSC vent and purge ports are connected to HEPA filters to allow the release of hydrogen gas created by potential radiolysis within the TMI-2 canisters.

As discussed below, this event postulates a direct release to the environment of 40.2 Ci (over a one month period) of fission product gases and other radioactive materials contained in the TMI-2 canisters. This nonmechanistic accident conservatively assumes that all 12 TMI-2 canisters rupture, plus either a DSC seam or both HEPA filter trains are instantaneously ruptured. All other components of the NUHOMS®-12T system remain intact.

8.2.7.1 Cause of Accident

There is no credible event that could result in the rupture of any TMI-2 canister component concurrent with an instantaneous rupture of the DSC seams or HEPA filter trains. The passive nature of the NUHOMS®-12T system and the various design features ensure that the integrity of the DSC shell confinement pressure boundary and HEPA filter trains are maintained. Nevertheless, this evaluation assumes that the TMI-2 canisters and the DSC pressure boundary or HEPA filter trains are ruptured due to an event of unspecified origin.

8.2.7.2 Accident Analysis

There are no structural or thermal consequences resulting from the DSC leakage accident described above. The radiological consequences of this accident are described in Section 8.2.7.3.

8.2.7.3 Accident Dose Calculations

The postulated accident assumes that the HEPA filter trains from one DSC are ruptured and that all 12 of the TMI-2 canisters fail simultaneously such that 40.2 Ci of the fission product gasses and other radioactive materials in the TMI-2 canisters are released to the atmosphere over a one month period. The nuclide composition of the postulated release is provided in Chapter 7. The total effective dose equivalent received by an individual at or beyond the INL controlled area boundary under the worst meteorological conditions was calculated using the RSAC-5 code. Contributions to this exposure include the 50-year committed effective dose equivalents from the inhalation and ingestion pathways and the effective dose equivalents from the ground surface and cloud gamma pathways. The resultant accident dose of 0.28 mrem is well within the 10 CFR 72.106 limit, which restricts the maximum whole body or organ dose beyond the owner

controlled area from any design basis accident to be less than five rem. A critical organ dose of 0.08 mrem was calculated for the thyroid. A worker spending 40 hours per week at the INTEC fence would receive a total effective dose equivalent of 0.11 rem as a result of this event.

8.2.7.4 Recovery

Recovery from this accident condition may be achieved by returning the challenged DSC to the TAN Hot Shop, or other appropriate facility, offloading the TMI-2 canister, repairing the canisters and/or DSC as appropriate, reloading and returning it to the ISFSI. Alternatively, a dry transfer cask-to-cask system may be used to replace the challenged DSC. An HSM with an overpack is provided to ensure that the challenged DSC can be safely stored at the ISFSI without the need to return it to the TAN Hot Shop, or other appropriate facility.

As shown on the Appendix A drawings, the overpack is similar to the DSC confinement boundary. The 5/8" steel shell has an inner diameter of 68.25 inches and a length sufficiently long to accommodate the DSC, HEPA filter blocks, and grapple ring. The inner end of the overpack is sealed with a shop-installed 1-1/2" thick plate. The method of construction, codes, and inspections will be the same as those invoked for the DSC confinement boundary to provide assurance of a leak-tight system. The steel overpack is installed onto the HSM rails and is welded to the front HSM access collar to resist longitudinal load and maintain the circularity of the front end over a long period of time.

After insertion of a challenged DSC, the front (outer) end of the overpack is sealed by welding a 1-1/2" thick closure plate across the shell opening. The rear plate of the opening contains HEPA filters similar to those described for the DSCs installed in the other HSMs. Those filters have the same design, operating, and maintenance criteria as the HEPA filter trains described in Chapter 6.

The changes required for the HSM to accommodate the overpack are: a slightly larger, steel lined, front access sleeve; support rails lowered by approximately one inch to maintain the same cask center line height during transfer; and an increase in the diameter of the rear wall recess to clear the overpack. These modifications do not alter the calculated behavior or reinforcement requirements described in Section 8.1. The HSM front access door, seismic restraint, and rear HEPA filter access door are similar to those described for the NUHOMS®-12T HSM and do not require re-analysis for this scenario.

The DSC overpack design loads for pressure, dead load, and seismic forces are of the same magnitude as those of a DSC loaded into an HSM. This assures that the reported maximum stresses for the DSC envelope the calculated stresses for the overpack.

8.2.8 Accident Pressurization of DSC

The analysis documented in Appendix C shows that the maximum hydrogen concentration under worst case conditions will be 4.8% in the TMI-2 canister, and less than 1.2% in the DSC. These

concentrations are less than the lower flammability limit of 5%. With a vented system there will be no pressure build-up within the DSC.

8.2.8.1 Cause of Accident

The TMI-2 canisters and DSC are configured to prevent hydrogen concentrations from reaching the flammability limit. However, hydrogen deflagration within one of the TMI-2 canisters is postulated as an accident scenario. For this event to occur, not only must the hydrogen concentration reach the 5% minimum required for flammable levels, but an ignition source must also occur within the TMI-2 canister to initiate combustion.

8.2.8.2 Accident Analysis

In the unlikely event that combustion occurs inside a TMI-2 canister, the hydrogen-air combustion can take the form of either a deflagration or a detonation. Hydrogen deflagrations are subsonic combustion processes that produce peak to initial pressure ratios of approximately 8:1. Hydrogen detonations are supersonic combustion processes that can produce shock waves with momentary face-on pressure ratios of up to 40:1 [8.36]. Detonations require hydrogen concentrations in excess of 18% in air, and certain types of geometry which allow the flame to accelerate up to its detonation velocity. As the maximum TMI-2 canister hydrogen concentration is less than 5%, the likelihood of both detonation conditions being met in the TMI-2 storage canisters is extremely remote. Therefore, only the deflagration process is considered. Since the hydrogen concentration buildup will always be higher in the TMI-2 canisters than in the DSCs, only the deflagration in one TMI-2 canister is considered.

The maximum calculated pressure in the TMI-2 canister and DSC during normal, off-normal, or accident conditions from Section 8.1.1.1.B is 11.4 psig (26.1 psia). Therefore, using a pressure ratio of 8:1, the maximum overpressure due to hydrogen deflagration in the canister will be approximately 209 psia (194 psig).

The specified design pressure of the TMI-2 canisters is 150 psig. The original Babcock and Wilcox ASME Stress Analysis [8.37] was reviewed to determine whether an internal pressure of 194 psig would overstress the TMI-2 canisters. The report indicates that the canisters were sufficiently over-designed to accommodate pressures in excess of 194 psig and still meet ASME Section VIII allowable stress values. Therefore, no degradation of the TMI-2 canister will occur in the event of a hydrogen deflagration.

Because of the very small ports in the TMI-2 canisters and the momentary nature of the over pressure condition, the amount of gas which would escape from a TMI-2 canister into the DSC cavity during a deflagration is too small to affect the DSC cavity pressure. No degradation of the DSC confinement boundary will occur in the event of a hydrogen deflagration inside a TMI-2 canister.

8.2.8.3 Accident Dose Calculations

There are no dose consequences as a result of accidental pressurization of the DSC. Any release that may occur is bounded by the evaluation in Section 8.2.7.

8.2.9 Fire and Explosion

8.2.9.1 Cause of Accident

A fire hazards analysis has been performed for the TMI-2 ISFSI. Because it is constructed of non-combustible materials, the ISFSI does not impose a fire or explosion hazard to the surrounding area or facilities. The buildings, storage yards, fuel storage tanks, and access roads nearest the ISFSI have been evaluated for potential impacts to the ISFSI due to fire and explosions. Because of the limited fuel quantities present and the substantial distances to the ISFSI, it has been determined that they pose no threat to the ISFSI structures or components. The most severe source of fire comes from burning fuel in the support vehicles used for loading and unloading the facility, and sampling and testing of the DSCs in storage. The consequences of a fire from these sources is evaluated below.

8.2.9.2 Accident Analysis

Any fire from ISFSI service vehicles would be very limited due to the small amount of combustible material available. At any given time, the total amount of fuel in service vehicles and other containers within the ISFSI boundaries will be limited to less than 300 gallons. This insures that any fire will be relatively small and slow burning since the fuel would be discharging at a low rate, or that the fire would be over in a relatively short time. Based on burn test data for gasoline, if all 300 gallons of fuel was pooled and available for burning, the fire would last less than 30 minutes. Since there is no place for the fuel to pool on the pad to support such a fire, the actual burn time of any ISFSI fire would be considerably less than 30 minutes. An infinitely large fire that burned for two hours around an HSM was evaluated in Reference 8.38. This evaluation showed that only the outer three inches of the HSM concrete would reach the ACI 349 accident temperature limit of 650^{o}F. Some minor concrete cracking may occur due to the differential heating of the HSM, but will be controlled by the steel reinforcement. The inside temperature of the HSMs will not vary significantly from normal operating limits due to the massive nature of the HSM concrete thickness'. Cracks, or surface spalling that may occur as a result of the worst case postulated fire would have no significant effect on the structural strength or the radiation protection provided by the HSM.

8.2.9.3 Accident Dose

Although local radiation levels may increase slightly, there will be no effect to the public. Any dose increase due to fire damage is bounded by the loss of shielding discussed in Section 8.2.1. There will be no increases in airborne releases due to this event since the DSC and vent are protected inside the HSM and are well above potential fuel sources for the fire.

8.2.9.4 Recovery

Recovery from the fire would involve a radiological and physical survey of the HSM and surrounding area to determine the extent of potential damage. As stated above, it is expected that there will be no significant structural damage to the HSMs or increases in radiation exposures due to this accident. Any damage to the HSMs can be repaired or replaced. Replacement would require that the loaded DSC be removed and a new HSM installed. Alternatively, surface spalling can be repaired, in place, and the HSM returned to service without the need to remove the loaded DSC.

8.2.10 Blockage of Space Between Adjacent HSMs

This accident conservatively postulates the complete blockage of the gap between the adjacent HSMs.

The debris is conservatively assumed to remain in place for an indefinite period of time.

8.2.10.1 Cause of Accident

Since the HSMs are located outdoors, there is a small probability that the gap between HSMs could become blocked by debris from such events as wind storms, floods, and tornadoes. Even though complete blockage of the entire gap is unlikely, such an accident is postulated to occur for this conservative analysis.

8.2.10.2 Accident Analysis

The structural consequences due to the weight of the debris blocking the gap between the modules are negligible and are bounded by the HSM loads induced for a postulated tornado (Section 8.2.2) or earthquake (Section 8.2.3).

The thermal effects of this accident result from the increased temperatures of the DSC and the HSM due to blockage of the gap between HSMs. Even though any blockage will be cleared by site personnel, it is conservatively assumed for this analysis that the blockage is there for an indefinite amount of time.

The thermal analysis of the HSM for the blocked gap condition is performed using the same model as the normal conditions described in Section 8.1.3. The only change is the use of an insulated boundary condition in the gap region simulating blocked gap conditions. A steady state analysis is carried out to determine the worst temperature distribution in the DSC and the HSM.

The results of the blocked gap case are included in Tables 8.1-8, through 8.1-10. The results show that the maximum concrete temperature is 179°F and the maximum core debris

temperature is below 219°F. Therefore, the concrete, fuel, and all the material temperatures are well within their limits for accident conditions.

These temperatures are below the levels at which safety-impairing damage would occur to the HSM or DSC. The maximum DSC internal pressure during this event is less than 15 psig as shown in Section 8.1.1.1.B.

8.2.10.3 Accident Dose Calculations

There are no off-site dose consequences as a result of this accident. The only significant dose increase is related to the recovery operation. It is conservatively estimated that the on-site workers will receive an additional dose of less than one man-rem during the estimated eight hour period that may be required for debris removal from the gap between the HSMs.

8.2.10.4 Recovery

Debris removal is all that is required to recover from a postulated blockage of the gap between the HSMs. Cooling will begin immediately following removal of the debris. The amount and nature of debris can vary, but even in the most extreme case, manual means or readily available equipment can be used to remove debris.

8.2.11 Basaltic Lava Flow

The analysis of normal, off-normal, and accident conditions have shown that a future basaltic lava flow represents an extremely unlikely (5×10^{-6}) but credible event that, without mitigation could have a potential to adversely affect facility performance.

8.2.11.1 Cause of Accident

The general topography and vent locations within the INL area suggest that any future lava will most likely erupt from vents along the axial volcanic zone or at the intersections of that zone with the volcanic-rift zones. The volcanic event could cause lava to flow from the south toward the central INL and INTEC, which includes the ISFSI.

8.2.11.2 Mitigation Actions and Design Features

8.2.11.2.1 Warning Time

Total warning time from time of identification of magma-induced seismicity to arrival of lava in the vicinity of INTEC will range from 1 week to greater that 1 month. An alert will be declared when the INL Seismic Monitoring Program reports to the Warning Communications Center that seismic activity recorded by seismographs indicates that a volcanic eruption is possible in the

near future. Equipment and workforce available at INL could construct a barrier to protect endangered facilities in as little time as one week.

8.2.11.2.2 Arrival Time

The distance from the volcanic event will be at least 12 km (55^{th} percentile length) and more likely in the range of 16 km (70^{th} percentile length), and the effusion rate is likely to be waning by the time it reaches the ISFSI area. Analogy to flow velocities in other areas of the world with similar terrain indicates that velocities of about 2 km/day are most likely, and thus it would take several days for lava from most of the critical volcanic source area to reach the site.

8.2.11.2.3 Mitigation Actions and Design Features

Either of the two following mitigation actions would protect facilities from the advance of a lava flow. The objective of these actions is not to stop the advancing lava but to divert or direct the flow of lava around INTEC, and on down the Big Lost River Valley.

8.2.11.2.4 Earthen Barrier:

Big Lost River alluvium in the vicinity of INTEC consists almost entirely of sandy and silty limestone gravel (pebbles and cobbles). This material could be used to construct a barrier to divert or direct the lava flow around the ISFSI. The high-density limestone gravel would not be subject to breaching, as has happened in cases where low-density volcanic ash barriers were used. To protect the ISFSI from an approaching lava flow, an earthen barrier could be constructed within the INTEC and immediately surrounding the ISFSI. The earthen barrier or berm (as shown in Figure 8.2-4) would be approximately 20 feet in height and 50 feet in width at the base. Such a structure would be adequate to divert the design basis lava flow reaching the ISFSI sight and could erected within a week using excavation equipment that is available at the INL and surrounding communities.

8.2.11.2.5 Water Spray

Diversion of lava flows by cooling with water sprays has been used successfully in Iceland, Japan, and Italy [8.40, 8.41, 8.42]. The combined pumping capacity of wells at INTEC, TRA, CFA, and RWMC (south-central INL facilities which have large pumping capacity) is over 14 million gallons per day. This capacity surpasses the pumping rate used on Heimaey, Iceland for a lava flow with a much higher effusion rate and much longer eruption duration than would occur at INL. The large capacity of the Snake River Plain aquifer is likely to be able to sustain those pumping rates for several days to several weeks because the water would be pumped from several high-capacity wells. The objective of this mitigation action is to cool and solidify a portion of the lava flow front and flank as it approaches INTEC, so that lava is forced to flow around the facilities.

The following factors provide a high degree of confidence that a lava flow could be diverted around INTEC:

- The Big Lost River Valley is broad and flat, with a gentle gradient to the north, so lava will not have a strong tendency to flow in any particular path down the valley.
- The distance from the volcanic vent will be at least 12 km (55th percentile length) and more likely in the range of 16 km (70th percentile length), and the effusion rate is likely to be waning by the time it reaches the ISFSI area.
- Although the INTEC is within the Big Lost River valley, there are no constrictions in the valley at or near the ISFSI that would cause ponding of lava.
- Local alluvium available for barrier construction is dense and easily moved with available equipment.
- Equipment and workforce available at INL could construct a barrier in as little time as one week.

These mitigation actions provide assurance that a basaltic lava flow will not adversely affect ISFSI facility performance because:

1) A seismic network is maintained such that characteristic volcanic earthquakes can be readily distinguished from tectonic earthquakes.

2) Criteria has been developed to determine what level of activity (e.g., earthquake clustering or rate of decrease in epicenter depth) constitutes a potentially significant volcanic event.

3) An alert will be declared when the INL Seismic Monitoring Program reports to the Warning Communications Center that seismic activity recorded by seismographs indicates that a volcanic eruption is possible in the near future.

4) A site area emergency will be declared when the INL Seismic Network reports shallow seismicity accompanied by observed ground fissures.

5) Mitigation plans consider that lava would not reach the site until a week after vent formation and thus action could be implemented before a new vent actually forms.

6) Lava diversion takes into account site topographic and lava flow characteristics.

7) Property removal, as a mitigation strategy is not required.

8.2.11.3 Accident Dose Calculations

In the unlikely event of a future basaltic lava flow, the ISFIS would experience no structural, thermal, or radiological consequences due to the implementation of the above mitigation actions.

8.2.11.4 Recovery

Adequate time is available for implementation of mitigation actions to preclude any impact on the ISFSI performance, therefore, recovery from this unlikely event is not required.

Table 8.2-1
Postulated Accident Loading Identification

Accident Load Type	Section Reference	NUHOMS®-12T Component Affected				
		DSC Shell Assembly	DSC Internal Basket	DSC Support Structure	HSM	On-Site Transfer Cask
Tornado Wind	8.2.2				X	X
Tornado Missiles	8.2.2				X	X
Earthquake	8.2.3	X	X	X	X	X
Accident Cask Drop	8.2.5	X	X			X
Loss of Cask Neutron Shield	8.2.5					X
Lightning	8.2.6				X	
DSC Leakage	8.2.7	(radiological consequence only)				
DSC Accident Internal Pressure	8.2.8	X				
Fire and Explosion	8.2.9				X	
Load Combinations	8.3	X	X	X	X	X

Table 8.2-2
Maximum HSM Reinforced Concrete Bending Moments and Shear Force for Accident Loads

Structural Section	Force Component	HSM Internal Forces (kip/ft, in-k/ft)[1]	
		Tornado Wind and Tornado Missile Load	Seismic
Floor Slab	Shear	1.2	0.86
	Moment	127.3	478.1
Side Wall	Shear	7.4	0.78
	Moment	212.4	61.2
Front Wall	Shear	25.6	10.5
	Moment	567.7	84.3
Rear Wall	Shear	17.5	10.8
	Moment	95.3	66.7
Roof Slab	Shear	9.8	1.4
	Moment	329.1	11.2

(1) Maximum loads shown are irrespective of location.

Table 8.2-3
Maximum NUHOMS®-12T DSC Stresses for Drop Accident Loads

DSC Components	Stress Type	Calculated Stress (ksi)(1, 2)	
		Vertical	Horizontal
DSC Shell	Primary Membrane	10.1	14.5
	Membrane + Bending	17.7	40.4
Top Shield Plug	Primary Membrane	1.1	14.9
	Membrane + Bending	38.9	26.6
Top Cover Plate	Primary Membrane	2.4	8.5
	Membrane + Bending	3.8	14.1
Inner Bottom Cover Plate	Primary Membrane	4.5	9.6
	Membrane + Bending	5.2	12.7
Outer Bottom Cover Plate	Primary Membrane	4.7	7.9
	Membrane + Bending	7.4	12.8
Top Cover Plate Weld	Primary	2.6	11.4
Bottom Cover Plate Weld	Primary	2.3	10.6

(1) Values shown are maximums irrespective of location.

(2) DSC was also included in corner drop analysis for cask, however, stresses are enveloping.

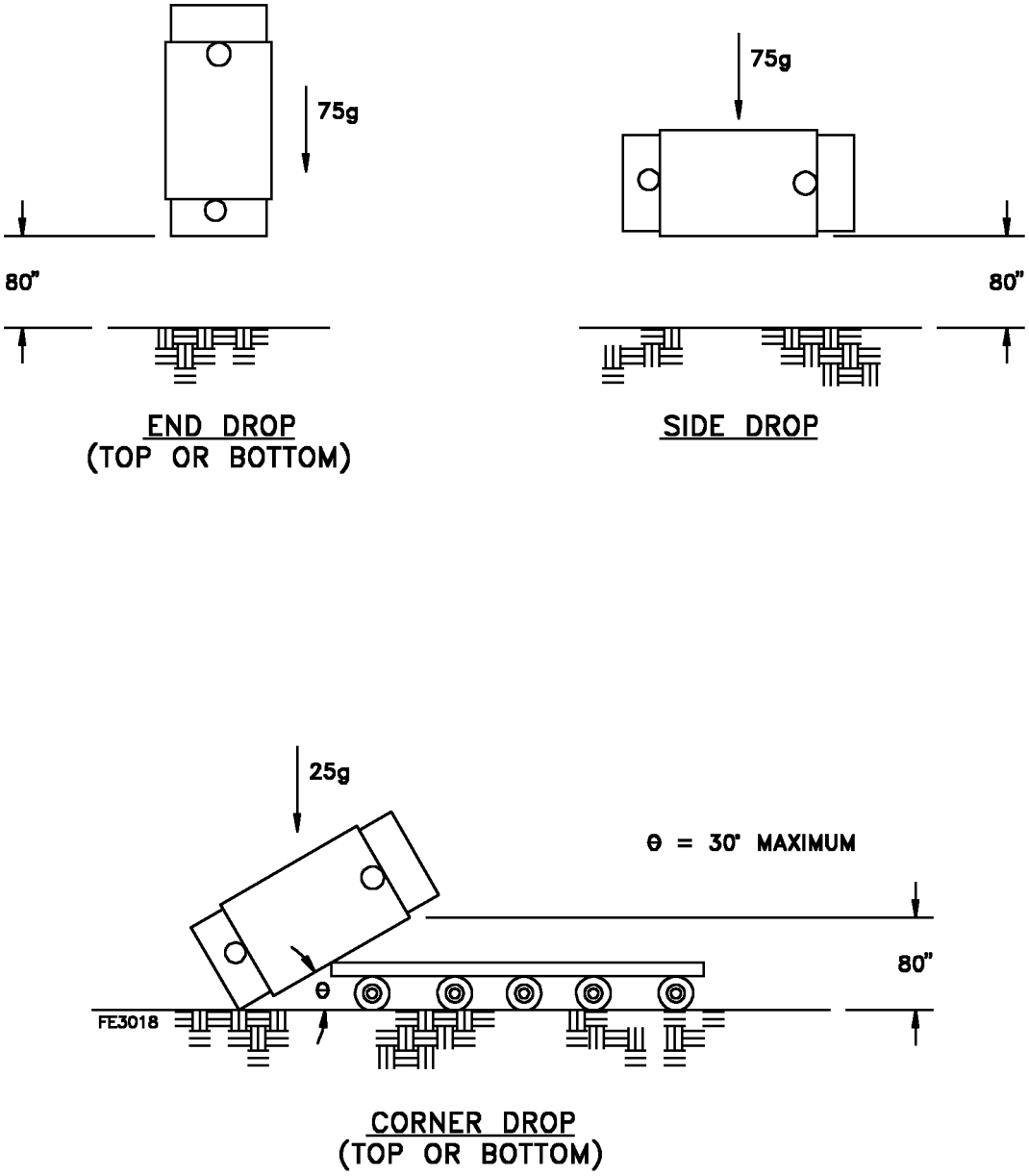

Figure 8.2-1
MP187 Cask Postulated Drop Accident Scenarios

Security-Related Information
Figure Withheld Under 10 CFR 2.390.

Figure 8.2-2
Tornado Missile Impact Model

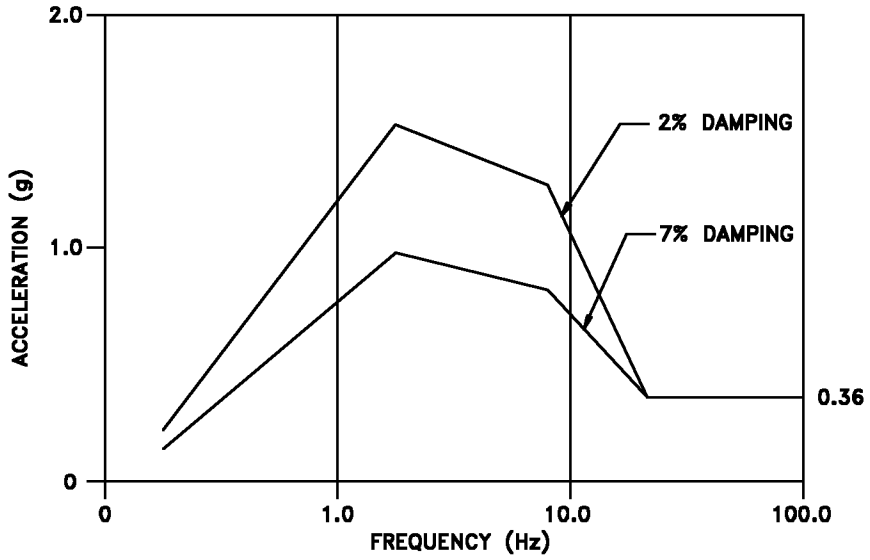

Horizontal Seismic Design Response Spectra

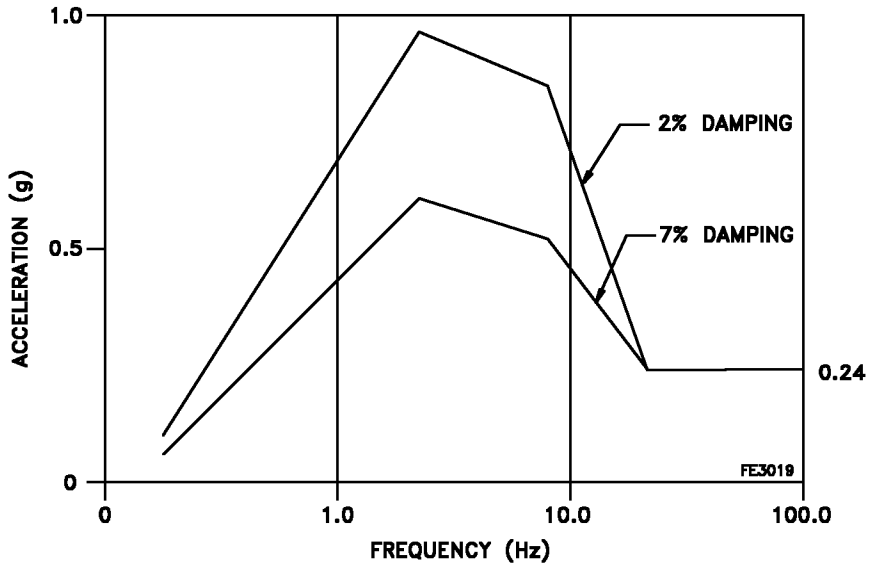

Vertical Seismic Design Response Spectra

Figure 8.2-3
Horizontal and Vertical Seismic Design Response Spectra

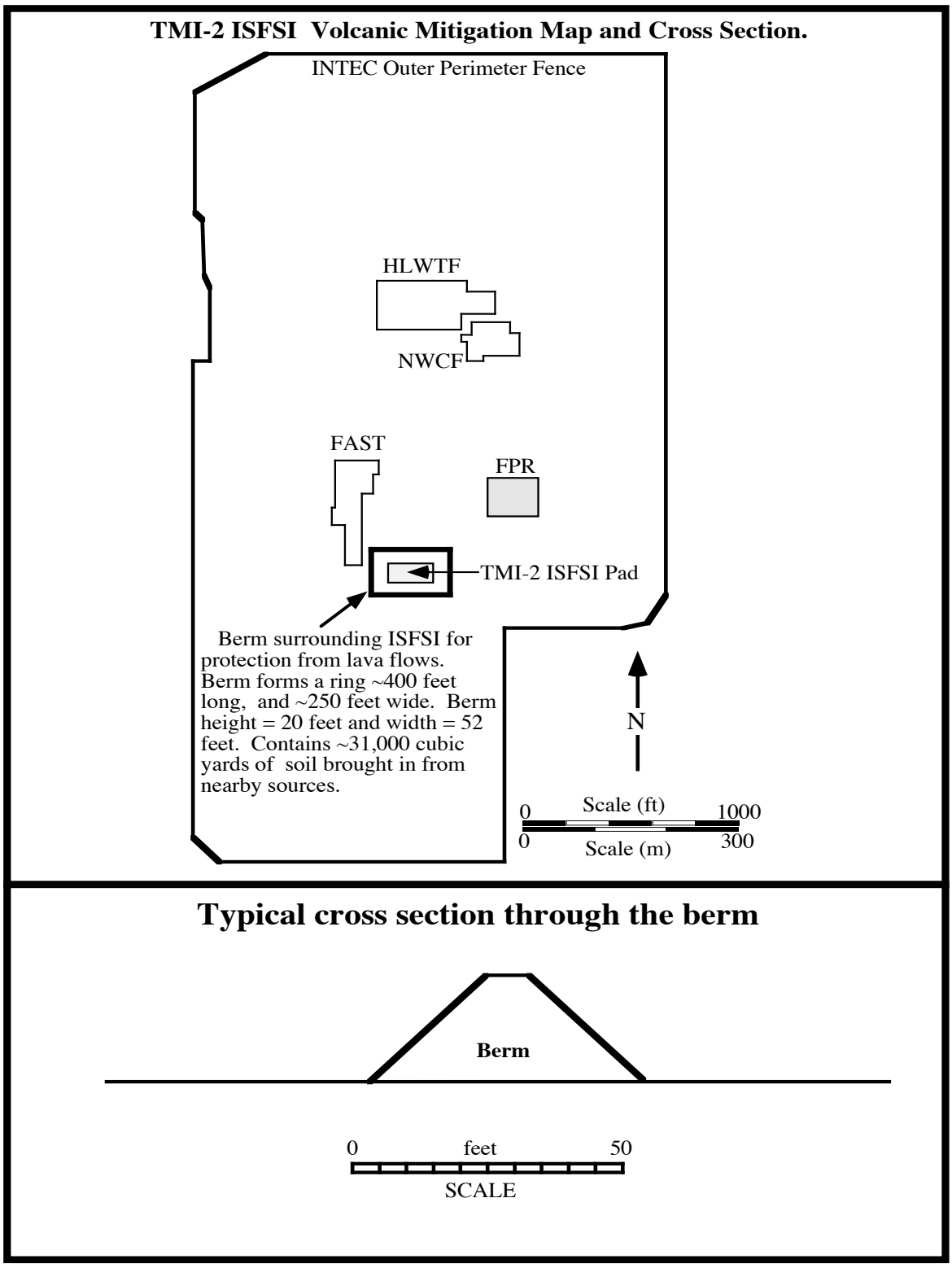

Figure 8.2-4
TMI-2 ISFSI Volcanic Mitigation Map and Cross Section

8.3 Load Combination Evaluation

The load categories associated with normal operating conditions, off-normal conditions, and postulated accident conditions are described and analyzed in previous sections. The load combination results for the NUHOMS®-12T components important to safety are presented in this section. Fatigue effects on the DSC confinement boundary are also addressed in this section.

8.3.1 DSC Confinement Boundary Load Combination Evaluation

As described in Section 3.2, the stress intensities in the DSC confinement boundary at various critical locations for the appropriate normal operating condition loads are combined with the stress intensities experienced by the DSC confinement boundary during postulated accident conditions. It is assumed that only one postulated accident event occurs at any one time. Since the postulated cask drop accidents are by far the most critical, the load combinations for these events envelope all other accident event combinations. Table 8.3-1 through Table 8.3-3 tabulate the maximum stress intensity for each component of the DSC confinement boundary calculated for the enveloping normal operating, off-normal, and accident load combinations. For comparison, the appropriate ASME Code allowables are also presented in these tables.

8.3.2 DSC Confinement Boundary Fatigue Evaluation

Table 8.3-1 through Table 8.3-3 present the calculated enveloping normal, off-normal and accident stress intensities for the DSC confinement boundary components. Fatigue effects on the DSC confinement boundary are addressed using the criteria contained in NB-3222.4 of the ASME Code [8.19]. Fatigue effects need not be specifically evaluated provided the six criteria contained in NB-3222.4(a) are met. As demonstrated in Appendix C.4.1 of the NUHOMS® generic SAR [8.9], an evaluation using these six criteria has been performed to show that the ASME Code fatigue requirements are satisfied for the DSC confinement boundary.

8.3.3 MP187 Cask Load Combination Evaluation

The MP187 cask load combination evaluations are addressed in the MP187 cask SAR [8.18] and the Rancho Seco ISFSI SAR [8.12].

8.3.4 MP187 Cask Fatigue Evaluation

Fatigue effects on the MP187 cask are addressed in the MP187 cask 10 CFR Part 72 evaluation presented in the Rancho Seco ISFSI SAR [8.12].

8.3.5 HSM Load Combination Evaluation

The maximum bending moments and shear forces induced in the HSM for the individual normal and off-normal loads are listed in Table 8.1-15. Similarly, the maximum moments and shears induced in the HSM for the individual accident loads are listed in Table 8.1-15. As described in Section 3.2.5.l, the load combination procedure of Section 6.17.3.1 of ANSI 57.9 [8.2] is used to combine the factored normal operation, off-normal, and postulated accident loadings imposed on the reinforced concrete HSM. Many of the general event combinations, shown in Table 3.2-4, are enveloped by others that contain the same load factors with additional applied load cases.

The governing calculated bending moments and shears for each load combination are tabulated in Table 8.3-4. The tabulated results represent the bounding shears and moments for either a single free-standing HSM or the array of HSMs. For comparison, the ultimate moment and shear capacity of the HSM for the controlling load combinations are also shown in Table 8.3-4. Comparison of the reported bending moment and shear for each load combination with the corresponding ultimate capacity shows that the design strength of the HSM is greater than the strength required for the most critical load combination.

8.3.6 Thermal Cycling of the HSM

The largest mean daily change of temperature at the TMI-2 ISFSI site is 50°F. Because of the massive concrete sections used in the HSM, a period of time greater than one week is needed to obtain steady state temperatures and a steady state thermal gradient. For conservatism, it is assumed that the 50°F maximum daily change could produce a steady state gradient every day for 50 years, for a total of 18,250 thermal cycles. For the TMI-2 HSM, the maximum moment caused by the worst case steady state normal operating thermal loads is bounded by the steady state off-normal operating thermal loads. The maximum moment caused by the off-normal operating thermal load for the concrete components of the HSM is 928.8 kip-in/ft and occurs in the rear wall. This loading is 46% of the minimum ultimate strength of the roof slab. Assuming this load amplitude is cycled daily, and referring to the S-N curve of Figure 6-46 of Reference 8.7, the number of cycles that occur before failure is greater than 10,000,000. Since this value is far greater than the postulated worst case 18,250 cycles, thermal cycling has a negligible effect on the HSM reinforced concrete.

8.3.7 DSC Support Structure Load Combination Evaluation

The applicable loads for the DSC support structure inside the HSM include the DSC and support assembly dead weight, seismic loads, and DSC handling loads. Three load combinations are evaluated. Load combination one consists of the DSC plus the support structure dead weight, plus the DSC handling loads for a typical normal operating load case. Load combination two includes the dead weight of the support structure plus DSC handling loads in the jammed condition representing an off-normal loading. The third load combination includes the total dead weight plus design basis seismic loads for an accident event. The resulting maximum stresses as compared to AISC code allowables [8.39] are shown in Table 8.3-5.

The same load combinations are used for the DSC support structure connecting elements. All end connection components are designed to meet the AISC Code requirements for these design loads. The structural steel design is based on the requirements of the AISC code, and the embedments are designed in accordance with the requirements of ACI 349.

Table 8.3-1
NUHOMS®-12T DSC Enveloping Load Combination Results for Normal and Off-Normal Loads (ASME Service Levels A and B)

DSC Components	Stress Type	Stress (ksi)		Controlling Load Combination
		Calculated	Allowable	
DSC Shell	Primary Membrane	16.3	23.1	A
	Membrane + Bending	32.7	34.6	A
	Primary + Secondary	54.7	69.3	B
Inner Bottom Cover Plate	Primary Membrane	1.8	23.1	A
	Membrane + Bending	2.6	34.6	A
	Primary + Secondary	3.9	69.3	B
Outer Bottom Cover Plate	Primary Membrane	7.9	23.1	B
	Membrane + Bending	28.2	34.6	B
	Primary + Secondary	34.7	69.3	B
Top Cover Plate	Primary Membrane	9.5	23.1	A
	Membrane + Bending	14.0	34.6	A
	Primary + Secondary	14.8	69.3	B
Top Shield Plug	Primary Membrane	5.3	19.3	A
	Membrane + Bending	7.8	29.0	A
	Primary + Secondary	8.0	57.9	A

Table 8.3-2
NUHOMS®-12T DSC Enveloping Load Combination Results for Accident Loads (ASME Service Level C)

DSC Components	Stress Type	Stress (ksi)	
		Calculated	Allowable
DSC Shell	Primary Membrane	16.4	34.6
	Membrane + Bending	28.0	51.9
Inner Bottom Cover Plate	Primary Membrane	2.2	34.6
	Membrane + Bending	3.6	51.9
Outer Bottom Cover Plate	Primary Membrane	5.1	34.6
	Membrane + Bending	9.1	51.9
Top Cover Plate	Primary Membrane	10.7	34.6
	Membrane + Bending	15.5	51.9
Top Shield Plug	Primary Membrane	5.4	32.8
	Membrane + Bending	8.5	49.2

Table 8.3-3
NUHOMS®-12T DSC Enveloping Load Combination Results for Accident Loads (ASME Service Level D)

DSC Components	Stress Types	Stress (ksi)	
		Calculated	Allowable
DSC Shell	Primary Membrane	26.4	49.0
	Membrane + Bending	51.6	70.0
Inner Bottom Cover Plate	Primary Membrane	11.1	49.0
	Membrane + Bending	15.0	70.0
Outer Bottom Cover Plate	Primary Membrane	11.9	49.0
	Membrane + Bending	20.5	70.0
Top Cover Plate	Primary Membrane	17.7	49.0
	Membrane + Bending	27.7	70.0
Top Shield Plug	Primary Membrane	19.8	40.6
	Membrane + Bending	46.5	58.0
Top Cover Plate Weld	Primary	17.9	56.0
Bottom Cover Plate Weld	Primary	13.7	56.0

Table 8.3-4
HSM Enveloping Load Combination Results

Load[1] Combination	Loading Combination Description	Governing Load[2, 3]		Capacities	
		V_{max} (k/ft)	M_{max} (k-in/ft)	V_u (k/ft)[4]	M_u (k-in/ft)
1	$1.4D+1.7L+1.7R_o$	60.4	834.2	100.9	1683.0
2	$0.75(1.4D+1.7L+1.7T_o+1.7W)$	20.0	2193.8	31.0	2576.0
3	$0.75(1.4D+1.7L+1.7T_o+1.7R_o)$	20.1	1471.2	31.0	1683.0
4	$D+L+T_o+E$	15.8	1791.9	31.0	2576.0
5	$D+L+T_o+W_t$	59.8	1197.2	100.9	1683.0
6	$D+L+T_a+R_a$	54.7	1265.3	100.9	1683.0

D = Dead Weight, E = Earthquake Load, L = Live Load, T_o = Normal Condition Thermal Load,
T_a = Off-normal or Accident Condition Thermal Load, W_t = Tornado Wind and Missile Loads,
R_o = Normal Handling Loads, R_a = Off-Normal Handling Loads, W = Normal Wind Load

---

(1) Load combinations are based on ANSI-57.9 as shown in Table 3.2.4.

(2) Governing loads shown are irrespective of locations. Loads reported have minimum margin to design capacity.

(3) Results of load combinations 2 through 6 are based on cracked section. Others based on uncracked sections.

(4) See Table 3.2-4 for definition of load terms.

Table 8.3-5
DSC Support Structure Enveloping Load Combination Results

Component	Load Combination	Calculated Stress[1]				Interaction[2] (Calc/ Allowable)	Allowable[2] Shear Stress (ksi)
		Axial (ksi)	Strong Axis Bending (ksi)	Weak Axis Bending (ksi)	Shear (ksi)		
Support Rail	Normal Operation $D + L + R_o$[3]	1.42	6.73	7.81	5.12	0.73	13.1
	Off-Normal Operation $D + L + R_a$[3]	2.84	10.47	9.94	5.70	1.09[4]	17.4
	Accident $D + L + E$[3]	0.02	6.23	5.36	4.91	.051[5]	18.3

(1) Maximum stresses reported irrespective of location.

(2) Allowable stresses taken at 200°F for all combinations.

(3) See Table 3.2-4 for definition of load terms.

(4) The permissible interaction ratio for this load combination is 1.33.

(5) The permissible interaction for this load combination is 1.6.

8.4 Site Characteristics Affecting Safety Analysis

All site characteristics affecting the safety analysis of the NUHOMS®-12T system are noted throughout this SAR where they apply. Specific site characteristics that were taken into consideration in the design were:

- Wind Loads
- Missile Loads
- Seismic Events
- Temperatures
- Precipitation
- Flooding

Intentionally Blank

8.5 References

8.1 U.S. Nuclear Regulatory Commission (U.S. NRC), "Standard Format and Content for the Safety Analysis Report for an Independent Spent Fuel Storage Installation (Dry Storage)," Regulatory Guide 3.48, August 1989.

8.2 American National Standard, "Design Criteria for an Independent Spent Fuel Storage Installation (Dry Storage Type)," ANSI/ANS 57.9-1984, American Nuclear Society, La Grange Park, Illinois, 1984.

8.3 Henry H. Bednar, P.E., Pressure Vessel Design Handbook, Van Nostrand Reinhold Co., 1981.

8.4 U. S. Nuclear Regulatory Commission, "Barrier Design Procedures," Standard Review Plan NUREG-0800, (Formerly NUREG-75/087) Revision 1, July 1981.

8.5 American Concrete Institute, Code Requirements for Nuclear Safety Related Concrete Structures and Commentary, ACI 349-85 and ACI 349R-85, American Concrete Institute, Detroit, MI, 1980.

8.6 C. Wang and C. G. Salmon, Reinforced Concrete Design, Third Edition, Harper and Row, New York, N. Y., 1979.

8.7 M. Fintel, Handbook of Concrete Engineering, Van Nostrand Reinhold Co., New York, N.Y., 1985.

8.8 Prestressed Concrete Institute, PCI Design Handbook, 2nd Edition, Prestressed Concrete Institute, 1978.

8.9 Safety Analysis Report for the Standardized NUHOMS® Horizontal Modular "Storage System for Irradiated Nuclear Fuel," NUH-003, Revision 4A, VECTRA Technologies, Inc., June 1996, File No. NUH003.0103.

8.10 H. K. Hilsdorf, J. Kropp, and H. J. Koch, "The Effects of Nuclear Radiation on the Mechanical Properties of Concrete," Paper 55-10, Douglas McHenry International Symposium on Concrete and Concrete Structures, American Concrete Institute, Detroit, MI, 1978.

8.11 American Nuclear Society, "American National Standard Guidelines on the Nuclear Analysis and Design of Concrete Radiation Shielding for Nuclear Power Plants," ANSI/ANS-6.4-1977, American National Standards Institute, Inc., 1977.

8.12 Safety Analysis Report for the Rancho Seco Independent Spent Fuel Storage Installation, Sacramento Municipal Utility District, October 1993, USNRC Docket Number 72-11.

8.13 R. J. Roark and W. C. Young, Formulas for Stress and Strain, Sixth Edition, McGraw-Hill, New York, N.Y., 1989.

8.14 "Climatography of the Idaho National Engineering Laboratory," DOE/ID-12118, 2nd Edition, December 1989.

8.15 "SCALE 4.2, Modular Code System for Performing Standardized Computer Analysis for Licensing Evaluation," NUREG/CR-0200, Revision 4, ORNL/NUREG/CSD-2/V2/R4, Prepared by Oak Ridge National Laboratory for USNRC, CCC-S45, Released November 1993.

8.16 F. Kreith, Principle of Heat Transfer, Third Edition, Harper and Row Publishers.

8.17 "TMI-2 Canister Dry Storage: Hydrogen Gas Generation and Transport Evaluation," GPU Nuclear, Inc., September 1996.

8.18 "Safety Analysis Report for the NUHOMS®-MP187 Multi-Purpose Cask," NUH-005, Revision 2, VECTRA Technologies, Inc., February 1996, USNRC Docket Number 71-9255.

8.19 American Society of Mechanical Engineers, ASME Boiler and Pressure Vessel Code, Section III, Division l, Subsections NB, NC, and Appendices, 1992 Edition with 1993 Addenda.

8.20 J. A. Buckholz, "Scoping Design Analyses for Optimized Shipping Casks Containing 1-, 2-, 3-, 5-, 7-, or 10-Year Old PWR Spent Fuel," ORNL/CSD/TM-149, Oak Ridge National Laboratory/Union Carbide Nuclear Division, p. 95, 1983.

8.21 "Safety Analysis Report for the NUPAC 125-B Fuel Shipping Cask," Nuclear Packaging, Inc., USNRC Docket Number 71-9200.

8.22 U.S. Atomic Energy Commission, "Design Basis Tornado for Nuclear Power Plants," Regulatory Guide 1.76, April 1974.

8.23 NUREG/CR-4461 Tornado Climatology of the Contiguous United States.

8.24 SECY-93-087 USNRC Policy Issue “Policy, Technical, and Licensing Issues Pertaining to Evolutionary and Advanced Light-Water Reactor (ALWR) Designs,” April 2, 1993.

8.25 R. P. Kennedy, Holmes and Narver, Inc., "A Review of Procedures for the Analysis and Design of Concrete Structures to Resist Missile Impact Effects," Nuclear & Systems Sciences Group, Anaheim, California, September 1975.

8.26 J. R. McDonald, K. C. Mehta, and J. E. Minor, "Design Guidelines for Wind-Resistant Structures," Institute for Disaster Research and Department of Civil Engineering, Texas Tech University, Lubbock, Texas, June 1975.

8.27 U.S. Atomic Energy Commission, "Design Response Spectra for Seismic Design of Nuclear Power Plants," Regulatory Guide 1.60, Revision 1, December 1973.

8.28 U.S. Atomic Energy Commission, "Damping Values for Seismic Design of Nuclear Power Plants," Regulatory Guide 1.61, October 1973.

8.29 R. D. Blevins, Formulas for Natural Frequency and Mode Shape, Van Nostrand Reinhold Co., New York, N.Y., 1979.

8.30 American Concrete Institute, Building Code Requirements for Reinforced Concrete (ACI 318-95) ACI, Detroit, MI, 1995.

8.31 Swanson Analysis Systems Inc., ANSYS Engineering Analysis System User's Manual, Version 5.3A, Swanson Analysis Systems Inc., Pittsburgh, PA.

8.32 U. S. Nuclear Regulatory Commission, "Combining Modal Responses and Spatial Components in Seismic Response Analysis," Regulatory Guide 1.92, Revision 1, February 1976.

8.33 Electric Power Research Institute, "The Effects of Target Hardness on the Structural Design of Concrete Storage Pads for Spent-Fuel Casks," EPRI Report NP-4830, October 1986.

8.34 “TMI-2 Defueling Canisters, Final Design Technical Report,” Document 77-1153937-04, Babcock and Wilcox Company, May 24, 1985

8.35 "ICPP Interim Storage System (ISS) Lightning Risk Assessment," INEL Engineering Design File 0566 dated Sept. 4, 1996

8.36 "Flammability Characteristics of Combustible Gases and Vapors" Zabetakis, M.J., Bureau of Mines Bulletin 627, United States Department of the Interior, 1965.

8.37 "TMI-2 Canister Stress Analysis," Babcock and Wilcox Company, Document No. 33-1153704

8.38 "ISFSI Fire Exposure Analysis", VECTRA File No. NUH004.0422.

8.39 American Institute of Steel Construction (AISC), Allowable Stress Design, 9th Edition..

8.40 Fisher, R.V., Heiken, G., and Hulen, J.B. (1997) Volcanoes, Crucibles of Change;Princeton University Press, Princeton, N.J., p. 137-146.

8.41 Barberi, F., Carapezza, M.L., Valenza, M., and Villari, L. (1993) The control of lava flow during the 1991-1992 eruption of Mt. Etna; Journal of Volcanology and Geothermal Research, v.56, p.1-34.

8.42 McPhee, J. (1991) The Control of Nature; Noonday Press, New York, chapter 2, Cooling the Lava.

8.43 N.B. Zolders, "Thermal Properties of Concrete Under Sustained elevated Temperatures," ACI Publication, Paper SP25-1, American Concrete Institute, Detroit, MI, 1970.

8.44 ASHRAE Handbook, 1981 Fundamentals, Fourth Printing, American Society of Heating, Refrigerating, and Air-Conditioning Engineering, Inc., 1983.

8.45 Hall, G. G., "Radiological Evaluation of TMI-2 ISFSI Technical Specification 3.1.1", Engineering Design File No. 4728, Revision 2, July, 2006.